ISSN 0971 - 6203

Journal of Medical Physics

Volume 42 | No 1 | Jan - Mar 2017

Full text at www.jmp.org.in

PubMed

Association of
Medical Physicists of India
An Affiliate of Indian National Science Academy
and
International Organization for Medical Physics
www.ampi.org.in

Medknow

Wolters Kluwer

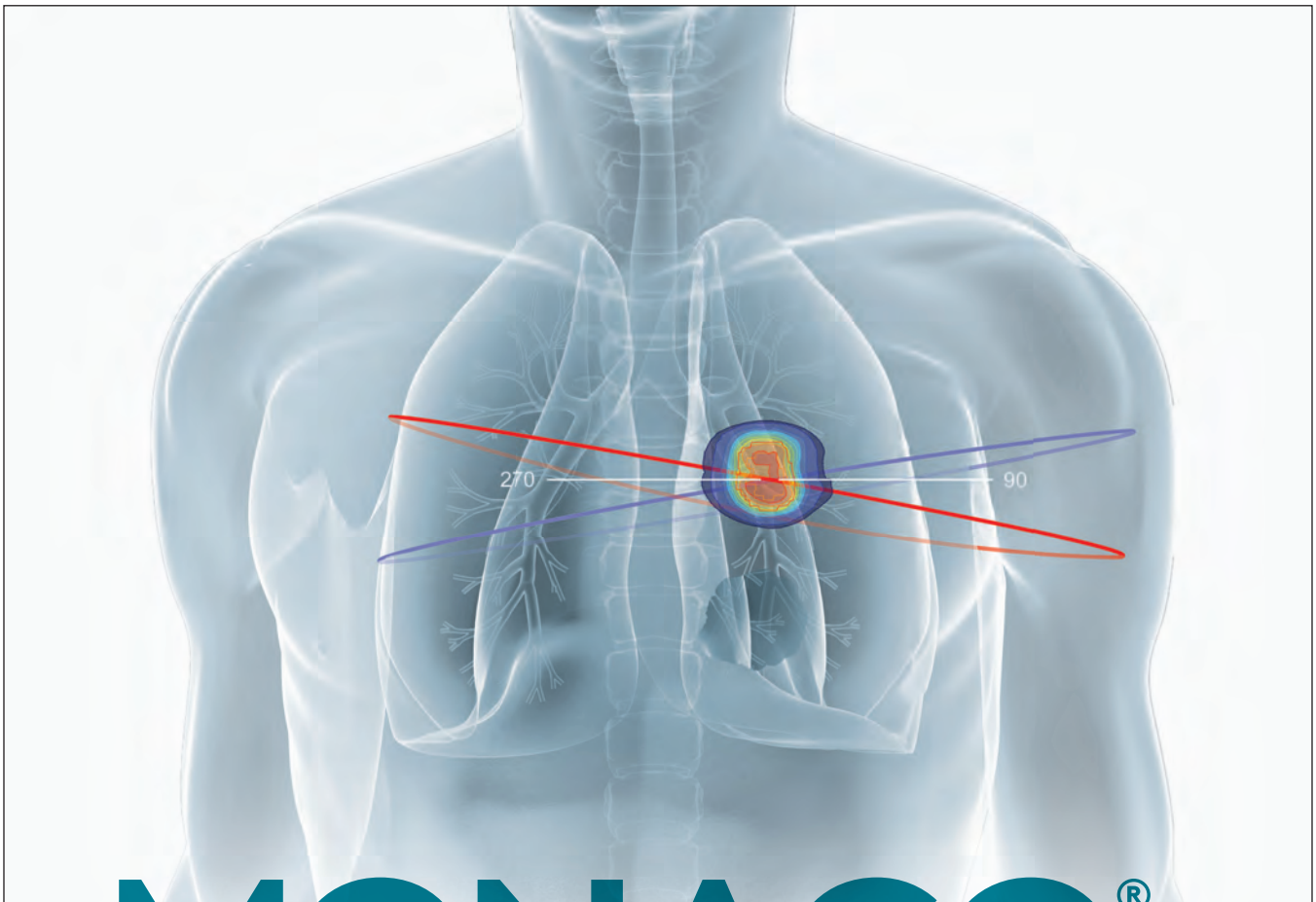

MONACO®

Accuracy without compromise

Monaco delivers the exquisite quality you expect at the speed you need.

The complete solution you know for planning accuracy now provides **faster, more efficient planning** from simple 3D to the most complex high definition stereotactic plans. Plus, Monaco is the only treatment planning solution with the gold standard Monte Carlo algorithm and multicriteria optimization, so you can be confident that the dose planned is the dose delivered.

VISIT ELEKTA.COM/MONACO

Elekta

LADMON072616 07.2016

ROSALINA INSTRUMENTS

FARMER TYPE CHAMBER FAR 65-GB

Preliminary Data Sheet

APPLICATIONS

- Absolute dosimetry in radiation therapy
- Photons and High Energy Electrons.
- Traditional chamber construction for absolute dosimetry in x-rays
- Standard reference detector for reference dosimetry and scientific applications

FEATURES

- Air ionisation chamber
- Chamber with graphite wall, for all applicable radiation conditions
- Non waterproof
- Vented through waterproof sleeve
- Guarded upto 15 mm from base
- Supplied with individual factory calibration certificate and user's guide (Provisional)

MATERIAL

- Outer electrode Graphite **(1.82 g/cm^3)**
- Inner electrode Aluminium **(2.70 g/cm^3)**
- Build-up cap for ^{60}Co Delrin **(1.42 g/cm^3)**

ACTIVE DIMENSIONS

- Volume (nominal) **0.65 cm^3**
- Total active length **23.1 mm**
- Inner diameter of cylinder **6.2 mm**
- Wall thickness 0.4 mm
- Diameter of inner electrode **1.0 mm**
- Wall thickness of build-up cap for ^{60}Co **3.9 mm**

CABLE AND CONNECTOR

- Connector type **TNC triaxial**
- Cable length **1.40 m**

OPERATIONAL DATA

- Leakage current **<± 10 x 10^{-15} A**
- Sensitivity **21 x 10^{-9} C/Gy**
- Radiation quality (e^-) **1.3 Mev - 50 MV**
- Polarising voltage **+ 300 V**
- Reference point w/o build-up cap **13 mm from the distal end of the chamber**
- Reference point with build-up cap **17 mm from the distal for ^{60}Co end of the build-up cap**

127, Bussa Udyog Bhavan,
T.J Road, Sewri (W)
Mumbai - 400 015.
India

91 22 24166630
support@rosalina.in
www.rosalina.in

5 Year Warranty

MADE IN INDIA

DOSEVIEW™ 3D

PREMIUM QUALITY
AFFORDABLE PRICE

PRECISION REDEFINED
INTUITIVE SOFTWARE • WIRELESS INTERFACE

Wi Fi

STANDARD IMAGING®
ADVANCING RADIATION QA™

ROSALINA
INSTRUMENTS

QA BEAMCHECKER™ PLUS

- **Wire-free operation**
- **Automatic energy detection**
- **Integrated build-up beyond dmax for all energies**
- **Unique "flip" feature**
- **Easy to use software**

The QUICK FLIP

Photon to electron with no additional build-up

The new ***QA BeamChecker Plus*** from Standard Imaging is a reliable and uncomplicated device for daily quality assurance testing of linear accelerator output.

With wire-free technology, integrated build-up and automatic determination of energy, technicians can quickly complete daily QA procedures, and physicists have access to powerful data, trending and analysis.

ROSALINA INSTRUMENTS

127, Bussa Udyog Bhavan, Tokershi Jivraj Road, Sewri, Mumbai - 400 015. INDIA
Tel : 91 22 24166630 / 24173493 Fax : 91 22 66627766
E-mail support@rosalina.in www.rosalina.in

ROSALINA INSTRUMENTS

RENTRANT WELL CHAMBER

BDS 1000 BRACYTHERAPY DOSIMETRY SYSTEM

BRACHYTHERAPY SOURCE CALIBRATION

The BDS 1000 Well Chamber is air vented chamber, Highly accurate for low dose rate and high dose rate brachytherapy. Source holders are available for most existing sources as well as custom made source holders.

Calibrations Available	^{60}Co ^{192}Ir and/or LDR radionuclides from various manufacturers as requested
Active Volume	240 cm^3
Connector	TNC triax (standard) Other Optional
Range	10 U to 80 MU 0.01 mCi to 20 Ci
Cable	5 ft, 1.5 m
Bias voltage	± 300 volts, typical
Leakage	Less than 25 fA
Stability	0.2% (Reproducibility over 2 years)
Response	± 0.5% over 25 mm at center of axis

5 Year Warranty

MADE IN INDIA

Preliminary Data Sheet

127, Bussa Udyog Bhavan T.J Road, Sewri (W) Mumbai - 400 015. INDIA
Tel : 91 22 241 66630, E-mail : support@rosalina.in www.rosalina.in

ROSALINA INSTRUMENTS

SURE DOSE Universal Radiation Dosimeter

We Make The Things That Make Indian Medical Physicist Proud

Cutting edge Indian technology, high calibre engineering expertise, decades of experience, devotion and total commitment to the nation.

Innovative Leadership in Radiation Oncology and Medical Physics

- Farmer type ionisation chambers
- Electro Meters
- Specialized phantoms
- IGRT Dosimetry
- Absolute Dosimetry
- Relative Dosimetry
- VMAT Dosimetry
- INVIVO Dosimetry

www.rosalina.in

STANDARD IMAGING®
ADVANCING RADIATION QA™

ROSALINA INSTRUMENTS

Exradin W1 Scintillator FFF - Small Field Dosimetry

The Exradin W1 Scintillator is a near-water equivalent detector that achieves paramount precision by signi‹cantly decreasing beam disturbance.

Minimize Beam Perturbation and Corrections

The unprecedented characteristics of the W1 Scintillator closely mimic water, easing data collection by negating many measurement corrections required with other detectors.

- Near water equivalence (within 5% of physical density)
- Linear dose response
- Dose rate independence
- Energy independence within the MV range
- Minimal temperature dependence

Ideal for Measurement and Characterization of Small Fields

1mm spatial resolution makes the W1 a perfect tool for stereotactic radiosurgery (SRS) and stereotactic body radiation therapy (SBRT) QA. This includes compatibility with the Lucy 3D QA Phantom and use in the following systems:

- Gamma Knife®
- CyberKnife®
- BrainLab®
- Varian®
- Elekta®
- TomoTherapy®

Automatically Correct for Cherenkov Effect

Pair the W1 Scintillator with the SuperMAX Electrometer to effectively eliminate Cherenkov effect without the need for extraneous hand calculations.

Consistent, Convenient Setup

Integration with the Exradin Scintillator Calibration Slab and solid water phantoms allows for easy, repeatable measurements.

Print ISSN: 0971-6203, E-ISSN: 1998-3913

Journal of Medical Physics

(Incorporating AMPI Medical Physics Bulletin)

Association of Medical Physicists of India

(Regd. No. 421/1976 GBBSD, Public Trust F 4238)
(An affiliate of the Indian National Science Academy & The International Organization for Medical Physics)
C/o Radiological Physics & Advisory Division, BARC
CT & CRS Building, Anushaktinagar, Mumbai - 400094, ● Website: www.ampi.org.in

The Association of Medical Physicists of India (AMPI) is a professional but a non-profit making / non-governmental organization, devoted to serving the needs of the country in the field of Medical Physics. Its membership is open to science graduates, engineers and physicians interested in the application of physics to medical and biological sciences. Medical Radiation Physicists, Radiation Safety Officers, Radiological and Hospital Physicists, Radiation Oncologists and Radiologists form the main group of the association. It publishes this quarterly journal. The association is having about 1200 active members. The journal is provided to its members and also to the libraries of almost all leading Cancer Centres in the country on a very nominal subscription. Other than publishing Journal of Medical Physics, the association holds a national/ international conference every year to exchange information among its members. The association also supports advanced training of Medical Physicists by offering Travel Fellowships. For public awareness, publication of articles related to medical physics and radiation safety in newspapers and periodicals is encouraged. The association also works towards worldwide exchange of information on medical physics.

The College of Medical Physics of India (CMPI) is an autonomous wing of AMPI which was established to function as the certifying and accreditation body. Membership of AMPI is prerequisite to appear for CMPI certification examination. A member of AMPI can become member of CMPI only by passing the certification examination. CMPI certification indicates that the holder has acquired, demonstrated, and maintained a minimum standard of knowledge in medical physics and the competence to practice as clinical physicist in Diagnostic Radiology, Radiation Oncology and Nuclear Medicine.

Membership Fee Details (w.e.f. February 07, 2015)

Annual Member	
Indian Resident	INR ₹ 1,280.00
Developing Countries	USD $ 50.00
Other Countries	USD $ 165.00
Life Member	
Indian Resident	INR ₹ 3,615.00
Developing Countries	USD $ 257.00
Other Countries	USD $ 970.00
Institution Member (India)	INR ₹ 4,780.00

AMPI Executive Committee (2015-2017)

President	Prof. Arun Chougule
Vice President	Mr. Balasubramanian Nagappan
Secretary	Dr. Vellaiyan Subramani
Treasurer	Mr. Varadharajan Ekambaram
Members	Dr. Lalit M Aggarwal
	Dr. Atul Tyagi
	Dr. Thayalan Kuppusamy
	Dr. Varatharaj Chandraraj
	Dr. Raghukumar P
	Dr. Arabinda Rath
	Mr. Vinod Pandey
	Mr. Suresh Pangam
	Mr. S Karthikeyan
	Dr. Om Prakash Gurjar
	Dr. Vinod Kumar Dangwal

AMPI Board of Trustees (2015-2017)

Chairman	Mr. Satya Pal Agarwal
Convener	Dr. Pankaj Tandon
Members	Dr. Deepak Deshpande
	Dr. Kamlesh Passi
	Mr. Radhakrishnan Balan Nair

College of Medical Physics of India (CMPI) Board 2015-2017

Chairman	Mr. V. K. Sathiyanarayanan
Vice Chairman	Dr. Tharmar Ganesh
Chief Examiner	Dr. Sunil Dutt Sharma
Registrar	Dr. Dayananda Shamurailtpam
Secretary-Treasurer	Dr. K. J. Maria Das
Members	Dr. Arabinda Kumar Rath
	Dr. Pratik Kumar
	Dr. Jamema Swamidas
	Mr. Raghavendra Holla

JMP H-Index = 13

Journal of Medical Physics

General Information

The journal

The Journal of Medical Physics (known as AMPI Medical Physics Bulletin till 1994) is a quarterly publication of Association of Medical Physicists of India (AMPI). Issues are published quarterly in January, April, July and October. The main objective of the Journal is to serve as a vehicle of communication to highlight all aspects of medical physics. The scope of this journal covers all aspects of the application of radiation physics to health science, mainly radiation therapy, radiodiagnosis, nuclear medicine, radiation dosimetry, radiation standards, quality assurance, calibration and radiation protection. Papers / manuscripts on radiobiology pertaining to cancer therapy also fall within the scope of the journal. Apart from the original research work, papers which are of practical importance to medical physicists e.g., those dealing with practices (performance and quality assurance tests, clinical investigations and follow-ups with novelty), radiation accidents and emergencies are also published in the journal. Brief manuscripts dealing with the validation of relatively newer concepts may be considered as technical notes or letter to editor. Reviews of publications (e.g., ICRP/ ICRU reports and books related to the scope of the journal) may also find a place in the journal. Manuscripts with no or oblique relevance to the scope may not find place.

Abstracting and indexing information

The journal is registered with the following abstracting partners: CNKI (China National Knowledge Infrastructure), EBSCO Publishing's Electronic Databases, Exlibris – Primo Central, Google Scholar, Hinari, Infotrieve, Journal Guide, National Science Library, OpenJGate, ProQuest, TdNet

The journal is indexed with: DOAJ, EMBASE/ Excerpta Medica, Emerging Sources Citation Index, Index Copernicus, Indian Science Abstracts, IndMed, Pubmed Central, Scimago Journal Ranking, SCOPUS

Information for Authors

Copies of the journal are provided free of cost to the AMPI members.

There are no page charges for JMP submissions. However, there are charges for color reproduction of photographs. Please check http://www.jmp.org.in/contributors.asp for details.

All manuscripts must be submitted online at www.journalonweb.com/jmp.

Subscription Information

A subscription to Journal of Medical Physics comprises 4 issues. Prices include postage. Annual Subscription Rate for non-members-

Annual Subscription Rates

Print	Personal	Institutional
India (INR)	1700.00	2800.00
Abroad (USD)	130.00	260.00
Online only		
India (INR)	1400.00	2200.00
Abroad (USD)	100.00	210.00
Print + Online		
India (INR)	2100.00	3500.00
Abroad (USD)	160.00	330.00
Single Issue		
India (INR)	581.00	925.00
Abroad (USD)	46.00	86.00

For mode of payment and other details, please visit www.medknow.com/subscribe.asp.

Claims for missing issues will be serviced at no charge if received within 60 days of the cover date for domestic subscribers, and 3 months for subscribers outside India. Duplicate copies cannot be sent to replace issues not delivered because of failure to notify publisher of change of address.

The journal is published and distributed by Wolters Kluwer India Private Limited. Copies are sent to subscribers directly from the publisher's address. It is illegal to acquire copies from any other source. If a copy is received for personal use as a member of the association/society, one cannot resale or give-away the copy for commercial or library use. The copies of the journal to the members of the association are sent by ordinary post. The editorial board, association or publisher will not be responsible for non receipt of copies. If any member/subscriber wishes to receive the copies by registered post or courier, kindly contact the publisher's office. If a copy returns due to incomplete, incorrect or changed address of a member/subscriber on two consecutive occasions, the names of such members will be deleted from the mailing list of the journal. Providing complete, correct and up-to-date address is the responsibility of the member/subscriber.

Please send change of address information to subscriptions@medknow.com.

Advertising policies

The journal accepts display and classified advertising. Frequency discounts and special positions are available. Inquiries about advertising should be sent to Wolters Kluwer India Private Limited, advertise@medknow.com.

The journal reserves the right to reject any advertisement considered unsuitable according to the set policies of the journal.

The appearance of advertising or product information in the various sections in the journal does not constitute an endorsement or approval by the journal and/or its publisher of the quality or value of the said product or of claims made for it by its manufacturer.

Annual Advertisement Tariffs

1. Back cover (Color) - ₹ 56,000.00
2. Back Inside cover (Color) - ₹ 45,000.00
3. First Page (Color) - ₹ 48,000.00
4. Front Inside cover (Color) - ₹ 48,000.00
5. Full page B/W - ₹ 22,500.00
6. Full page color - ₹ 30,000.00
7. Gate Fold cover - ₹ 90,000.00
8. Art-Card (Back2Back) - ₹ 79,000.00

Copyright

Permissions

For information on how to request permissions to reproduce articles/information from this journal, please visit www.medknow.com.

Disclaimer

The information and opinions presented in the Journal reflect the views of the authors and not of the Journal or its Editorial Board or the Publisher. Publication does not constitute endorsement by the journal. Neither the Journal of Medical Physics nor its publishers nor anyone else involved in creating, producing or delivering the Journal of Medical Physics or the materials contained therein, assumes any liability or responsibility for the accuracy, completeness, or usefulness of any information provided in the Journal of Medical Physics, nor shall they be liable for any direct, indirect, incidental, special, consequential or punitive damages arising out of the use of the Journal of Medical Physics. The Journal of Medical Physics, nor its publishers, nor any other party involved in the preparation of material contained in the Journal of Medical Physics represents or warrants that the information contained herein is in every respect accurate or complete, and they are not responsible for any errors or omissions or for the results obtained from the use of such material. Readers are encouraged to confirm the information contained herein with other sources.

Editorial Office
Dr. A. S. Pradhan
Editor-in-Chief
Journal of Medical Physics,
Association of Medical Physicists of India (AMPI)
C/o Radiological Physics & Advisory Division,
Bhabha Atomic Research Centre,
CTCRS, Anushaktinagar, Mumbai - 400094, India.
E-mail: editor@jmp.org.in / Website: www.jmp.org.in

Published by
Wolters Kluwer India Private Limited,
A-202, 2nd Floor, The Qube,
C.T.S. No.1498A/2 Village Marol, Andheri (East),
Mumbai - 400 059, India.
Phone: 91-22-66491818
Print at Website: www.medknow.com

Printed at
Dhote Offset Technokrafts Pvt. Ltd., Jogeshwari, Mumbai, India

Journal of Medical Physics

Volume. 42 - No. 1 - January-March 2017

Contents

Contents (Contd...)

Journal of Medical Physics on Web

http://www.journalonweb.com/jmp

The Journal of Medical Physics now accepts articles electronically. It is easy, convenient and fast. Check following steps:

1 Registration

- Register from http://www.journalonweb.com/jmp as a new author (Signup as author)
- Two-step self-explanatory process

2 New article submission

- Read instructions on the journal website or download the same from manuscript management site
- Prepare your files (Article file, First page file and Images, Copyright form & Other forms, if any)
- Login as an author
- Click on 'Submit new article' under 'Submissions'
- Follow the steps (guidelines provided while submitting the article)
- On successful submission you will receive an acknowledgement quoting the manuscript ID

3 Tracking the progress

- Login as an author
- The report on the main page gives status of the articles and its due date to move to next phase
- More details can be obtained by clicking on the ManuscriptID
- Comments sent by the editor and reviewer will be available from these pages

4 Submitting a revised article

- Login as an author
- On the main page click on 'Articles for Revision'
- Click on the link "Click here to revise your article" against the required manuscript ID
- Follow the steps (guidelines provided while revising the article)
- Include the reviewers' comments along with the point to point clarifications at the beginning of the revised article file.
- Do not include authors' name in the article file.
- Upload the revised article file against New Article File - Browse, choose your file and then click "Upload" OR Click "Finish"
- On completion of revision process you will be able to check the latest file uploaded from Article Cycle (In Review Articles-> Click on manuscript id -> Latest file will have a number with 'R', for example XXXX_100_15R3.docx)

Facilities

- Submission of new articles with images
- Submission of revised articles
- Checking of proofs
- Track the progress of article until published

Advantages

- Any-time, any-where access
- Faster review
- Cost saving on postage
- No need for hard-copy submission
- Ability to track the progress
- Ease of contacting the journal

Requirements for usage

- Computer and internet connection
- Web-browser (Latest versions - IE, Chrome, Safari, FireFox, Opera)
- Cookies and javascript to be enabled in web-browser

Online submission checklist

- First Page File (rtf/doc/docx file) with title page, covering letter, acknowledgement, etc.
- Article File (rtf/doc/docx file) - text of the article, beginning from Title, Abstract till References (including tables). File size limit 4 MB. Do not include images in this file.
- Images (jpg/jpeg/png/gif/tif/tiff): Submit good quality colour images. Each image should be less than 10 MB) in size
- Upload copyright form in .doc / .docx / .pdf / .jpg / .png / .gif format, duly signed by all authors, during the time mentioned in the instructions.

Help

- Check Frequently Asked Questions (FAQs) on the site
- In case of any difficulty contact the editor

Original Article

The Feasibility Study of a Hybrid Coplanar Arc Technique Versus Hybrid Intensity-modulated Radiotherapy in Treatment of Early-stage Left-sided Breast Cancer with Simultaneous-integrated Boost

Yuan-Gui Chen, An-Chuan Li, Wen-Yao Li, Miao-Yun Huang, Xiao-Bo Li, Ming-Qiu Chen, Mutian Zhang[1], Ben-Hua Xu

Department of Radiation Oncology, Fujian Medical University Union Hospital, Fuzhou, Fujian Province, China, [1]Department of Radiation Oncology, University of Nebraska Medical Center, Omaha, Nebraska, USA

Abstract

This study demonstrated the feasibility and advantages of a hybrid, volumetric arc therapy technique that used two 90° coplanar arcs and two three-dimensional conformal tangential beams in the simultaneous-integrated boost radiotherapy of left-sided breast cancer after breast-conserving surgery. A total of nine patients with stage I, left-sided breast cancer who underwent breast-conserving surgery were selected for this retrospective study. For each patient, a hybrid arc plan was generated and then compared with two hybrid intensity-modulated radiotherapy plans. All plans were optimized using the same objectives and dose constraints. The prescription dose was 50.4 Gy to the planning target volume with simultaneous boost to 60 Gy to the expanded gross target volume in 28 fractions. The differences among these hybrid plans were analyzed by the Kolmogorov–Smirnov test or the Wilcoxon rank sum test. The hybrid arc plans achieved the clinical requirements of target dose coverage and normal tissue (NT) dose constraints. It was found that the hybrid arc plans showed advantages in the conformity index of the expanded gross target volume, the V_5 of the heart, the D_2 of the left ventricle, and the D_2 and $V_{50.4}$ of NTs. The average beam-on time and monitor units of the hybrid arc plans were significantly lower ($P < 0.001$).

Keywords: Breast cancer, hybrid treatment plan, simultaneous-integrated boost, whole breast irradiation

Received on: 01-10-2016 **Review completed on: 26-01-2017** **Accepted on: 27-01-2017**

Introduction

Nearly 1.2 million women are diagnosed with breast cancer all over the world every year, and 500,000 women die of it.[1] With the development of treatment strategies, an enhanced awareness of medical examination, and the popularity of breast cancer screening, the 5-year overall survival of breast cancer patients has improved in the last 30 years.[1] The 5-year, 10-year, and 15-year overall survival is 89%, 83%, and 78%, respectively. Analyses of randomized clinical trials have proven that breast-preserving surgery achieves survival equivalent to mastectomy in patients with early-stage breast cancer.[2-4] Adjuvant whole-breast irradiation is performed on these patients as the standard of care.

Radiotherapy following breast-conserving surgery for early-stage disease significantly reduces local recurrence and improves overall survival and thus has become an integrated part of breast cancer treatment.[5,6] Conventional radiotherapy regimens for these patients usually consist of two opposed tangential fields, followed by a boost with electron beam, achieving satisfactory local control with relatively low incidence of radiation complications.[7] However, dose inhomogeneity in the target and doses to the organs at risk (OAR), especially the heart, ipsilateral lung,

Access this article online

Quick Response Code:

Website: www.jmp.org.in

DOI: 10.4103/jmp.JMP_105_16

Address for correspondence: Dr. Ben-Hua Xu, Department of Radiation Oncology, Fujian Medical University Union Hospital, Fuzhou, Fujian Province, China. E-mail: benhuaxu@163.com

How to cite this article: Chen YG, Li AC, Li WY, Huang MY, Li XB, Chen MQ, *et al*. The feasibility study of a hybrid coplanar: Arc Technique versus hybrid intensity-modulated radiotherapy in treatment of early-stage left-sided breast cancer with simultaneous-integrated boost. J Med Phys 2017;42:XX.

and contralateral breast, are the major limitations of this technique.[8] Intensity-modulated radiotherapy (IMRT) with simultaneous-integrated boost (SIB) technique is adapted for breast cancer patients after breast-conserving surgery. This therapy is capable of shortening treatment course, improving dose homogeneity and conformity, and sparing normal tissues (NTs).[9-11] Currently, volumetric-modulated arc therapy (VMAT) has become one option for postoperative radiotherapy in breast cancer. However, the effectiveness of VMAT is controversial: some oncologists claim that VMAT has better protection for the adjacent organs than IMRT,[12-14] while others think that VMAT only reduces the treatment time without any advantage in the protection of NT.[15,16]

Recently, Jöst *et al*.[17] recommended the use of the VMAT + IMRT hybrid technique in radiation treatment of breast cancer after breast-conserving surgery, with the whole breast treated with IMRT and the boost volume treated with VMAT. Lin *et al*.[18] demonstrated that the VMAT and IMRT techniques could be applied simultaneously and that the hybrid-VMAT plan was feasible for whole-breast irradiation of left sided, early breast cancer. It is well known that during radiotherapy, the breast may have setup uncertainties of more than 1 cm. Respiratory motions will cause additional uncertainties in the radiation dose delivery to the target. Although breath hold and active breath control techniques can reduce errors, these techniques might not be feasible for every patient and not all the clinics are implementing these techniques. Previously, Mayo *et al*.[19] developed a hybrid technique of IMRT plus tangential beams, which could take into account the effect of breathing movement as well as achieve dose uniformity and NT protection. However, little is known about whether VMAT has advantages over IMRT when combined with tangential beams, especially in the SIB radiotherapy of breast cancer patients after breast-conserving survey.

The purpose of the present study was to demonstrate the feasibility and advantages of a hybrid VMAT technique in SIB radiotherapy of breast cancer. Specifically, plans of two coplanar 90° VMAT arcs plus tangential beams were compared with plans of IMRT beams plus tangential beams. We investigated dosimetric parameters, including the conformity index (CI), heterogeneity index (HI), and the radiation dose to NTs, especially the left ventricle. Our results provided clinical evidence for validating the use of the hybrid VMAT technique in radiotherapy with SIB for early-stage left breast cancer.

Materials and Methods

Patient selection and image acquisition

Nine patients were enrolled in this retrospective study under an Institutional Review Board-approved protocol. These patients had left sided, early-stage invasive mammary carcinoma (pT1N0M0), and underwent breast-conserving surgery followed by radiotherapy at our hospital between February 2014 and August 2015. Patients between 34 and 46 years old, with adequate function of the liver, kidney, heart, and hematopoietic system were considered eligible for the study. Patients with positive axillary or supraclavicular lymph nodes and distant metastasis were excluded from the study. All patients were immobilized in the supine position with the arm abducted (90° or greater) on the disease side. A computed tomography (CT) scan (LightSpeed RT4, GE Healthcare, USA) with 5 mm slice thickness was acquired for each patient, with coverage from the mandible to 4–6 cm below the inframammary fold to cover the entire lung volume. Imaging data were then transferred to the Eclipse treatment planning system (Varian Medical Systems, USA) for delineation of targets and critical structures.

Definition of target volumes and organs at risk

Clinical target volume (CTV) and gross tumor volume (GTV) were delineated according to the Radiation Therapy Oncology Group (RTOG) guidelines.[20] The planning target volume (PTV) and the boost volume (primary gross tumor volume [PGTV]) were expanded by an 8 mm margin from CTV and GTV, respectively, and were restricted to the breast tissue within 3 mm from the skin. Contralateral breast, contralateral lung, ipsilateral lung, heart, left ventricle, and NT were contoured by the same physician on the CT images. The heart was contoured from the pulmonary trunk branches into the left and right pulmonary arteries, and to its apex according to the RTOG 0413 protocol. The left ventricle was contoured from the mitral valve at the cephalic direction along the smooth appearance of the left ventricular outflow tract, and the posterior border was along the diaphragmatic cardiac surface.[21] NT represents the external contour of the patient's body minus the breast PTV, with an additional distance of 0.5 cm.

Treatment planning techniques

Patients were treated with conventional three-dimensional conformal radiotherapy (3D-CRT) technique of two opposite tangential photon beams. These 3D-CRT plans were not included in dosimetric comparison of the present study because there are reports showing that in left breast treatment, IMRT can improve dose homogeneity and conformity, and spare NTs.[22-24] Using the identical planning CT datasets and the contours, three types of treatment plans were created:

1. The "hybrid 15°-IMRT plan" combined two tangential beams and four IMRT beams. The standard medial and lateral 3D-CRT beams with control points were created by adding a 2.5 cm expansion margin on the surface of the chest wall skin, and a 0.5 cm margin was added in the other directions. Two IMRT beams had the same gantry angles as that of the tangential beams, and the other two beams were 15° anterior from the nearest tangential beams [Figure 1 Left].
2. The "hybrid 45°-IMRT plan" combined two tangential beams and four IMRT beams. Compared to the hybrid 15°-IMRT plan, the hybrid 45° plan is only different in that two IMRT beams were 45° anterior from the nearest tangential beams [Figure 1 Middle].

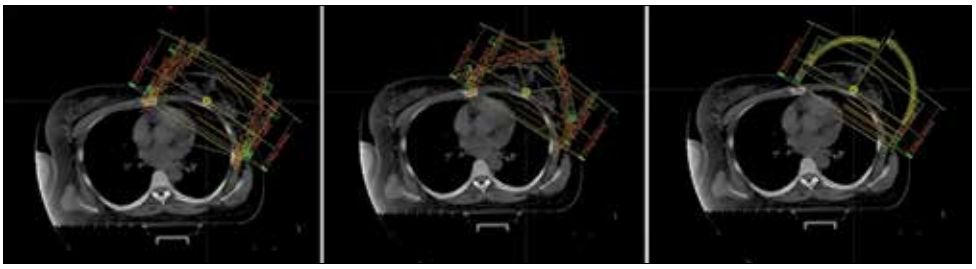

Figure 1: Beam arrangements of the three hybrid planning techniques. Left, hybrid 15°-intensity-modulated radiotherapy; Middle, hybrid 45°-intensity-modulated radiotherapy; Right, hybrid volumetric-modulated arc therapy.

3. The "hybrid VMAT plan" combined two tangential beams and two coplanar 90° arcs. The start angles of the arcs were the angles of the tangential beams, respectively. Each ran clockwise and counter-clockwise for 90° [Figure 1 Right]. The dose rate was set to 600 monitor unit (MU)/min. The collimator angles of the two arcs were set to 10° and 350°.

These treatment plans could be delivered using 6 MV photon beams commissioned for a Varian Trilogy linac (Varian Medical Systems, USA). The Linac was equipped with a 120-leaf multileaf collimator, with a maximal leaf speed of 2.5 cm/s, a maximal jaw speed of 1.5 cm/s, a maximal gantry speed of 6°/s, and a variable dose rate of up to 600 MU/min. The isocenter of all plans was placed at the center of the PTV. The IMRT plan was used by sliding window mode. For all patients, the prescribed doses of PTV and PGTV were 50.4 Gy and 60 Gy to at least 95% of the volumes in 28 fractions. In all the hybrid plans, 30% of the PTV dose was delivered by IMRT beams or arcs. Both treatment planning and optimization were performed with Eclipse version 10.0. The optimization objectives and relative priorities were the same for all plans [Table 1].[21] The dose calculation grid was set at 2.5 mm. The skin flash function was not used. All plans were created by the same radiotherapy physicist and evaluated by the same radiation oncologist.

Evaluation parameters

Dose-volume histograms (DVH) were generated for the target volumes and all OARs for dosimetric analysis. Following established conventions, the percentage of a volume that received at least *m* dose was denoted by V_m and the dose to q% of the volume by D_q. The plans were compared through three parameters: PTV dose conformity, dose homogeneity, and volume of irradiated NTs.

To evaluate the quality of the plans, the maximum dose D_{max}, V_{107}, D_{98}, D_2, the CI and the HI of the PTV were analyzed from the DVHs. The conformity index (CI) is calculated by

$$CI = \frac{V_{PTV,ref}}{V_{PTV}} \times \frac{V_{PTV,ref}}{V_{ref}} \quad (1)$$

where $V_{PTV, ref}$ refers to a volume of the PTV covered by the prescribed dose, V_{PTV} refers to the volume of the contoured PTV, and V_{ref} refers to the volume covered by the prescribed dose. For good PTV coverage, a CI approaching unity is desired. The HI is calculated by

$$HI = \frac{D_2 - D_{98}}{D_{50}} \quad (2)$$

The lower the HI value, the higher the dose homogeneity within the PTV.[25]

Table 1: Plan optimization objectives and dose constraints for all hybrid plans

Structures	Criteria	Dose limit
PGTV	D_{95}	≥60 Gy
	D_{max}	<107%
PTV	D_{95}	≥50.4 Gy
	D_{max}	<107%
Contralateral breast	D_{max}	10 Gy
	V_5	<5%
	V_{10}	<0.5%
Contralateral lung	V_5	<20%
	V_{10}	<0.5%
Ipsilateral lung	V_5	<45%
	V_{10}	<30%
	V_{20}	<15%
Heart	V_5	<60%
	V_{10}	<30%
	V_{30}	<2.5%
Left ventricle	V_{25}	<5%
	V_{30}	<2.5%

PGTV: Planning gross tumor volume, PTV: Planning target volume

The following dosimetric parameters were compared for the NTs: contralateral breast (D_2, D_{mean}, V_5, V_{10}), contralateral lung (D_2, D_{mean}, V_5, V_{10}), ipsilateral lung (D_2, D_{mean}, V_5, V_{10}, V_{20}, V_{30}, V_{40}), heart (D_2, D_{mean}, V_5, V_{25}, V_{30}), left ventricle (D_2, D_{mean}, V_{25}, V_{30}), and NT (D_2, D_{mean}, V_5, $V_{50.4}$). The beam-on time and total MUs per fraction were recorded.

Statistical analysis

All statistical computations were performed using the IBM SPSS statistical package (version 21; SPSS Inc., Chicago, IL, USA). All data in the text, tables, and figures are presented as the mean ± standard deviation as appropriate. Statistical significance was detected using the paired *t*-test after checking for normal distribution (Kolmogorov–Smirnov test).

The Wilcoxon rank sum test was used for values that were not distributed normally. A two-tailed $P < 0.05$ was considered statistically significant.

Results

Patient characteristics are listed in Table 2. All the hybrid plans achieved the dosimetric requirements for the target volumes [Table 1]. The dose constraints of NTs were satisfied. The mean volumes of PGTV and PTV were 46.8 ± 17.0 cc and 767.7 ± 159.2 cc, respectively. Examples of isodose distributions are shown in Figure 2.

The three types of hybrid plans were different in PTV dose coverage [Table 3]. The D_{98} of the PTV in the hybrid 45°-IMRT plans was the highest ($P < 0.001$). The D_{50} of the PTV in the hybrid 15°-IMRT plans was the highest. The HI of the PTV in the hybrid 45°-IMRT plans was the lowest but was not significantly different between the hybrid 15°-IMRT plans and the hybrid VMAT plans. The CI of the PTV in the hybrid 45°-IMRT plans was the highest but not significantly different from the hybrid VMAT plans ($P = 0.613$). The D_{98} of the PGTV in the hybrid 15°-IMRT plans was the highest but was not significantly different in the other two types of plans. The HI of the PGTV in the hybrid 45°-IMRT plans was the lowest but not significantly different from the hybrid 15°-IMRT plans. The CI of the PGTV in the hybrid VMAT plans was the highest ($P < 0.001$). The differences in other parameters were not statistically significant in the three hybrid plans.

The three hybrid plans were different in their OAR dosimetric parameters [Table 4]. The D_{mean}, $V_{5,}$ and D_2 of the contralateral breast and the contralateral lung in the hybrid 15°-IMRT plans were the lowest, but the difference in V_{10} was not statistically significant in the three hybrid plans. The D_2 of the ipsilateral lung in the hybrid 45°-IMRT plans was lowest, but not significantly different from that of the hybrid VMAT plans. The D_{mean}, V_5, V_{10}, V_{20}, V_{30}, and V_{40} of the ipsilateral lung were not statistically significantly different in the three hybrid plans. The V_5 of the heart in the hybrid VMAT plans was lower ($P < 0.015$) than that of the hybrid 45°-IMRT plans. The D_2, D_{mean}, V_{25}, and V_{30} of the heart were not statistically significantly different between the three hybrid plans. The D_2 of the left ventricle in the hybrid VMAT plans was the lowest, but the differences in D_{mean}, V_{25}, and V_{30} were not statistically significant. The D_2 and $V_{50.4}$ of NTs in the hybrid VMAT plan were the lowest in the three hybrid plans. The D_{mean} and V_5 of NT in the hybrid 15°-IMRT plans were the lowest, but the difference was not significant between the other two plans.

By comparison, in the 3D-CRT plans for the same patients, the HI of the PTV and PGTV was 0.30 ± 0.04 and 0.17 ± 0.08; the CI of the PTV and PGTV was 0.54 ± 0.10 and 0.56 ± 0.06, respectively. These parameters were poorer than their counterparts in the hybrid plans [Table 3].

As to the beam-on time and total MUs, there was a significant difference between the hybrid VAMT plans and the other two plans [Table 5]. The beam-on time and total MUs of the hybrid VMAT plans were the least in the three hybrid plans.

Table 2: Patient characteristics (staged according to the Union for International Cancer Control)

Patient	Age (year)	Disease stage	GTV (cc)	CTV (cc)
1	44	I	13.9	579.0
2	38	I	9.2	495.2
3	41	I	18.2	442.8
4	41	I	72.0	601.2
5	38	I	13.7	385.9
6	44	I	26.2	571.2
7	34	I	21.7	848.5
8	46	I	3.4	548.0
9	39	I	23.1	611.2

GTV: Gross tumor volume, CTV: Clinical target volume

Discussion

The VMAT technique has been used in postoperative radiotherapy for early-stage breast cancer after breast-conserving surgery; however, we believe it is for the first time that a hybrid VMAT technique is used in such treatment. The rationale of using two coplanar 90° arcs in the hybrid VMAT technology is as follows: (1) In the VMAT plan, two arcs are needed to optimize dose distribution when dealing with a complex target;[26] (2) the target is an arc that was nearly 90° along the chest wall, and the 90° arc in tangential direction enters the target without irradiating much of the lung. A hybrid VMAT plan achieves better dose conformality than a 3D-CRT plan, in the meantime reduces radiation dose to NTs than a pure VMAT plan.[27] An additional advantage of using hybrid VMAT plan is a shorter radiotherapy course due to the SIB.

In regard to the HI and CI, Mayo *et al*.[19] found that improvement in the uniformity and conformality of target dose may be achieved by the hybrid IMRT plan of two 3D-conformal

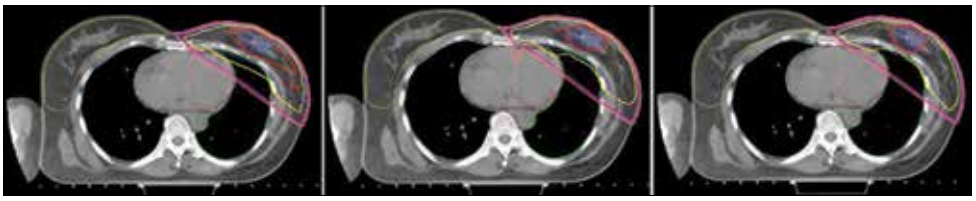

Figure 2: Dose distributions of the hybrid 15°-intensity-modulated radiotherapy (left), the hybrid 45°-intensity-modulated radiotherapy (middle) and the hybrid volumetric-modulated arc therapy (right) plans for the same patient. The isodose lines represent 50.4 Gy (yellow), 60 Gy (red), 30 Gy (magenta), and 20 Gy (pink).

Table 3: Comparison of the planning target volume dosimetric parameters among the three hybrid plans

Structures	Dosimetric parameters	Hybrid			P^a	P^b	P^c
		15°-IMRT	45°-IMRT	VMAT			
PTV	D_{max} (Gy)	65.2±1.3	64.8±1.1	65.1±1.2	0.574	0.855	0.703
	D_2 (Gy)	62.6±0.9	62.0±0.5	62.6±1.0	0.156	0.912	0.128
	D_{98} (Gy)	48.7±0.4	49.9±0.4	49.1±0.4	<0.001	0.058	<0.001
	D_{95} (Gy)	50.4±0.3	50.8±0.3	50.6±0.3	0.002	0.485	0.013
	D_{50} (Gy)	56.5±4.0	53.5±0.4	54.0±0.7	0.014	0.033	0.702
	HI	0.27±0.02	0.23±0.01	0.26±0.02	<0.001	0.404	0.001
	CI	0.70±0.05	0.79±0.03	0.76±0.06	<0.001	<0.001	0.613
PGTV	D_{max} (Gy)	64.7±1.1	63.9±0.9	64.8±1.0	0.09	0.859	0.063
	V_{107} (%)	2.36±4.4	0.14±0.32	3.28±7.7	0.367	0.707	0.206
	D_2 (Gy)	63.5±1.1	62.7±0.6	63.8±1.0	0.072	0.381	0.011
	D_{98} (Gy)	60.0±0.6	59.8±0.3	59.8±0.5	0.126	0.007	0.191
	D_{95} (Gy)	60.6±0.6	60.3±0.2	60.4±0.4	0.087	0.015	0.413
	D_{50} (Gy)	62.6±1.8	61.8±0.4	62.4±0.5	0.118	0.712	0.223
	HI	0.06±0.01	0.05±0.01	0.07±0.02	0.252	0.023	0.001
	CI	0.52±0.1	0.69±0.11	0.74±0.03	<0.001	<0.001	0.173

[a]The hybrid 15°-IMRT versus the hybrid 45°-IMRT, [b]The hybrid 15°-IMRT versus the hybrid VMAT, [c]The hybrid 45°-IMRT versus the hybrid VMAT. CI: Conformity index, HI: Heterogeneity index, IMRT: Intensity-modulated radiotherapy, VMAT: Volumetric-modulated arc therapy, PTV: Planning target volume, PGTV: Planning gross tumor volume

Table 4: Comparison of the organs at risk dosimetric parameters for the three hybrid plans

Structures	Dosimetric parameters	Hybrid			P^a	P^b	P^c
		15°-IMRT	45°-IMRT	VMAT			
Contralateral breast	D_{mean} (Gy)	1.09±0.77	1.99±0.62	2.38±0.84	0.007	<0.001	0.125
	D_2 (Gy)	4.81±1.99	6.43±1.53	7.01±1.43	0.051	0.010	0.464
	V_5 (%)	2.60±2.92	5.65±3.20	7.60±4.34	0.081	0.006	0.253
	V_{10} (%)	0.28±0.49	0.33±0.38	0.45±0.56	0.813	0.466	0.620
Contralateral lung	D_{mean} (Gy)	0.59±0.80	1.32±0.33	1.96±0.87	0.040	<0.001	0.066
	D_2 (Gy)	2.47±2.06	4.02±0.88	5.90±2.13	0.078	<0.001	0.035
	V_5 (%)	1.10±3.07	0.79±0.62	5.71±4.63	0.840	0.006	0.004
	V_{10} (%)	0.06±0.17	0.03±0.09	0.26±0.43	0.835	0.125	0.084
Ipsilateral lung	D_{mean} (Gy)	14.13±1.93	14.41±1.84	13.81±2.42	0.781	0.784	0.550
	D_2 (Gy)	53.06±2.30	49.89±2.08	50.33±2.50	0.004	0.012	0.660
	V_5 (%)	49.97±6.68	56.61±8.86	49.31±11.25	0.136	0.879	0.103
	V_{10} (%)	34.84±5.47	35.01±5.24	33.56±7.01	0.954	0.651	0.610
	V_{20} (%)	25.74±3.51	25.55±3.59	25.49±3.89	0.971	0.886	0.969
	V_{30} (%)	22.10±3.21	21.92±3.20	21.95±3.68	0.908	0.925	0.983
	V_{40} (%)	15.34±2.68	14.63±2.69	14.48±4.13	0.646	0.580	0.925
Heart	D_{mean} (Gy)	8.00±2.61	9.58±2.14	7.81±1.60	0.146	0.849	0.104
	D_2 (Gy)	48.37±3.72	45.48±2.82	45.99±2.79	0.062	0.120	0.734
	V_5 (%)	36.11±13.28	52.70±12.09	36.57±13.69	0.013	0.941	0.015
	V_{25} (%)	9.97±4.65	9.70±4.31	9.44±4.25	0.900	0.801	0.899
	V_{30} (%)	8.95±4.41	8.38±4.19	8.48±3.92	0.773	0.815	0.956
Left ventricle	D_{mean} (Gy)	13.64±3.63	13.03±2.32	11.65±2.09	0.650	0.140	0.297
	D_2 (Gy)	52.20±2.74	47.14±2.17	46.60±2.84	<0.001	<0.001	0.664
	V_{25} (%)	19.39±6.53	18.75±6.12	18.71±5.70	0.828	0.816	0.988
	V_{30} (%)	17.48±6.12	17.02±5.84	16.93±5.32	0.868	0.842	0.973
NT	D_{mean} (Gy)	2.61±0.35	3.23±0.39	3.20±0.52	0.005	0.007	0.909
	D_2 (Gy)	38.70±2.66	38.39±2.66	38.25±2.92	0.816	0.733	0.914
	V_5 (%)	9.71±1.50	12.82±2.06	13.03±2.36	0.003	0.002	0.833
	$V_{50.4}$ (%)	0.51±0.22	0.21±0.09	0.13±0.13	<0.001	<0.001	0.329

[a]Hybrid 15°-IMRT versus hybrid 45°-IMRT, [b]Hybrid 15°-IMRT versus hybrid VMAT, [c]Hybrid 45°-IMRT versus hybrid VMAT. NT: Normal tissue, IMRT: Intensity-modulated radiotherapy, VMAT: Volumetric-modulated arc therapy

Table 5: Comparison of monitor units and beam-on time for the three planning techniques

Parameters	Hybrid			P^a	P^b	P^c
	15°-IMRT	45°-IMRT	VMAT			
MUs	738±105	756±90	349±63	0.658	<0.001	<0.001
Beam-on time	1.84±0.26	1.74±0.50	1.01±0.054	0.515	<0.001	<0.001

[a]Hybrid 15°-IMRT versus hybrid 45°-IMRT, [b]Hybrid 15°-IMRT versus hybrid VMAT, [c]Hybrid 45°-IMRT versus hybrid VMAT. MUs: Monitor units, IMRT: Intensity-modulated radiotherapy, VMAT: Volumetric-modulated arc therapy

beams and four IMRT beams. However, the comparison between the hybrid VMAT plan and the hybrid IMRT plan has rarely been reported. In our study, the dosimetric parameters of the hybrid VMAT plans are generally close to those of the hybrid IMRT plans. It is worth noting that the CI of the hybrid VMAT plans is significantly higher than that of the hybrid IMRT plans. This fact suggests that hybrid VMAT plans might be more suitable for whole-breast irradiation with SIB than are hybrid IMRT plans.

In breast radiotherapy, the lung is the primary and critical organ of concern. The D_{mean}, V_5, and V_{20} are good predictors for radiation-induced lung toxicity.[28,29] However, if the V_{20} of the ipsilateral lung was <30% for breast cancer patients, clinically significant pneumonitis should be rare.[30] It has been also reported that the expected complication rate is 20% if more than 50% of the lung volume receives 10 Gy.[31] In our study, the V_5 and V_{10} of the contralateral lung are 5.71% and 0.26% in the hybrid VMAT plan; the D_2 of the ipsilateral lung in the hybrid VMAT plan was not significant compared with the hybrid 45°-IMRT plan; and the V_{10} and V_{20} of the ipsilateral lung in the hybrid VMAT plan were lowest (33.56% and 25.49%, respectively). Thus, lung toxicity associated with the hybrid VMAT plans should be reasonably low.

The heart is the most important organ to protect during left breast radiation therapy. In our study, the D_{mean} of the heart was the lowest (7.81 ± 1.60 Gy) in the hybrid VMAT plans, much less than the 12.2 ± 1.8 Gy reported by Goddu *et al*.[32] for tomotherapy, and 8.7–21.1 Gy for the IMRT cases reported by Fogliata *et al*.[33] Radiation-induced injuries of the heart appear mainly in the coronary arteries and connective tissues.[34,35] In our study, the D_2 of the left ventricle in the hybrid VMAT plan was reduced by 6% ($P < 0.001$) compared with the hybrid 15°-IMRT plan. The dosimetric parameters of the heart in the hybrid VMAT plan overall were moderately better than those of the hybrid IMRT plans, demonstrating that hybrid VMAT plans are also safer for the heart.

For patients enrolled in the present study, the mean radiation doses to the ipsilateral lung, and the heart in 3D-CRT plans were 10.95 ± 1.93 Gy and 5.86 ± 1.90 Gy, respectively. These values were moderately lower than that in the hybrid IMRT or VMAT plans [Table 4]. The 3D-CRT plans included boost dose from electron beams. These data confirmed that using tangential beams in the hybrid plans could take advantage of the low NT doses in 3D-CRT plans.

The dose to the contralateral breast is another critical factor to consider, especially for younger patients. Stovall *et al*.[36] found an elevated long-term risk of developing secondary contralateral breast cancer, with the D_{mean} of 3.2 Gy to the contralateral breast with RapidArc. In our study, although the D_{mean} of the contralateral breast in the hybrid VMAT plans was higher than the other hybrid plans, the value (2.38 ± 0.84 Gy) was shown to be <4.3 ± 0.7 Gy reported by Goddu *et al*.[32] and 2.82 Gy by Boice *et al*.[37]

More monitor units and extended therapy lead to higher doses to outfield NTs from leakage and scattered radiation, which in turn are likely to increase the incidence of radiation-induced malignancy. Hall and Wuu[38] evaluated the secondary neoplasia rate after 10 years and found that the rate of radiation-induced malignancy was 1% in 3D-CRT and increased to 1.75% in IMRT. Kry *et al*.[39] demonstrated that compared with 3D-CRT, IMRT plans had an increased MU and varied dose distribution and that this difference would double the incidence of secondary solid tumors. In our study, the hybrid VMAT plans using two coplanar 90° arcs resulted in a much lower beam-on time and MUs ($P < 0.001$) than the hybrid IMRT plans.

The effects of respiratory motion should be addressed for patients for whom breath control is not utilized. The interplay of respiratory motions and dose delivery will cause deviations from the planned dose distributions, which are more pronounced for IMRT or VMAT techniques.[40] To reduce interplay effects or setup uncertainties, sufficient target expansion margin and daily image guidance maybe considered for patients who are treated with the hybrid plans investigated in this manuscript.

Conclusions

Overall, our results show that the hybrid VMAT technique is feasible for adjuvant irradiation with SIB for left sided, early-stage breast cancer. Hybrid VMAT plans are especially superior to the hybrid IMRT plans with regard to heart dose and treatment delivery time.

Acknowledgments

The authors would like to thank Dr. Adrian Koesters, Research Editor at University of Nebraska Medical Center, for her editorial contribution.

Financial support and sponsorship

Nil.

Conflicts of interest

There are no conflicts of interest.

References

1. Byers T, Wender RC, Jemal A, Baskies AM, Ward EE, Brawley OW. The American Cancer Society challenge goal to reduce US cancer mortality by 50% between 1990 and 2015: Results and reflections. CA Cancer J Clin 2016;66:359-69.
2. Fisher B, Anderson S, Redmond CK, Wolmark N, Wickerham DL, Cronin WM. Reanalysis and results after 12 years of follow-up in a randomized clinical trial comparing total mastectomy with lumpectomy with or without irradiation in the treatment of breast cancer. N Engl J Med 1995;333:1456-61.
3. Fisher B, Anderson S, Bryant J, Margolese RG, Deutsch M, Fisher ER, *et al.* Twenty-year follow-up of a randomized trial comparing total mastectomy, lumpectomy, and lumpectomy plus irradiation for the treatment of invasive breast cancer. N Engl J Med 2002;347:1233-41.
4. Early Breast Cancer Trialists' Collaborative Group (EBCTCG), Darby S, McGale P, Correa C, Taylor C, Arriagada R, *et al.* Effect of radiotherapy after breast-conserving surgery on 10-year recurrence and 15-year breast cancer death: Meta-analysis of individual patient data for 10,801 women in 17 randomised trials. Lancet 2011;378:1707-16.
5. Clarke M, Collins R, Darby S, Davies C, Elphinstone P, Evans V, *et al.* Effects of radiotherapy and of differences in the extent of surgery for early breast cancer on local recurrence and 15-year survival: An overview of the randomised trials. Lancet 2005;366:2087-106.
6. Vinh-Hung V, Verschraegen C. Breast-conserving surgery with or without radiotherapy: Pooled-analysis for risks of ipsilateral breast tumor recurrence and mortality. J Natl Cancer Inst 2004;96:115-21.
7. Favourable and unfavourable effects on long-term survival of radiotherapy for early breast cancer: An overview of the randomised trials. Early Breast Cancer Trialists' Collaborative Group. Lancet 2000;355:1757-70.
8. Buchholz TA, Gurgoze E, Bice WS, Prestidge BR. Dosimetric analysis of intact breast irradiation in off-axis planes. Int J Radiat Oncol Biol Phys 1997;39:261-7.
9. Kestin LL, Sharpe MB, Frazier RC, Vicini FA, Yan D, Matter RC, *et al.* Intensity modulation to improve dose uniformity with tangential breast radiotherapy: Initial clinical experience. Int J Radiat Oncol Biol Phys 2000;48:1559-68.
10. Dogan N, Cuttino L, Lloyd R, Bump EA, Arthur DW. Optimized dose coverage of regional lymph nodes in breast cancer: The role of intensity-modulated radiotherapy. Int J Radiat Oncol Biol Phys 2007;68:1238-50.
11. Beckham WA, Popescu CC, Patenaude VV, Wai ES, Olivotto IA. Is multibeam IMRT better than standard treatment for patients with left-sided breast cancer? Int J Radiat Oncol Biol Phys 2007;69:918-24.
12. Zhao LR, Zhou YB, Sun JG. Comparison of plan optimization for single and dual volumetric-modulated arc therapy versus intensity-modulated radiation therapy during post-mastectomy regional irradiation. Oncol Lett 2016;11:3389-94.
13. Popescu CC, Olivotto IA, Beckham WA, Ansbacher W, Zavgorodni S, Shaffer R, *et al.* Volumetric modulated arc therapy improves dosimetry and reduces treatment time compared to conventional intensity-modulated radiotherapy for locoregional radiotherapy of left-sided breast cancer and internal mammary nodes. Int J Radiat Oncol Biol Phys 2010;76:287-95.
14. Nicolini G, Clivio A, Fogliata A, Vanetti E, Cozzi L. Simultaneous integrated boost radiotherapy for bilateral breast: A treatment planning and dosimetric comparison for volumetric modulated arc and fixed field intensity modulated therapy. Radiat Oncol 2009;4:27.
15. Jin GH, Chen LX, Deng XW, Liu XW, Huang Y, Huang XB. A comparative dosimetric study for treating left-sided breast cancer for small breast size using five different radiotherapy techniques: Conventional tangential field, filed-in-filed, tangential-IMRT, multi-beam IMRT and VMAT. Radiat Oncol 2013;8:89.
16. Badakhshi H, Kaul D, Nadobny J, Wille B, Sehouli J, Budach V. Image-guided volumetric modulated arc therapy for breast cancer: A feasibility study and plan comparison with three-dimensional conformal and intensity-modulated radiotherapy. Br J Radiol 2013;86:20130515.
17. Jöst V, Kretschmer M, Sabatino M, Würschmidt F, Dahle J, Ueberle F, *et al.* Heart dose reduction in breast cancer treatment with simultaneous integrated boost: Comparison of treatment planning and dosimetry for a novel hybrid technique and 3D-CRT. Strahlenther Onkol 2015;191:734-41.
18. Lin JF, Yeh DC, Yeh HL, Chang CF, Lin JC. Dosimetric comparison of hybrid volumetric-modulated arc therapy, volumetric-modulated arc therapy, and intensity-modulated radiation therapy for left-sided early breast cancer. Med Dosim 2015;40:262-7.
19. Mayo CS, Urie MM, Fitzgerald TJ. Hybrid IMRT plans – Concurrently treating conventional and IMRT beams for improved breast irradiation and reduced planning time. Int J Radiat Oncol Biol Phys 2005;61:922-32.
20. White J, Tai A, Arthur D, Buchholz T, MacDonald S, Marks L, *et al.* RTOG Breast Cancer Atlas for Radiation Therapy Planning: Consensus Definitions. Available from: https://www.rtog.org/CoreLab/ContouringAtlases/BreastCancerAtlas.aspx. [Last accessed on 2016 Aug 30].
21. Tsai PF, Lin SM, Lee SH, Yeh CY, Huang YT, Lee CC, *et al.* The feasibility study of using multiple partial volumetric-modulated arcs therapy in early stage left-sided breast cancer patients. J Appl Clin Med Phys 2012;13:3806.
22. Donovan E, Bleakley N, Denholm E, Evans P, Gothard L, Hanson J, *et al.* Randomised trial of standard 2D radiotherapy (RT) versus intensity modulated radiotherapy (IMRT) in patients prescribed breast radiotherapy. Radiother Oncol 2007;82:254-64.
23. Pignol JP, Olivotto I, Rakovitch E, Gardner S, Sixel K, Beckham W, *et al.* A multicenter randomized trial of breast intensity-modulated radiation therapy to reduce acute radiation dermatitis. J Clin Oncol 2008;26:2085-92.
24. Selvaraj RN, Beriwal S, Pourarian RJ, Lalonde RJ, Chen A, Mehta K, *et al.* Clinical implementation of tangential field intensity modulated radiation therapy (IMRT) using sliding window technique and dosimetric comparison with 3D conformal therapy (3DCRT) in breast cancer. Med Dosim 2007;32:299-304.
25. Wu Q, Mohan R, Morris M, Lauve A, Schmidt-Ullrich R. Simultaneous integrated boost intensity-modulated radiotherapy for locally advanced head-and-neck squamous cell carcinomas. I: Dosimetric results. Int J Radiat Oncol Biol Phys 2003;56:573-85.
26. Guckenberger M, Richter A, Krieger T, Wilbert J, Baier K, Flentje M. Is a single arc sufficient in volumetric-modulated arc therapy (VMAT) for complex-shaped target volumes? Radiother Oncol 2009;93:259-65.
27. Jiang QF, Bai S, Fu YC, Li GJ, Zhang H, Ai P, *et al*. Feasibility of volumetric modulated arc therapy applied to breast cancer radiotherapy after radical surgery. J North Sichuan Med Coll 2012;27:102-8.
28. Kimura T, Togami T, Takashima H, Nishiyama Y, Ohkawa M, Nagata Y. Radiation pneumonitis in patients with lung and mediastinal tumours: A retrospective study of risk factors focused on pulmonary emphysema. Br J Radiol 2012;85:135-41.
29. Wang S, Liao Z, Wei X, Liu HH, Tucker SL, Hu CS, *et al.* Analysis of clinical and dosimetric factors associated with treatment-related pneumonitis (TRP) in patients with non-small-cell lung cancer (NSCLC) treated with concurrent chemotherapy and three-dimensional conformal radiotherapy (3D-CRT). Int J Radiat Oncol Biol Phys 2006;66:1399-407.
30. Blom Goldman U, Wennberg B, Svane G, Bylund H, Lind P. Reduction of radiation pneumonitis by V20-constraints in breast cancer. Radiat Oncol 2010;5:99.
31. Yorke ED, Jackson A, Rosenzweig KE, Braban L, Leibel SA, Ling CC. Correlation of dosimetric factors and radiation pneumonitis for non-small-cell lung cancer patients in a recently completed dose escalation study. Int J Radiat Oncol Biol Phys 2005;63:672-82.
32. Goddu SM, Chaudhari S, Mamalui-Hunter M, Pechenaya OL, Pratt D, Mutic S, *et al.* Helical tomotherapy planning for left-sided breast cancer patients with positive lymph nodes: Comparison to conventional multiport breast technique. Int J Radiat Oncol Biol Phys 2009;73:1243-51.
33. Fogliata A, Nicolini G, Alber M, Asell M, Dobler B, El-Haddad M, *et al*. IMRT for breast. A planning study. Radiot Oncol 2005;76:300-10.
34. Giordano SH, Kuo YF, Freeman JL, Buchholz TA, Hortobagyi GN,

Goodwin JS. Risk of cardiac death after adjuvant radiotherapy for breast cancer. J Natl Cancer Inst 2005;97:419-24.
35. Yu X, Zhou S, Prosnitz RG, Kahn D, Hardenbergh PH, Hollis D, *et al*. Persistence of radiation (RT)-induced cardiac dysfunction 3-5 years post RT. Int J Radiat Oncol Biol Phys 2004;60:S390-1.
36. Stovall M, Smith SA, Langholz BM, Boice JD Jr., Shore RE, Andersson M, *et al.* Dose to the contralateral breast from radiotherapy and risk of second primary breast cancer in the WECARE study. Int J Radiat Oncol Biol Phys 2008;72:1021-30.
37. Boice JD Jr., Harvey EB, Blettner M, Stovall M, Flannery JT. Cancer in the contralateral breast after radiotherapy for breast cancer. N Engl J Med 1992;326:781-5.
38. Hall EJ, Wuu CS. Radiation-induced second cancers: The impact of 3D-CRT and IMRT. Int J Radiat Oncol Biol Phys 2003;56:83-8.
39. Kry SF, Salehpour M, Followill DS, Stovall M, Kuban DA, White RA, *et al.* The calculated risk of fatal secondary malignancies from intensity-modulated radiation therapy. Int J Radiat Oncol Biol Phys 2005;62:1195-203.
40. Zhou S, Zhu X, Zhang M, Zheng D, Lei Y, Li S, *et al.* Estimation of internal organ motion-induced variance in radiation dose in non-gated radiotherapy. Phys Med Biol 2016;61:8157-79.

Original Article

Measurement of Total Scatter Factor for Stereotactic Cones with Plastic Scintillation Detector

Suresh H Chaudhari, Rishabh Dobhal[1], Rajesh A. Kinhikar[2], Sudarshan S. Kadam[2], Deepak D. Deshpande[2]

Department of Radiation Oncology, Apollo Hospitals, Navi Mumbai, Maharashtra, [1]Department of Radiation Oncology, Batra Hospital and Medical Research Centre, New Delhi, [2]Department of Medical Physics, Tata Memorial Hospital, Mumbai, Maharashtra, India

Abstract

Advanced radiotherapy modalities such as stereotactic radiosurgery (SRS) and image-guided radiotherapy may employ very small beam apertures for accurate localized high dose to target. Accurate measurement of small radiation fields is a well-known challenge for many dosimeters. The purpose of this study was to measure total scatter factors for stereotactic cones with plastic scintillation detector and its comparison against diode detector and theoretical estimates. Measurements were performed on Novalis Tx™ linear accelerator for 6MV SRS beam with stereotactic cones of diameter 6 mm, 7.5 mm, 10 mm, 12.5 mm, and 15 mm. The advantage of plastic scintillator detector is in its energy dependence. The total scatter factor was measured in water at the depth of dose maximum. Total scatter factor with plastic scintillation detector was determined by normalizing the readings to field size of 10 cm × 10 cm. To overcome energy dependence of diode detector for the determination of scatter factor with diode detector, daisy chaining method was used. The plastic scintillator detector was calibrated against the ionization chamber, and the reproducibility in the measured doses was found to be within ± 1%. Total scatter factor measured with plastic scintillation detector was 0.728 ± 0.3, 0.783 ± 0.05, 0.866 ± 0.55, 0.885 ± 0.5, and 0.910 ± 0.06 for cone sizes of 6 mm, 7.5 mm, 10 mm, 12.5 mm, and 15 mm, respectively. Total scatter factor measured with diode detector was 0.733 ± 0.03, 0.782 ± 0.02, 0.834 ± 0.07, 0.854 ± 0.02, and 0.872 ± 0.02 for cone sizes of 6 mm, 7.5 mm, 10 mm, 12.5 mm, and 15 mm, respectively. The variation in the measurement of total scatter factor with published Monte Carlo data was found to be −1.3%, 1.9%, −0.4%, and 0.4% for cone sizes of 7.5 mm, 10 mm, 12.5 mm, and 15 mm, respectively. We conclude that total scatter factor measurements for stereotactic cones can be adequately carried out with a plastic scintillation detector. Our results show a high level of consistency within our data and compared well with published data.

Keywords: Plastic scintillator, small field dosimetry, total scatter factor

Received on: 24-10-2016 **Review completed on: 05-02-2017** **Accepted on: 06-02-2017**

Introduction

Advanced radiotherapy modalities such as stereotactic radiosurgery (SRS), intensity modulated radiotherapy (IMRT) and volumetric modulated arc therapy (VMAT) may employ very small beam apertures for accurate localized high dose to target. A small photon field is generally defined as the one having dimensions smaller than the lateral range of the charged particles that contribute to the dose deposited at a point along the central axis of the beam.[1,2]

Nonstandard fields are either made of small fields or whenever nonequilibrium conditions exist; this occurs, for example, when the size of the penumbra is similar to the field size.[3] According to these criteria, field sizes of <3 cm × 3 cm are considered to be small for 6 MV photon beam. For these fields, dosimetric errors may be larger than that in conventional beams as the reference conditions recommended by conventional codes of practice[4] cannot be established and the measurement of absorbed dose to water in composite fields is not standardized.[5]

Accurate measurement of small radiation fields is a well-known challenge for many dosimeters. Lack of lateral charged-particle equilibrium, dose averaging within the sensitive volume of dosimeters, and differences between the composition of detectors and their surrounding media all cause perturbations of the radiation field. Thus, discrepancies are seen between the measured dose and the actual dose that would be deposited in the medium in the absence of a detector. The use of small fields is becoming popular in radiation therapy and may be a source of

Address for correspondence: Mr. Suresh H. Chaudhari, Department of Radiation Oncology, Apollo Hospitals, Navi Mumbai - 400 614, Maharashtra, India.
E-mail: chaudhari_suresh@yahoo.com

Access this article online

Quick Response Code:

Website: www.jmp.org.in

DOI: 10.4103/jmp.JMP_114_16

How to cite this article: Chaudhari SH, Dhobal R, Kinhikar RA, Kadam SS, Deshpande DD. Measurement of total scatter factor for stereotactic cones with plastic scintillation detector. J Med Phys 2017;42:XX-XX.

errors if measurements are not conducted properly. Discrepancies have been observed between doses calculated by treatment planning systems and actual dose measurements which can be attributed to the presence of small fields.

An important issue of the dosimetry in small field is the size of detector. The construction can significantly perturb the fluence, and the major cause of error in the measurement is due to the volume of the detector. Every detector averages the dose over its volume and this volume averaging[6,7] may underestimate dose in the center of a small field. To overcome volume averaging effect, the most straightforward and logical method is to employ a detector with a small active volume and high spatial resolution. Detectors in this category include microchambers, diodes, scintillation detector, diamond detectors, gel dosimeters, and radiographic/radiochromic film.

The use of unshielded diodes has been shown to be most promising. Diodes partially solve the detector volume averaging issue. However, because of the small electron range in common diode material (such as silicon), they still represent intermediate-sized cavities for typical SRS fields. In addition, they introduce new issues that are associated with the energy, dose rate, and directional dependence of their responses. For small fields, the measurements of scatter factors are subject to many uncertainties that in turn may lead to significant errors in dose calculations. The difficulties in the accurate measurements of total scatter factor can be traced to three "equilibrium factors:" (a) The size of the detector used in the measurements, (b) the lateral electronic equilibrium in the irradiated medium and detector material, and (c) the partial occlusion of the viewable part of the X-ray source (focal spot on the target). Since there is no single detector that obeys all the three equilibrium conditions simultaneously under small and reference field conditions, different detectors, such as diode for small fields and ion chamber for reference field, should be used.[8]

The purpose of this study was to measure total scatter factors for stereotactic cones with plastic scintillation detector and its comparison against diode detector and theoretical estimates.

Materials and Methods

Detector specifications

Plastic scintillator detector

The Extradin W1 plastic scintillator detector (Standard Imaging, USA) employs a 1 mm diameter × 3 mm length polystyrene-based scintillating fiber coupled to a 3 m long poly methyl methacrylate-based optical fiber. The radiation-induced light signals from scintillator and fiber are chromatically separated into a blue and a green component and converted into charge signals by a dual-channel photodiode enclosure attached to the distal end of the optical fiber. The photodiode signals are transmitted to an electrometer located outside the treatment bunker. In this study, the signals from the photodiodes were read using the SUPERMAX electrometer (Standard Imaging, USA), which employs software dedicated to dose measurements using the Extradin W1 scintillator detector.[9] The characteristics of the scintillator can be found elsewhere.[10]

Diode detector

The EDGE Diode detector (Sun Nuclear Corporation, USA) is a waterproof dosimeter with a design that nearly eliminates the convolution of high-dose gradient regions during profile and depth measurements. It is intended for the measurement of fields as small as 5 mm. The Edge Detector diode has an active volume of 0.8 mm × 0.8 mm × 0.03 mm (0.019 mm^3). The intended field size for Edge Detector is 0.5 cm × 0.5 cm –10 cm × 10 cm. Compared to ion chambers, EDGE Detector gives approximately 100 times more signal even though it is over 6000 times smaller in volume.

Experimental setup

Measurements were performed on Novalis Tx™ linear accelerator (Varian Medical Systems, Palo Alto) for 6 MV SRS beam with stereotactic cones (Brainlab AG, Germany) of diameter 6 mm, 7.5 mm, 10 mm, 12.5 mm, and 15 mm. The jaw settings used for all the cones were 2 cm × 2 cm as per the recommendation of manufacturer. Total scatter factor was measured in three-dimensional Scanner Radiation Field Analyzer (Sun Nuclear Corporation, USA) of diameter 65 cm and 40 cm height and controlled by software for accurate, reproducible detector positioning [Figure 1].

Measurements were made at a depth of 1.5 cm at target to surface distance (TSD) of 100 cm with the long axis of the plastic scintillator and diode detector placed parallel to the beam axis such that the active volume was positioned at isocenter.

Calibration of plastic scintillator detector

The plastic scintillator detector directly measures dose to medium with appropriate calibration unlike diode detector which measures charge produced in medium. The calibration was performed in a 30 cm × 30 cm × 30 cm plastic water phantom slab (Standard Imaging, USA) of density 1.03 g/cm^3, at 10 cm depth at TSD of 100 cm as shown in Figure 2.

Figure 1: Experimental setup for measurement of total scatter factor.

Cross-calibration was performed against reference class ionization chamber A19 (Standard Imaging, USA) of volume 0.62 cm^3 using TRS 398 protocol[4] at reference field size of 10 cm × 10 cm. Calibration procedure recommended by the manufacturer involves a stem effect baseline correction to determine the Čerenkov light ratio (CLR) coefficient and dose-to-water calibration to determine the gain coefficient which is described elsewhere.[11]

Measurement of total scatter factors

Plastic scintillator detector

The plastic scintillation detector has energy independent response,[10] so in the calculation of total scatter factor, 10 cm × 10 cm was directly used as normalization field and there is no need of intermediate field size.

The total scatter factor of circular collimator of diameter "A" can be calculated by the following formula:

$$S_t = \frac{M\ (A, d_{ref})}{M\ (f, d_{ref})} \times k^{fclin,\ fmsr}_{Qclin,\ Qmsr} \quad (1)$$

Where, S_t is total scatter factor, M is meter reading for fixed number of monitor units, f is reference field size, and d_{ref} is depth of measurement. $k^{fclin,\ fmsr}_{Qclin,Qmsr}$ is a factor that corrects for the differences between the conditions of field size, geometry, phantom material, and beam quality of the conventional clinical field f_{clin} and the machine-specific reference field f_{msr}.[5] Q_{clin} is the beam quality of the clinical field f_{clin}.

Figure 2: Experimental setup for calibration of plastic scintillator detector (buildup is removed for clear view of detector).

But, in daisy chain method, this will be modified as follows:

$$S_t = \left[\frac{M\ (A, d_{ref})}{M\ (f_1, d_{ref})} \times k^{fclin,\ fmsr}_{Qclin,\ Qmsr}\right] \text{diode} \times \left[\frac{M\ (f_1, d_{ref})}{M\ (f_2, d_{ref})}\right] \text{IC} \quad (2)$$

Where, f_1 is intermediate field size and f_2 is reference field size.

Diode detector

Detector-specific output ratios were calculated with respect to a square jaw collimated field. For determination of scatter factor for diode detector, daisy chaining method was used.[12] The strategy involves measurement of the ratio of readings for collimator-defined fields at the reference field size and at a medium-sized field using a suitable ion chamber, then factors were measured with a diode for the medium-sized field and the cone-defined fields, and finally the diode measurements were renormalized to the reference field ion chamber measurement by applying the ratio of the two detector readings at the intermediate field. In this study, the reference field size was 10 cm × 10 cm and intermediate field size was 5 cm × 5 cm.

The accuracy of measurement of total scatter factor with plastic scintillator detector was also validated with Monte Carlo-derived theoretical estimates.[8] The Monte Carlo simulations in the referred paper were performed by EGSnrc/BEAMnrc code with the similar machine and cone geometry of the present study.

Results

The plastic scintillator detector was calibrated against the ionization chamber, and the reproducibility in the measured doses was found to be within ± 1%.

Total scatter factor measured with plastic scintillator, diode detector, and Monte Carlo estimates is summarized in Table 1. The measured values are reported at 1 σ.

$k^{fclin,\ fmsr}_{Qclin,Qmsr}$ for plastic scintillator is unity across all field sizes as its performance is demonstrated to be near ideal.[13,14] For diode detector correction factor, $k^{fclin,\ fmsr}_{Qclin,Qmsr}$ was applied from published data.[15]

Table 1: Measured total scatter factor with plastic scintillator, diode detector, and Monte Carlo estimates

Cone diameter (mm)	Diode	Plastic scintillator	Monte Carlo	Diode/plastic scintillator	Monte Carlo/plastic scintillator
6	0.733±0.03	0.728±0.3	NA	0.7	NA
7.5	0.782±0.02	0.783±0.05	0.793±0.011	−0.02	−1.3
10	0.834±0.07	0.866±0.55	0.850±0.011	3.67	1.9
12.5	0.854±0.02	0.885±0.5	0.889±0.011	3.43	−0.4
15	0.872±0.02	0.910±0.06	0.906±0.011	4.11	0.4

NA: Not available

Discussion

Dosimetry of small field is challenging, and the dosimetry protocols are still evolving. Although accelerators with stereotactic cones are routinely utilized for SRS treatment, there is no general agreement for total scatter factor.[16] A range of relative output factors are in clinical use.

Diodes exhibit dependence on dose rate and energy. High photoelectric cross-section of silicon (Z = 14) results in overresponse to low-energy scattered radiation.[17,18] Diode overresponse is most significantly affected by the field size and diode type. The overresponse can be corrected mathematically and was found to be at an average of 0.25%.[19] In our study, we have applied "daisy-chained" diode output factors to overcome the overresponse of silicon to low-energy scattered photons within large fields.

The daisy chaining method was not used for plastic scintillator as the energy dependence of CLR calibration coefficient was found to exhibit variations within 0.4%.[20]

Literature reports beam quality correction factors for absolute dosimetry accounting for the difference between the responses of an ionization chamber in the reference field and small treatment fields.[5] For Edge Diode, the literature reports $k_{Qclin,Qmsr}^{fclin,\ fmsr}$ for square fields from 0.6 cm × 0.6 cm to 2 cm. Francescon *et al*.[21] reported $k_{Qclin,Qmsr}^{fclin,\ fmsr}$ corrections of Edge Detector using Monte Carlo simulations for Primus (Siemens) and the Synergy (Elekta). They reported that Edge Detector correction factors for 5 mm, 7.5 mm, 10 mm, 12.5 mm, and 15 mm square fields are 0.933, 0.952, 0.966, 0.976, and 0.983, respectively. Qin *et al*.[15] have reported that Edge Detector correction factors for square field of 5 mm, 10 mm, 15 mm, and 20 mm are 0.97, 0.95, 0.96, and 0.96, respectively, for 6FFF beam of Varian make. We have adapted a generic $k_{Qclin,Qmsr}^{fclin,\ fmsr}$ of 0.97 to correct diode measurements.

Dosimetry in small field is investigated by several investigators for square fields defined by collimator jaws.[22-27] Wiant *et al*.[28] have reported output factors for 6 MV beam of Truebam STX (Varian) with cone diameters of 6 mm, 10 mm, 12.5 mm, and 15 mm as 0.79, 0.83, 0.871, 0.890, and 0.901, respectively. Our data are in agreement with 5.12 ± 1.75, however Wiant *et al*. have reported the output factors without accounting for $k_{Qclin,Qmsr}^{fclin,\ fmsr}$. If their data are corrected for, the data agree well within 1.97 ± 1.70.

Morales *et al*.[29] have reported a field factor for Novalis equipped with circular cones using a 6 MV SRS X-ray beam with micro Diamond (PTW 60019 microDiamond) and diode detector stereotactic filed diode, IBA). They found that, for microDiamond chamber, the field factors for 4 mm, 7.5 mm, 10 mm, and 20 mm cones are 0.644, 0.799, 0.856, and 0.929, respectively, and that for diode are 0.662, 0.798, 0.851, and 0.925, respectively.

We have used cones of various sizes and compared our results with the published work with similar machine and cone geometry. The measured data for both detectors agree within 5% of published Monte Carlo results.

Conclusion

Total scatter factor measurements for stereotactic cones can be adequately carried out with a plastic scintillation detector. Our results show a high level of consistency within our data and were compared well with the published data. Validation measurements with Sun Nuclear Edge Detector diode show acceptable dosimetric agreement.

Financial support and sponsorship

Nil.

Conflicts of interest

There are no conflicts of interest.

References

1. Das IJ, Ding GX, Ahnesjö A. Small fields: Nonequilibrium radiation dosimetry. Med Phys 2008;35:206-15.
2. Aspradakis M, Byrne J, Palmans H, Conway J, Rosser K, Warrington J, *et al*. Small Field MV Photon Dosimetry. IPEM Report No. 103. York, UK: Institute of Physics and Engineering in Medicine; 2010.
3. Charles PH, Cranmer-Sargison G, Thwaites DI, Crowe SB, Kairn T, Knight RT, *et al.* A practical and theoretical definition of very small field size for radiotherapy output factor measurements. Med Phys 2014;41:041707.
4. IAEA. Absorbed Dose Determination in External Beam Radiotherapy: An International Code of Practice for Dosimetry Based on Absorbed Dose to Water. Tech. Series No. 398. Vienna: IAEA; 2000.
5. Alfonso R, Andreo P, Capote R, Huq MS, Kilby W, Kjäll P, *et al.* A new formalism for reference dosimetry of small and nonstandard fields. Med Phys 2008;35:5179-86.
6. Laub WU, Wong T. The volume effect of detectors in the dosimetry of small fields used in IMRT. Med Phys 2003;30:341-7.
7. Bouchard H, Seuntjens J, Duane S, Kamio Y, Palmans H. Detector dose response in megavoltage small photon beams. I. Theoretical concepts. Med Phys 2015;42:6033-47.
8. Khelashvili G, Chu J, Diaz A, Turian J. Dosimetric characteristics of the small diameter brainLab™ cones used for stereotactic radiosurgery. J Appl Clin Med Phys 2012;13:3610.
9. Therriault-Proulx F, Briere TM, Mourtada F, Aubin S, Beddar S, Beaulieu L. A phantom study of an *in vivo* dosimetry system using plastic scintillation detectors for real-time verification of 192Ir HDR brachytherapy. Med Phys 2011;38:2542-51.
10. Carrasco P, Jornet N, Jordi O, Lizondo M, Latorre-Musoll A, Eudaldo T, *et al.* Characterization of the Exradin W1 scintillator for use in radiotherapy. Med Phys 2015;42:297-304.
11. Guillot M, Gingras L, Archambault L, Beddar S, Beaulieu L. Spectral method for the correction of the Cerenkov light effect in plastic scintillation detectors: A comparison study of calibration procedures and validation in Cerenkov light-dominated situations. Med Phys 2011;38:2140-50.
12. Dieterich S, Sherouse GW. Experimental comparison of seven commercial dosimetry diodes for measurement of stereotactic radiosurgery cone factors. Med Phys 2011;38:4166-73.
13. Underwood TS, Rowland BC, Ferrand R, Vieillevigne L. Application of the Exradin W1 scintillator to determine Ediode 60017 and microDiamond 60019 correction factors for relative dosimetry within small MV and FFF fields. Phys Med Biol 2015;60:6669-83.
14. Francescon P, Beddar S, Satariano N, Das IJ. Variation of kQclin, Qmsr (fclin, fmsr) for the small-field dosimetric parameters percentage

depth dose, tissue-maximum ratio, and off-axis ratio. Med Phys 2014;41:101708.
15. Qin Y, Zhong H, Wen N, Snyder K, Huang Y, Chetty IJ. Deriving detector-specific correction factors for rectangular small fields using a scintillator detector. J Appl Clin Med Phys 2016;17:6433.
16. Fan J, Paskalev K, Wang L, Jin L, Li J, Eldeeb A, *et al.* Determination of output factors for stereotactic radiosurgery beams. Med Phys 2009;36:5292-300.
17. Bucciolini M, Buonamici FB, Mazzocchi S, De Angelis C, Onori S, Cirrone GA. Diamond detector versus silicon diode and ion chamber in photon beams of different energy and field size. Med Phys 2003;30:2149-54.
18. Griessbach I, Lapp M, Bohsung J, Gademann G, Harder D. Dosimetric characteristics of a new unshielded silicon diode and its application in clinical photon and electron beams. Med Phys 2005;32:3750-4.
19. Liu PZ, Suchowerska N, McKenzie DR. Can small field diode correction factors be applied universally? Radiother Oncol 2014;112:442-6.
20. Beierholm AR, Behrens CF, Andersen CE. Dosimetric characterization of the Exradin W1 plastic scintillator detector through comparison with an in-house developed scintillator system. Radiat Meas 2014;69:50-6.
21. Francescon P, Cora S, Satariano N. Calculation of k (Q(clin), Q (msr)) (f (clin), f (msr)) for several small detectors and for two linear accelerators using Monte Carlo simulations. Med Phys 2011;38:6513-27.
22. Klein DM, Tailor RC, Archambault L, Wang L, Therriault-Proulx F, Beddar AS. Measuring output factors of small fields formed by collimator jaws and multileaf collimator using plastic scintillation detectors. Med Phys 2010;37:5541-9.
23. Sauer OA, Wilbert J. Measurement of output factors for small photon beams. Med Phys 2007;34:1983-8.
24. Scott AJ, Nahum AE, Fenwick JD. Using a Monte Carlo model to predict dosimetric properties of small radiotherapy photon fields. Med Phys 2008;35:4671-84.
25. Ding GX, Duggan DM, Coffey CW. Commissioning stereotactic radiosurgery beams using both experimental and theoretical methods. Phys Med Biol 2006;51:2549-66.
26. Gonzalez-Lopez A, Vera-Sanchez JA, Lago-Martin JD. Small fields measurements with radiochromic films. J Med Phys 2015;40:61-7.
27. Lárraga-Gutiérrez JM. Experimental determination of field factors for small radiotherapy beams using the daisy chain correction method. Phys Med Biol 2015;60:5813-31.
28. Wiant DB, Terrell JA, Maurer JM, Yount CL, Sintay BJ. Commissioning and validation of brainLab cones for 6X FFF and 10X FFF beams on a varian trueBeam STx. J Appl Clin Med Phys 2013;14:4493.
29. Morales JE, Crowe SB, Hill R, Freeman N, Trapp JV. Dosimetry of cone-defined stereotactic radiosurgery fields with a commercial synthetic diamond detector. Med Phys 2014;41:111702.

Original Article

Comparison of Rapid Arc and Intensity-modulated Radiotherapy Plans Using Unified Dosimetry Index and the Impact of Conformity Index on Unified Dosimetry Index Evaluation

Jayapalan Krishnan, Jayarama Shetty[1], Suresh Rao, Sanath Hegde, Shambhavi C

Department of Radiation Oncology, Mangalore Institute of Oncology, [1]Department of Radiation Oncology, K. S. Hegde Medical Academy, Mangalore, Karnataka, India

Abstract

The aim of this study was to evaluate the impact of conformity index in the unified dosimetry index (UDI) score for two different planning techniques namely intensity-modulated radiotherapy (IMRT) and Rapid Arc. Rapid Arc and IMRT plans of 57 patients were evaluated and compared using UDI score which incorporates four indices. To determine the impact of conformity index on the IMRT and Rapid Arc plans, UDI at conformity index one of all plan (UDI_{unit_CI}) score was calculated by assuming conformity index is equal to one. Mean and standard deviations of all indices were calculated. Rapid Arc technique plans of different treatment sites of all patients scored lesser UDI than IMRT plans, and the conformity index of Rapid Arc plan was significantly better than IMRT plan. The average dose gradient, homogeneity, coverage, and conformity index of all sites with Rapid Arc plans were 0.212 ± 0.05, 1.123 ± 0.03, 0.959 ± 0.03, and 1.056 ± 0.09; with IMRT plans were 0.190 ± 0.05, 1.113 ± 0.04, 0.950 ± 0.04, and 1.172 ± 0.16, respectively. UDI score value with actual conformity index of Rapid Arc and IMRT plans differed significantly ($P < 0.001$). However, UDI_{unit_CI} score values with assumed conformity index equal to one did not differ significantly ($P = 0.528$). In the comparison of IMRT and Rapid Arc plans using the UDI score, the impact of conformity index was significant.

Keywords: Conformity index, intensity-modulated radiotherapy, Rapid Arc, unified dosimetry index

Received on: 20-10-2016 **Review completed on: 29-12-2016** **Accepted on: 03-01-2017**

Introduction

The basic principle of radiotherapy is to deliver higher and uniform dose to tumour and to reduce dose to organ at risks (OARs) as low as possible which reduces the morbidity and in turn improves the quality of life of patients. Although the conventional techniques provide better tumor coverage, there is some limitation in achieving OARs tolerance dose.

To overcome this difficulty, modern delivery techniques such as intensity-modulated radiotherapy (IMRT) and Rapid Arc have been used widely. These techniques can deliver a higher dose to tumor and limit the dose to OARs. The degree of confirmed dose delivery using these techniques improves the plan quality. Usually, plan quality has been evaluated using various dosimetry indices. Most of the articles contain conformity index, coverage index, homogeneity index, and dose gradient (DG) index for plan evaluation. The conformity can be determined in many ways using a different definition.[1] An ideal plan is defined as one with full uniform dose coverage; exact conformed to the target and step-wise fall-off dose outside the target.[2-5] Akpati *et al*.[6] introduced one more approach called unified dosimetry index (UDI) that computes an overall score which integrates contribution from all four dosimetry components mentioned above. The UDI score of each plan can be ranked and selected the least scored plan as a better plan. There are fewer articles published that employed UDI score. This study utilized UDI score for the comparison of IMRT and Rapid Arc plans of various sites and also studied the impact of conformity index on UDI-based plan evaluation.

Access this article online

Quick Response Code:

Website: www.jmp.org.in

DOI: 10.4103/jmp.JMP_112_16

Address for correspondence: Mr. Jayapalan Krishnan, Department of Radiation Oncology, Mangalore Institute of Oncology, Mangalore, Karnataka, India.
E-mail: nkjayapalceg37@gmail.com

How to cite this article: Krishnan J, Shetty J, Rao S, Hegde S, Shambhavi C. Comparison of Rapid Arc and IMRT plans using unified dosimetry index and the impact of conformity index on unified dosimetry index evaluation. J Med Phys 2017;42:XX.

Materials and Methods

Dose coverage is defined as 100% of the planning target volume (PTV) receiving the prescribed dose. It gives a measure of how well the PTV is covered by the prescribed dose. Dose conformity, on the other hand, is defined as the ratio of the total volume of all tissues receiving prescribed dose versus the PTV. Dose conformity gives a measure of how well the prescribed dose is confined to the PTV. DG is defined as the ratio of the volume receiving the prescribed dose and the volume receiving half the prescribed dose. Homogeneity index (HI) is defined as the ratio of the maximum dose at any point 2 mm beyond the PTV (D_{Max}) to the prescribed dose.[6]

The mathematical logic-based UDI formula is:

$$UDI = \left(\prod_{k=1}^{4} W_k \left[\left|1.0 - DI_k\right| + 0.1\right]\right) \times 10^4 \quad (1)$$

Where DI_k is dosimetry index of each index of the four indices and W_k denotes weighting factors that reflect the relative importance of the four components.

For ideal plan, unified index (UDI) is equal to 1:

$$UDI = UDI\ (C) \times UDI\ (CF) \times UDI\ (HI) \times UDI\ (DG) = 1.0 \quad (2)$$

Where C-coverage index (DI_1), CF-conformity index (DI_2), HI (DI_3) and DG-gradient index (DI_4). Akpati *et al*.[6] used the following equations to calculate all indices and explained full detail about UDI and method of calculation.

$$\text{Coverage Index (C)} = PTV_{PI}/PTV \quad (3)$$

$$\text{Conformity Index (CF)} = DV_{PI}/PTV \quad (4)$$

$$HI = D_{Max}/D_{PI} \quad (5)$$

$$\text{DG Index (DG)} = DV_{PI}/DV_{HPI} \quad (6)$$

Where PTV is the PTV; PTV_{PI} = PTV receiving the prescribed isodose (PI); DV_{PI} = Dose volume of the PI; DV_{HPI} = dose volume of the half the prescribed dose; D_{Max} = Maximum dose at any point 2 mm beyond the PTV; D_{PI} = Dose value of the PI.

Using this approach, we compared two different techniques IMRT and Rapid Arc. CT data of 57 patients (13 Ca. Prostate, 12 Ca. Endometrium, 6 Ca. Cervix, and 26 Ca. Oesophagus) were utilized in this study. IMRT and Rapid Arc plans were generated by inverse planning method using Eclipse treatment planning system (V-10.0.39, Varian Medical Systems, USA). All plans use 6MV photon energy and optimized by assigning the target and OAR goals.

The plans were evaluated using all four indices separately. The UDI scoring values of all plans were ranked and lesser value scored plan considered as a better plan for the patient. For determining the impact of conformity index in the comparison of IMRT and Rapid Arc plan, a UDI score of the plans was calculated by assuming confidence interval = 1 UDI at conformity index one of all plan (UDI_{unit_CI}), and it was compared against the UDI score calculated with actual conformity index. Mean and standard deviations of all indices were calculated, and statistical analysis was performed using SPSS (version 16.0.0, SPSS, Chicago, USA).

Results

Table 1 shows an overview of the mean and standard deviations of DG index, HI, coverage index, conformity index, UDI score and UDI_{unit_CI} score for IMRT and Rapid Arc techniques planned for each site of the patients. Table 2 shows the mean and standard deviations of the different indices for all 57 patients compared.

It is observed that the conformity index and UDI of Rapid Arc plan were significantly better than IMRT plan. The average DG index, HI, coverage index and conformity index of all sites with Rapid Arc plans were 0.212 ± 0.05, 1.123 ± 0.03, 0.960 ± 0.03, and 1.056 ± 0.09; with IMRT plans were 0.190 ± 0.05, 1.113 ± 0.04, 0.950 ± 0.04, and 1.172 ± 0.16, respectively.

Figures 1-3 show the radar graph of UDI scores from Rapid Arc and IMRT plans of various treatment sites. In the figures, the lowest score denotes the minimum deviation from an ideal dosimetry plan (toward to one), and highest score denotes the maximum deviation from an ideal dosimetry plan (outward from one). The radar graph shows that Rapid Arc plans are better than IMRT plans for all treatment sites.

Table 1: Mean and standard deviations of dose gradient index, homogeneity index, coverage index conformity index, unified dosimetry index score and unified dosimetry index at conformity index one of all plans score of each treatment site

Technique	Mean±SD		
	Prostate (*n*=13)	Esophagus (*n*=26)	Cervix and endometrium (*n*=18)
DG_index			
RapidArc	0.206±0.04	0.204±0.06	0.223±0.02
IMRT	0.185±0.04	0.171±0.06	0.211±0.03
HI_index			
RapidArc	1.103±0.02	1.135±0.02	1.118±0.03
IMRT	1.088±0.05	1.127±0.03	1.112±0.03
Coverage_index			
RapidArc	0.944±0.03	0.947±0.03	0.973±0.02
IMRT	0.936±0.05	0.893±0.09	0.983±0.01
Confirmity_index			
RapidArc	0.977±0.05	1.003±0.04	1.152±0.07
IMRT	1.110±0.11	1.045±0.21	1.300±0.11
UDI			
RapidArc	43.072±15.22	43.133±13.34	60.183±17.87
IMRT	57.266±20.96	120.532±227.82	90.602±41.03
UDI_{unit_CI}			
RapidArc	28.322±6.73	32.660±7.66	24.723±6.66
IMRT	28.635±12.21	46.469±35.35	22.217±5.21

DG: Dose gradient, HI: Homogeneity index, UDI: Unified dosimetry index, UDI_{unit_CI}: Unified dosimetry index at conformity index one of all plans, IMRT: Intensity-modulated radiation therapy, SD: Standard deviation

Discussion

The method of UDI score-based plan evaluation and comparison of different techniques plans can be useful for establishing a benchmark.[6] Although many numbers of indices have been proposed for plan evaluation, it is difficult to understand as to which system is better or useful. The radiation therapy oncology group has suggested that a quality treatment plan has to evaluate using three separate indices of dose coverage, conformity, and homogeneity.[1] The UDI used here incorporates all four dosimetry indices into a single overall score. In this study, the plans of similar techniques were analyzed and compared to find a better plan for patient treatment using this UDI score.

Conformity index may vary according to the isodose selected. The conformity index can be reduced while selecting lower isodose level as the reference, and therefore increasing the volume of reference isodose.[7] Therefore, in the evaluation of different techniques, this index would help to take clinical decision.

It is observed that the conformity index was significantly higher with Rapid Arc plan than IMRT ($P < 0.001$). While considered the conformity index as unit, the UDI_{unit_CI} of both plans did not differ significantly ($P = 0.527$). However, the UDI score values of both planning techniques were calculated with actual conformity index was better with Rapid Arc than IMRT significantly ($P < 0.001$). Subsequent effect of better conformity index, better DG index could be achieved with Rapid Arc plans. Therefore, critical structure dose (especially prescribed dose region) was controlled with Rapid Arc plan significantly than IMRT plan ($P < 0.011$). The dose-volume histogram values of different critical structures in the treatment of different sites were controlled significantly with Rapid Arc plans than IMRT.

From Figures 1-3, it is noted that the UDI score spikes for few plans. This result was observed in the bulky patients and whose tumor size is relatively large. The conformity index was relatively lesser due to the higher dose spillage outside the target.

For all plans studied, the coverage index, HI did not differ significantly between both IMRT and Rapid Arc. The same results were observed in various studies.[8-12] Therefore, it can be concluded that the higher degree of confined dose delivery of Rapid Arc technique provides better treatment plans when compared with IMRT.

Table 2: Mean and standard deviations of dose gradient index, homogeneity index, coverage index conformity index, unified dosimetry index score, and unified dosimetry index at conformity index one of all plans score of all patients

Technique	All sites (n=57), mean±SD
DG_index	
RapidArc	0.212±0.05
IMRT	0.190±0.05
HI_index	
RapidArc	1.123±0.03
IMRT	1.113±0.04
Coverage_index	
RapidArc	0.960±0.03
IMRT	0.950±0.04
Confirmity_index	
RapidArc	1.056±0.09
IMRT	1.172±0.16
UDI	
RapidArc	46.055±16.31
IMRT	74.463±40.44
UDI_{unit_CI}	
RapidArc	27.877±6.54
IMRT	29.443±10.44

DG: Dose gradient, HI: Homogeneity index, UDI: Unified dosimetry index, UDI_{unit_CI}: Unified dosimetry index at conformity index one of all plans, IMRT: Intensity-modulated radiation therapy, SD: Standard deviation

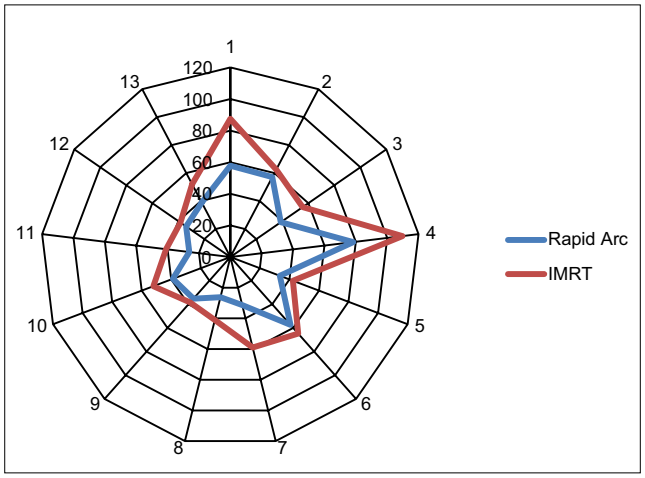

Figure 1: The unified dosimetry index score of each patient's Rapid Arc and intensity-modulated radiotherapy plans of Ca.Prostate.

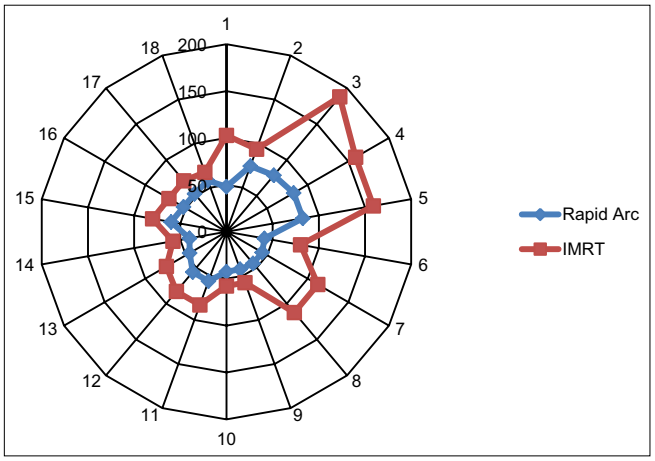

Figure 2: The unified dosimetry index score of each patient's Rapid Arc and intensity-modulated radiotherapy plans of Ca.Cervix and endometrium.

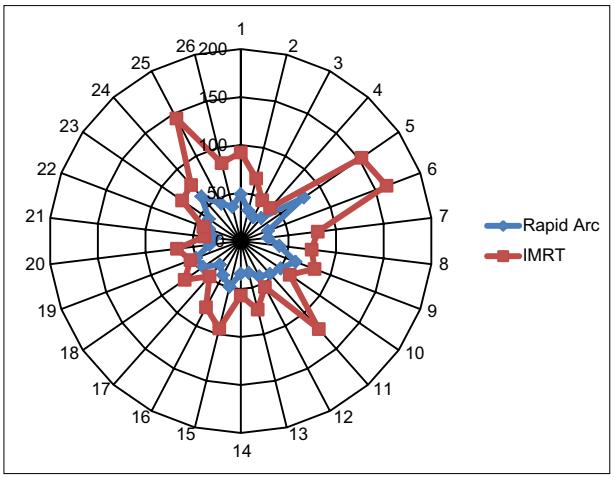

Figure 3: The unified dosimetry index score of each patient's Rapid Arc and intensity-modulated radiotherapy plans of Ca.lower third oesophagus.

Conclusion

For all compared treatment sites in this study, Rapid Arc plans scored better UDI value as well as better OARs sparing. In the comparison of IMRT and Rapid Arc plans using the UDI score, the impact of conformity index was significant.

Financial support and sponsorship

Nil.

Conflicts of interest

There are no conflicts of interest.

References

1. Shaw E, Kline R, Gillin M, Souhami L, Hirschfeld A, Dinapoli R, *et al.* Radiation therapy oncology group: Radiosurgery quality assurance guidelines. Int J Radiat Oncol Biol Phys 1993;27:1231-9.
2. Wagner TH, Bova FJ, Friedman WA, Buatti JM, Bouchet LG, Meeks SL. A simple and reliable index for scoring rival stereotactic radiosurgery plans. Int J Radiat Oncol Biol Phys 2003;57:1141-9.
3. van't Riet A, Mak AC, Moerland MA, Elders LH, van der Zee W. A conformation number to quantify the degree of conformality in brachytherapy and external beam irradiation: Application to the prostate. Int J Radiat Oncol Biol Phys 1997;37:731-6.
4. Paddick I. A simple scoring ratio to index the conformity of radiosurgical treatment plans. Technical note. J Neurosurg 2000;93 Suppl 3:219-22.
5. Baltas D, Kolotas C, Geramani K, Mould RF, Ioannidis G, Kekchidi M, *et al.* A conformal index (COIN) to evaluate implant quality and dose specification in brachytherapy. Int J Radiat Oncol Biol Phys 1998;40:515-24.
6. Akpati H, Kim C, Kim B, Park T, Meek A. Unified dosimetry index (UDI): A figure of merit for ranking treatment plans. J Appl Clin Med Phys 2008;9:2803.
7. Feuvret L, Noël G, Mazeron JJ, Bey P. Conformity index: A review. Int J Radiat Oncol Biol Phys 2006;64:333-42.
8. Krishnan J, Rao S, Hegde S, Shetty J, Shambhavi C. A dosimetric comparison of double arc volumetric modulated arc therapy with large field intensity modulated radiation therapy for head and neck cancer. Int J Med Phys Clin Eng Radiat Oncol 2015;4:353-63.
9. Cozzi L, Dinshaw KA, Shrivastava SK, Mahantshetty U, Engineer R, Deshpande DD, *et al.* A treatment planning study comparing volumetric arc modulation with RapidArc and fixed field IMRT for cervix uteri radiotherapy. Radiother Oncol 2008;89:180-91.
10. Palma D, Vollans E, James K, Nakano S, Moiseenko V, Shaffer R, *et al.* Volumetric modulated arc therapy for delivery of prostate radiotherapy: Comparison with intensity-modulated radiotherapy and three-dimensional conformal radiotherapy. Int J Radiat Oncol Biol Phys 2008;72:996-1001.
11. Clivio A, Fogliata A, Franzetti-Pellanda A, Nicolini G, Vanetti E, Wyttenbach R, *et al.* Volumetric-modulated arc radiotherapy for carcinomas of the anal canal: A treatment planning comparison with fixed field IMRT. Radiother Oncol 2009;92:118-24.
12. Wagner D, Christiansen H, Wolff H, Vorwerk H. Radiotherapy of malignant gliomas: Comparison of volumetric single arc technique (RapidArc), dynamic intensity-modulated technique and 3D conformal technique. Radiother Oncol 2009;93:593-6.

Original Article

Structural Shielding Design of a 6 MV Flattening Filter Free Linear Accelerator: Indian Scenario

Bibekananda Mishra, T. Palani Selvam[1], P. K. Dash Sharma

Radiological Safety Division, Atomic Energy Regulatory Board, Niyamak Bhavan, [1]Radiological Physics and Advisory Division, Health Safety and Environmental Group, Bhabha Atomic Research Centre, Mumbai, Maharashtra, India

Abstract

Detailed structural shielding of primary and secondary barriers for a 6 MV medical linear accelerator (LINAC) operated with flattening filter (FF) and flattening filter free (FFF) modes are calculated. The calculations have been carried out by two methods, one using the approach given in National Council on Radiation Protection (NCRP) Report No. 151 and the other based on the monitor units (MUs) delivered in clinical practice. Radiation survey of the installations was also carried out. NCRP approach suggests that the primary and secondary barrier thicknesses are higher by 24% and 26%. respectively, for a LINAC operated in FF mode to that of a LINAC operated in both FF and FFF modes with an assumption that only 20% of the workload is shared in FFF mode. Primary and secondary barrier thicknesses calculated from MUs delivered on clinical practice method also show the same trend and are higher by 20% and 19%, respectively, for a LINAC operated in FF mode to that of a LINAC operated in both FF and FFF modes. Overall, the barrier thickness for a LINAC operated in FF mode is higher about 20% to that of a LINAC operated in both FF and FFF modes.

Keywords: Flattening filter, flattening filter free, medical linear accelerator, monitor units, primary barrier, secondary barrier

Received on: 15-09-2016 **Review completed on: 17-01-2017** **Accepted on: 06-02-2017**

Introduction

Standard medical linear accelerators (LINACs) used in radiotherapy are equipped with a flattening filter (FF). The FF is designed to produce uniform dose distribution across the field in a homogeneous medium. Recently, there has been an increasing interest in operating medical LINAC without FF. A FF free (FFF) LINAC is basically a standard LINAC with the FF removed from the beam line. The main advantages of removing the FF are increased dose rate in addition to reduced scatter and leakage radiation inside and outside the target volume.[1-5] These benefits result from removal of attenuation of the primary beam, reduction of the scatter radiation originating from the FF, and reduction of leakage radiation due to decrease in beam energy. Reduction of the head scatter also improves dosimetry of the FFF beams due to reduction of output variation with field size and field size-dependent parameters.[6-8] FFF LINAC has been investigated in detail and is used in radiotherapy treatments including advanced modalities such as intensity-modulated radiation therapy treatments and stereotactic radiosurgery.[9-13] As expected, there are differences in the beam characteristics of LINAC operated in FFF mode to that of LINAC with the FF mode. FFF LINAC beam is softer, for example, the central axis percent depth dose in water for a 6 MV FFF beam resembles a 4 MV FF beam.[14] In addition, the lateral dose profile is peaked on the central axis, and less integral target current is required to generate the same dose to the tumor.[15,16] As a result, the shielding parameters, such as the tenth-value layers (TVLs) and scatter fractions, calculated for flattened beams, may not be appropriate for shielding evaluations for unflattened beams.[17-19] Since FFF beam is used for advanced modalities requiring higher monitor units (MUs) to be delivered, it must be determined whether shielding needs to be enhanced or reduced to use an FFF machine in comparison to vault of FF machine.

Considering the LINACs with FFF beam available in India and their growth, this study was carried out to find the impact

Access this article online

Quick Response Code:

Website: www.jmp.org.in

DOI: 10.4103/jmp.JMP_99_16

Address for correspondence: Mr. Bibekananda Mishra, Radiological Safety Division, Atomic Energy Regulatory Board, Mumbai - 400 094, Maharashtra, India.
E-mail: m.bibek@gmail.com

How to cite this article: Mishra B, Selvam TP, Sharma PKD. Structural shielding design of a 6 MV flattening filter free linear accelerator: Indian scenario. J Med Phys 2017;42:XX-XX.

of FFF beam on bunker design of LINAC facility in Indian scenario. The present study is to assess the structural shielding requirements of a 6 MV LINAC operated in both FF and FFF modes in comparison to a standard 6 MV LINAC. This study includes the detailed calculations of thicknesses required for the shielding of primary and secondary barriers of 6 MV LINAC bunker operated for FF and FFF photon beams. The calculations have been carried out by two methods, one using the approach given in National Council on Radiation Protection (NCRP) Report No. 151[20] and the other one is based on the MUs delivered in clinical practice. In recent times, several technical changes have been augmented in the treatment delivery modality which enables higher dose escalation to tumor and rapid dose fall off outside the tumor. The technologies involved for such delivery enhance the MUs generated from the LINAC due to the presence of different beam modifying techniques. This study also includes the radiation survey of the installations.

Materials and Methods

National Council on Radiation Protection approach of calculation of basic shielding parameters

A standard layout of 6 MV accelerator bunker used in this study is presented in Figure 1. Radiation generated by LINAC can be divided into primary and secondary components, the latter can further be divided into scatter and leakage radiation. The calculations for basic shielding parameters includes workload (W), use factor (U), occupancy factor (T), distance from the radiation source (d), and permissible dose limit (P) as prescribed by the regulatory authority of the country.

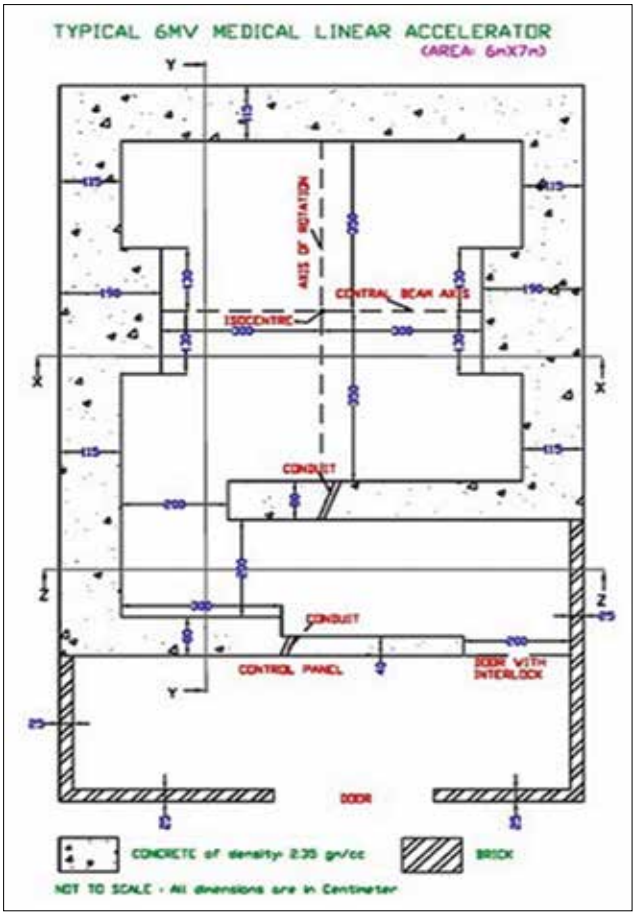

Figure 1: Standard layout of a 6 MV medical linear accelerator bunker.

Workload (W)

W for radiotherapy is the time integral of the absorbed dose rate at the depth of the maximum absorbed dose at 1 m from the source considering maximum possible number of the patient treated and physics work. The most common period of time over which W specified is 1 week and is expressed in cGy/week at 1 m. Here, we have considered only the delivered radiation dose for clinical use. Physics workload is not included since it is significantly less except commissioning measurements and for measurements after major repair work. W is calculated as below by considering an average of 200 cGy dose given per patient at 10 cm as the average depth of dose delivery in clinical cases:

$$W = D_p \times N_p \times N_d \times \frac{1}{DD_{10}} \quad (1)$$

where D_p is dose (in cGy) delivered per patient, N_p is number of patients treated per day, N_d is number of days per week, and DD_{10} is central axis dose at 10 cm depth normalized to dose value where dose maximum occurs.

Use factor (U) and occupancy factor (T)

U is the fraction of time that the beam is likely to be incident on the barrier and is considered as 0.25 for primary wall and 1 for secondary wall. T is defined as the kind of occupancy around the installation. In this study, T is considered as 1 for all the locations.

Distance (d)

The distance between source and point of interest, which has been considered with reference to the standard plan as provided in Figure 1 and measured in centimeter for all purposes.

Permissible dose limit (P)

In India, P is 20 μSv/week and 400 μSv/week for general public and radiation workers, respectively.

Primary barrier

Expression for the reduction factor (RF) to achieve the radiation level "P" is given by:

$$RF = \frac{WUT}{Pd^2} \quad (2)$$

where W, U, T, P, and d have their usual meaning. Then, the primary barrier thickness (t_{pri}) can be determined using number of TVLs, n, based on energy of the treatment unit and the type of shielding material being used.

$$t_{pri} = n \times TVL = \log(RF) \times TVL = \log\left(\frac{WUT}{Pd^2}\right) \times TVL \quad (3)$$

It may be noted that wall thicknesses determined for primary barriers will be more than the thickness required to shield

leakage and scattered radiation, which are comparatively insignificant, and hence, no further calculations are required. The values of TVL reported for corresponding energy of FF and FFF beams are different,[18] and accordingly, they have been used in our calculation.

Secondary barrier

These barriers are not in the direct line of the radiation beam but necessary to shield from leakage radiation from the treatment head and scatter from the patient and the treatment room walls.

Leakage radiation

For LINAC, International Electrotechnical Commission standards state that the leakage from the treatment head shall not exceed 0.5% of the primary beam.[21] In general, manufacturers provide adequate shielding on head of the LINAC resulting in leakage of <0.1% of primary. Therefore, it is reasonable to consider leakage as 0.1% in the shielding calculations. RF required to achieve design goal (P) against head leakage radiation is as follows:

$$RF = \frac{\alpha_0 WUT}{P\left(d_s\right)^2} = \frac{0.001 \times \mathrm{WUT}}{P\left(d_s\right)^2} \quad (4)$$

where α_0 is the leakage from the head (0.1%), d_s is the distance from the isocenter to the point of interest in meters, U is unity for secondary barriers. Then, the secondary barrier thickness $(t_{sec})_L$ can be determined as,

$$\left(t_{sec}\right)_L = n \times TVL = \log\left(RF\right) \times TVL = \log\left(\frac{0.001 \times \mathrm{WUT}}{P(d_s)^2}\right) TVL \quad (5)$$

Scattered radiation

Patient scatter

RF against radiation scattered by the patient to achieve design dose limit (P) is given by:

$$RF = \frac{\alpha_s WUT\left(\frac{F}{400}\right)}{P\left(d_{sca} \times d_s\right)^2} \quad (6)$$

where, P, W, and T have their usual meaning. The scatter primary ratio (α_s) depends on the energy of the photon and the scattering angle. Values of α_s are available for 400 cm^2 irradiated field area for all clinical beams, F is the field area incident on the patient in cm^2, d_{sca} is the distance (in meter) from the radiation source to the patient in meters, and d_s is the distance from the patient to the point of interest in meters. Radiation scattered by a patient is usually <0.1% of the incident radiation per 1000 cm^2 (0.1 m^2) area irradiated. For large scatter angles, the energy of the scattered radiation will be degraded and the protection designed against leakage radiation should provide adequate protection against scattered radiation from the patient.

Wall scatter

RF against scattered radiation when the primary beam strikes a wall is given by the following expression:

$$RF = \frac{\alpha_{w,s}\ AWUT}{Pd_w^{\ 2}d_r^{\ 2}} \quad (7)$$

where $\alpha_{w,s}$ is the wall reflection coefficient, which depends on the wall material, scattering angle, and beam energy, A is the field area projected on the scattering surface (wall) in m^2, d_w is the distance from the radiation source to the scattering surface (wall) in meter, and d_r is the distance from the scattering surface (wall) to the point of interest, in meter. The photons scattered by the wall and by the patient are of about the same energy. If the thickness required to shield from patient scatter is different from that needed to shield from wall scatter by one tenth-value thickness (TVT) or more, the larger thickness is used, otherwise, one half-value thickness (HVT) is added to the larger thickness. Similarly, one HVT is added to higher thickness if the thickness required to protect from leakage differs from that required to protect from scatter by <1 TVT.

Roofs

The roof section that can be struck directly by the primary radiation is also a primary barrier and the formula used to determine the required thicknesses are the same as that for primary.

Mazes

Since for LINAC operating below 10 MV, there is no production of neutron, the scatter and transmission of primary, leakage, and scattered radiation need to be considered while estimating dose at maze entrance.

When the gantry rotation axis is perpendicular to the maze axis, the total dose at the entrance door, that is, D_d (Photon dose) will be given by:

$$D_d = \sum_G D_P + \sum_G f \times D_W + \sum_G D_L + \sum_G D_T \quad (8)$$

where $\sum_G$ integrates through all gantry angles, D_P is the dose arising from patient scatter, f is the primary radiation transmitted through the patient, D_w is the primary radiation scattered by the wall into the maze, D_L is the leakage radiation scattered down the maze [Figure 2], and D_T is the leakage radiation transmitted through the maze wall.

When gantry rotation axis is parallel to the maze axis (i.e., maze is a primary barrier), the above expression can be written as:

$$D_d = \sum_G D_P + \sum_G f \times D_{W,T} + \sum_G D_L + \sum_G D_T \quad (9)$$

All the symbols have the same meaning except $D_{W,T}$, which will be primary radiation transmitted through the maze wall and further scattered to the maze entrance.

Monitor unit data from different radiotherapy centers

Around one thousand patients' data were taken from geographically different regions, considering the variation

in patients' physique and from accelerators of different manufacturers (Varian Medical System, USA and Elekta Medical System, UK) capable of delivering FF and FFF beam. Patients' data were grouped for five different major clinical sites such as brain, head and neck, thoracic, abdomen, and pelvic region. Actual MUs delivered have been obtained from the planning systems for these different cases using the 6 MV photon beam in both FF and FFF modes. The data, hence, generated are presented in Table 1. The small field treatment cases are not included as variation in MU delivered in FF and FFF mode is not significant.

Practical workload, W is arrived at by analyzing these data of MU delivered. The workload for FF mode is the cumulative MU delivered for 5 days, which is estimated from the daily average dose for stated clinical sites observed over a period of 6 months. Over this period, we have noted that 80% of the patients are treated in FF mode and only 20% of patients are treated in FFF mode. Therefore, in this study, the workload for a facility using both FF and FFF mode is assumed to be the combination of workloads for 80% of beam in FF mode and 20% of beam in FFF mode. Based on the W, barrier thicknesses are evaluated using the values of TVL reported for corresponding energy of FF and FFF beams.[18]

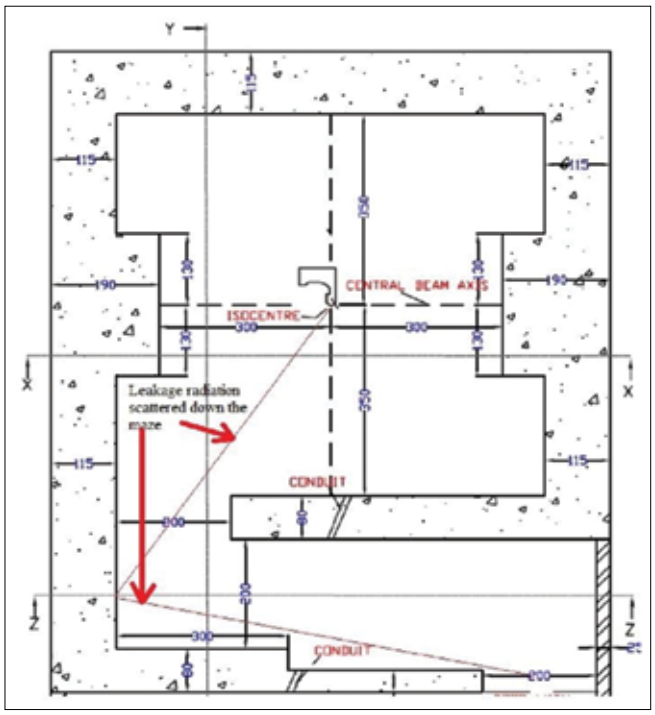

Figure 2: Layout of a 6 MV medical linear accelerator bunker indicating leakage radiation scattered down the maze.

Radiation survey measurements

The radiation survey measurements were carried out in these installations, from where the patient data were used. In this study, we have measured the instantaneous dose rate (IDR) for both FF and FFF modes all around the installation at different locations. For radiation level measurement, a calibrated pressurized ion chamber-based Fluke Biomedical, USA make 450R survey meter was used. The LINAC was operated in maximum available dose rate for both FF and FFF modes. All measurements were performed with the maximum achievable field size for both FF and FFF modes. For primary beam, the radiation level measurement was carried out without a phantom in the beam path considering the worst possible scenario. For secondary beam, the radiation levels were measured with a water phantom of dimension 40 cm × 40 cm × 40 cm to simulate full scattering condition. The phantom was positioned on the treatment couch with the center of the phantom at the isocenter. On each wall, a matrix of dimension 20 cm × 20 cm had been created. For each location, measurements were taken at the point where the survey meter reading was maximum. Radiation levels were measured at seven locations, that is, primary wall 1, primary wall 2, ceiling, secondary wall (gantry side), secondary wall (couch side), door location, and the control console. At each point, measurements were taken at four gantry angles 0°, 90°, 180°, and 270°. The measured data are presented in Table 2. Weekly radiation level (R_w) expressed in μSv/week was estimated for 6 MV beam in both FF and FFF modes as per the International Atomic Energy Agency Safety Reports Series[22] using the equation:

$$R_w = IDR \times \frac{WU}{\dot{D}} \quad (10)$$

where, IDR is the instantaneous dose rate and is the dose rate of the photon beam. W and U have their usual meaning.

Table 1: Details of monitor units delivered for major clinical cases using 6 MV photon beam with flattening filter and flattening filter free modes

Major clinical treatment sites	Average MUs delivered for ten number of patients treated in 6 MV using FF mode	Average MUs delivered for ten number of patients treated in 6 MV using FFF mode
Brain	500	900
Head and neck	550	1400
Thorax	450	1300
Abdomen	1200	1650
Pelvic	1200	2200

MUs are considered for intensity modulated beam delivery. MUs presented here are the average of 1000 clinical cases divided in twenty such groups, five major clinical sites in each group and ten number of patients for each site (rounded to nearest value of multiple of 10). MUs: Monitor units, FFF: Flattening filter free, FF: Flattening filter

Table 2: Measured radiation survey data in μSv/h, with maximum achievable field size and dose rate of 1400 MU/min at normal treatment distance for seven different locations for different gantry positions

Gantry angle (°)	Without phantom			With phantom			
	Primary wall1	Primary wall2	Ceiling	Secondary wall (gantry side)	Secondary wall (couch side)	Door location	Console
0	0.13	0.08	0.06	0.72	0.87	2.80	0.18
90	0.15	0.09	0.07	0.48	0.30	2.40	1.10
180	0.05	0.07	2.30	0.52	0.41	2.90	0.30
270	0.10	5.70	0.04	1.45	1.30	6.20	0.13

Results and Discussion

National Council on Radiation Protection approach

Workload

FF beam is harder with higher average beam energy and percentage depth dose (PDD). For example, PDD at a depth of 10 cm for FF beam is 66.1% whereas for FFF beam, it is 63.4%.[14] In conventional FF LINACs, the workload has been calculated considering seventy patients treated in a day and 5 days in a week. However, it is observed that number of patients treated in a LINAC capable of delivering FF and FFF beam is maximum 50 instead of 70. Using equation 1, W is found to be around 33% less for FFF beam than the W calculated for FF beam (i.e., W is about 1.04×10^5 for FF and 0.78×10^5 for FFF).

Since in clinical practice around 80% of the patients are treated in FF mode and 20% in FFF mode, W is calculated using the weighted W for FF and FFF beams, that is, total workload, $W = 0.8 \times W_{FF} + 0.2 \times W_{FFF}$.

Using D_P = 200 cGy/patient, N_d = 5 for FF and FFF, and using N_P = 40 and DD_{10} = 0.661 for FF and N_P = 10 and DD_{10} = 0.634 for FFF, total workload, W is found to be 0.76×10^5 cGy/week at 1 m.

Primary barrier

For primary barriers, the values of U and T are 0.25 and 1, respectively. Thickness for primary wall is calculated using equation 2 and published value of TVL for FF and FFF beam has been used for concrete of density 2.35 g/cm^3.[18] Since the initial considerations are 100 cm from source to isocenter distance and a clearance of 300 cm from isocenter to the point of interest where the P value is desired, calculations have been carried out for multiple iterations till the thickness becomes constant. It is found that primary barrier thickness for a LINAC operated in FF mode is higher by 24% to that a LINAC operated in both FF and FFF modes with an assumption that only 20% of the workload is shared in FFF mode.

Secondary barrier

Leakage radiation

Similarly, for secondary barrier thickness calculations, the total radiation level is contributing with respect to head leakage as well as scatter from patient. The thickness required was calculated using equation 3 and found that the secondary barrier thickness for a LINAC operated in FF mode only is higher by 26% to that a LINAC operated in both FF and FF mode with an assumption that only 20% of the workload is shared in FFF mode.

Scattered radiation

Using equations 4-6, patient scatter, wall scatter, and maze scatter were calculated. It was found that secondary barrier thickness calculated for leakage radiation is adequate to shield the scattered radiation as well. Considering the length of the paper, the detailed calculations are avoided.

Calculations based on actual monitor unit data from different radiotherapy centers

Workload

The data of delivered MUs in FF and FFF mode for different clinical sites have been analyzed to arrive at a practical workload [Table 1], which is the major factor in shielding calculation. A total of thousand patients were considered, that is, twenty groups, each group with five major clinical sites and ten patients for each site. The major clinical sites chosen are brain, head and neck, thoracic, abdomen, and pelvic region. MUs delivered per patient for both FF and FFF modes are presented in Table 1. Hence, W is the total MUs delivered in 5 days (in 1 week period). It is found that W is about 1.95×10^5 cGy/week at 1 m for FF beam and 2.3×10^5 cGy/week at 1 m for FFF beam.

Primary barrier

The same modality of calculation is adopted for evaluating shielding adequacy of accelerator bunker, that is, the contribution of FF beam is 80% and to that of FFF beam is only 20%. For barrier calculations, workload $W = 1.95 \times 10^5$ cGy/week in case of 6 MV beam in FF mode and 2.3×10^5 cGy/week in case of FFF mode has been considered. It is found that primary barrier thickness for a LINAC operated in FF mode only is higher by 20% to that of a LINAC operated in both FF and FFF modes.

Secondary barrier

Similarly, secondary barrier thickness was calculated and found that the secondary barrier thickness for a LINAC operated in FF mode is higher only by 19% to that a LINAC operated in both FF and FFF modes.

Earlier investigations by Kry *et al*.[18,19] on the vault shielding of LINAC operated in FF and FFF mode estimated an overall reduction of 20% in the primary and secondary wall

thickness of the LINAC bunker for FFF mode of operation in comparison to FF mode of operation. In our study also, it is observed that the reduction in primary and secondary wall thickness of the LINAC bunker for practical situations is 20% for primary and 21% for secondary, which is consistent with those reported in literature.

Radiation survey measurements

R_w is estimated using equation 8 for both FF and FFF modes LINAC. In this calculation, W is the clinical workload, IDR is measured for both FF and FFF modes using the maximum dose rate available, and the suitable value for U is considered depending on the location. The radiation survey was carried out in all installations from where the clinical data were taken for this study. However, representative data of the radiation survey of only one installation have been presented in Table 2. As bunkers were constructed for FF mode of use, the measured radiation level is further scaled for FFF mode with a factor of $\left\{\frac{e^{-\mu t_{FFF}}}{e^{-\mu t_{FF}}}\right\}$, where t_{FFF} and t_{FF} are the thicknesses estimated for FFF and FF mode, respectively. It is found that the radiation level all around the installations are within the acceptable limit.

Conclusions

The removal of FF significantly decreases local dose rates outside the treatment vault. In the present study, shielding requirements of a 6 MV medical LINAC operated both with and without the FF are assessed using the NCRP Report No. 151 and also by MUs delivered for clinical practice in Indian scenario. The results based on NCRP approach suggest that the primary and secondary barrier thicknesses are higher by 24% and 26%, respectively, for a LINAC operated in FF mode to that of a LINAC operated in both FF and FFF modes with an assumption that only 20% of the workload is shared in FFF mode. Primary and secondary barrier thicknesses calculated from the data on clinical practice also show the same trend and are higher by 20% and 19%, respectively, for a LINAC operated in FF mode to that of a LINAC operated in both FF and FFF modes. Hence, it is found that overall the barrier thickness for a LINAC operated in FF mode is higher about 20% to that of a LINAC operated in both FF and FFF. As a result, the wall thickness can be saved by about 20% for a LINAC operated in both FF and FFF modes in comparison to the LINAC operated in FF modes only. Hence, the lower consumption of shielding material and space for new treatment vaults housing the LINACs with FFF and FF modes may reduce the building cost, whereas for existing facilities, one might take the benefits in terms of increased weekly workload. We are of the view to use similar workload while estimating the weekly radiation level around the LINAC bunker. Further, this approach of calculations of shielding thickness for 6 MV bunker can also be extended for higher energies such as 10, 15, and 18 MV as well.

Acknowledgment

We would like to thank Dr. A. U. Sonawane, Head, Radiological Safety Division, Atomic Energy Regulatory Board, Mumbai, India, for his encouragement and support throughout the study.

Financial support and sponsorship

Nil.

Conflicts of interest

There are no conflicts of interest.

References

1. Titt U, Vassiliev ON, Pönisch F, Dong L, Liu H, Mohan R. A flattening filter free photon treatment concept evaluation with Monte Carlo. Med Phys 2006;33:1595-602.
2. Cashmore J. The characterization of unflattened photon beams from a 6 MV linear accelerator. Phys Med Biol 2008;53:1933-46.
3. Georg D, Knöös T, McClean B. Current status and future perspective of flattening filter free photon beams. Med Phys 2011;38:1280-93.
4. Tsiamas P, Sajo E, Cifter F, Theodorou K, Kappas C, Makrigiorgos M, *et al.* Beam quality and dose perturbation of 6 MV flattening-filter-free linac. Phys Med 2014;30:47-56.
5. Georg D, Kragl G, Wetterstedt Sa, McCavana P, McClean B, Knöös T. Photon beam quality variations of a flattening filter free linear accelerator. Med Phys 2010;37:49-53.
6. Pönisch F, Titt U, Vassiliev ON, Kry SF, Mohan R. Properties of unflattened photon beams shaped by a multileaf collimator. Med Phys 2006;33:1738-46.
7. Kragl G, af Wetterstedt S, Knäusl B, Lind M, McCavana P, Knöös T, *et al.* Dosimetric characteristics of 6 and 10 MV unflattened photon beams. Radiother Oncol 2009;93:141-6.
8. Kragl G, Baier F, Lutz S, Albrich D, Dalaryd M, Kroupa B, *et al.* Flattening filter free beams in SBRT and IMRT: Dosimetric assessment of peripheral doses. J Med Phys 2011;21:91-101.
9. Lang S, Reggiori G, Puxeu Vaquee J, Calle C, Hrbacek J, Klock S, *et al.* Pretreatment quality assurance of flattening filter free beams on 224 patients for intensity modulated plans: A multicentric study. Med Phys 2012;39:1351-6.
10. Cashmore J, Ramtohul M, Ford D. Lowering whole-body radiation doses in pediatric intensity-modulated radiotherapy through the use of unflattened photon beams. Int J Radiat Oncol Biol Phys 2011;80:1220-7.
11. Stathakis S, Esquivel C, Gutierrez A, Buckey CR, Papanikolaou N. Treatment planning and delivery of IMRT using 6 and 18 MV photon beams without flattening filter. Appl Radiat Isot 2009;67:1629-37.
12. O'Brien PF, Gillies BA, Schwartz M, Young C, Davey P. Radiosurgery with unflattened 6-MV photon beams. Med Phys 1991;18:519-21.
13. Fu W, Dai J, Hu Y, Han D, Song Y. Delivery time comparison for intensity-modulated radiation therapy with/without flattening filter: A planning study. Phys Med Biol 2004;49:1535-47.
14. Vassiliev ON, Titt U, Pönisch F, Kry SF, Mohan R, Gillin MT. Dosimetric properties of photon beams from a flattening filter free clinical accelerator. Phys Med Biol 2006;51:1907-17.
15. Vassiliev ON, Titt U, Kry SF, Pönisch F, Gillin MT, Mohan R. Monte Carlo study of photon fields from a flattening filter-free clinical accelerator. Med Phys 2006;33:820-7.
16. Huang Y, Siochi RA, Bayouth JE. Dosimetric properties of a beam quality-matched 6 MV unflattened photon beam. J Appl Clin Med Phys 2012;13:3701.
17. Dalaryd M, Kragl G, Ceberg C, Georg D, McClean B, af Wetterstedt S, *et al.* A Monte Carlo study of a flattening filter-free linear accelerator verified with measurements. Phys Med Biol 2010;55:7333-44.
18. Kry SF, Howell RM, Polf J, Mohan R, Vassiliev ON. Treatment vault shielding for a flattening filter-free medical linear accelerator. Phys Med Biol 2009;54:1265-73.
19. Jank J, Kragl G, Georg D. Impact of a flattening filter free linear

accelerator on structural shielding design. Z Med Phys 2014;24:38-48.
20. NCRP. Structural Shielding Design and Evaluation for Megavoltage X- and Gamma-Ray Radiotherapy Facilities. Report No. 151. Bethesda, Maryland, USA: National Council on Radiation Protection and Measurements (NCRP); 2005.
21. IEC. Medical Electrical Equipment: Particular Requirements for the basic safety and essential performance of Electron Accelerators in the Range 1 MeV to 50 MeV (60601-2-1). 3rd ed. Geneva, Switzerland: International Electrotechnical Commission (IEC); 2009.
22. IAEA. Radiation Protection in the Design of Radiotherapy Facilities. Safety Reports Series No. 47. Vienna, Austria: International Atomic Energy Agency (IAEA); 2006.

Original Article

Hesperidin as Radioprotector against Radiation-induced Lung Damage in Rat: A Histopathological Study

Gholam Hassan Haddadi, Abolhasan Rezaeyan[1], Mohammad Amin Mosleh-Shirazi[2], Massood Hosseinzadeh[3], Reza Fardid, Masoud Najafi[4], Ashkan Salajegheh

Department of Radiology, School of Paramedical Sciences, Shiraz University of Medical Sciences, Departments of [2]Radiotherapy and [3]Pathology, School of Medicine, Shiraz University of Medical Sciences, Shiraz, [1]Department of Medical Physics, School of Medicine, Iran University of Medical Sciences, [4]Department of Medical Physics and Biomedical Engineering, Faculty of Medicine, Tehran University of Medical Sciences, Tehran, Iran

Abstract

Reactive oxygen species (ROS) are generated by ionizing radiation, and one of the organs commonly affected by ROS is the lung. Radiation-induced lung injury including pneumonia and lung fibrosis is a dose-limiting factor in radiotherapy (RT) of patients with thorax irradiation. Administration of antioxidants has been proved to protect against ROS. The present study was aimed to assess the protective effect of hesperidin (HES) against radiation-induced lung injury of male rats. Fifty rats were divided into three groups. G1: Received no HES and radiation (sham). G2: Underwent γ-irradiation to the thorax. G3: Received HES and underwent γ-irradiation. The rats were exposed to a single dose of 18 Gy using cobalt-60 unit and were administered HES (100 mg/kg) for 7 days before irradiation. Histopathological analysis was performed 24 h and 8 weeks after RT. Histopathological results in 24 h showed radiation-induced inflammation and presence of more inflammatory cells as compared to G1 ($P < 0.05$). Administration of HES significantly decreased such an effect when compared to G2 ($P < 0.05$). Histopathological evaluation in 8 weeks showed a significant increase in mast cells, inflammation, inflammatory cells, alveolar thickness, vascular thickness, pulmonary edema, and fibrosis in G2 when compared to G1 ($P < 0.05$). HES significantly decreased inflammatory response, fibrosis, and mast cells when compared to G2 ($P < 0.05$). Administration of HES resulted in decreased radiation pneumonitis and radiation fibrosis in the lung tissue. Thus, the present study showed HES to be an efficient radioprotector against radiation-induced damage in the lung of tissue rats.

Keywords: Hesperidin, lung fibrosis, pneumonia, radioprotector

Received on: 09-11-2016 **Review completed on: 19-01-2017** **Accepted on: 22-01-2017**

Introduction

Ionizing radiation (IR) generates reactive oxygen species (ROS) and disrupts the structure of chemical bonds. Absorbed energy of IR causes ionization of different atoms and molecules, comprising H_2O and essential macromolecules such as DNA and membrane lipids.[1,2] The harmful role of IR is mainly due to ROS, including superoxide radical ($O_2^{\circ-}$), hydroxyl radical (OH°), and hydrogen peroxide generated by the decomposition of water.[3] ROS play significant role in many physiological and pathological reactions that may cause injury or disease. IR can increase production of ROS through interaction with water molecules, activation of redox system, and inhibition of antioxidant enzymes.[4] The lung is a radiosensitive organ and one of the organs commonly affected by ROS.

Radiotherapy (RT) is commonly applied as a part of cancer treatment, and it is assessed that more than half of all cancer patients will receive RT.[5] The lung is irradiated in patients with thoracic-region tumors that include breasts, lung, esophagus, lymphomas, and other mediastinal neoplasms.[6] Lung injuries are classified into two phases. The first (early) phase is named radiation pneumonitis (acute syndrome). According to histopathological evaluation, acute syndrome evidenced by loss of Type I pneumocytes, alveolar capillary congestion, increased capillary permeability, inflammatory cell accumulation, and interstitial edema in the alveolar space. These injuries reveal at approximately 1–6 months after RT in 10%–15% of patients who received chest region

Access this article online

Quick Response Code:

Website: www.jmp.org.in

DOI: 10.4103/jmp.JMP_119_16

Address for correspondence: Dr. Abolhasan Rezaeyan, Department of Medical Physics, School of Medicine, Iran University of Medical Sciences, Tehran, Iran.
E-mail: ahrezaeyan@gmail.com

How to cite this article: Haddadi GH, Rezaeyan A, Mosleh-Shirazi MA, Hosseinzadeh M, Fardid R, Najafi M, *et al*. Hesperidin as radioprotector against radiation-induced lung damage in rat: A histopathological study. J Med Phys 2017;42:XX.

irradiation.[7-10] According to histopathological changes in this phase, the first symptom of a lung injury is extensive alveolar damage.[11] The second or latent phase (chronic syndrome) is pulmonary fibrosis that occurs months to years after RT. The pathologic findings in pulmonary fibrosis characterized by excessive accumulation of extracellular matrix (ECM) and reshaping of the lung structure.[12] Pulmonary fibrosis is the repair process of pneumonitis radiation that usually develops with the loss of capillaries, thickened alveolar septa, and obliteration of the alveolar space.[10] Mast cells are immune effectors involved in allergic and hypersensitivity reactions that are actively implicated in a number of physiological and pathological situations, varying from normal wound healing and host defense to tissue inflammation and tumor growth.[13-15] Pathologically, mast cells contribute to alveolitis development through the secretion of chemokines and cytokines that serve to recruit inflammatory cells.[16,17]

In spite of improving the clinical RT treatment planning and delivery technologies, there is a considerable toxicity of RT for normal tissues.[18] To attain optimum treatment, the normal tissues should be protected against radiation damage. Thus, radioprotective compounds are essential in clinical RT.[19] Among varieties of radioprotectors, most failed because of their toxicity and side effects. The search for radioprotectors with less toxicity has motivated interest in the development of natural products that prevent damaging effects of IR and have some proven therapeutic advantages.[20]

Hesperidin (HES) (hesperetin-7-rhamnoglucoside), a flavanone glycoside, is a member of the flavonoids. Flavonoids are a family of natural polyphenolic structures that are found in fruits and vegetables. HES is the major flavonoids that discovered in sweet orange and lemon. In immature oranges, it has up to 14% of the weight of the fruit.[21,22] HES has been reported to exert a wide range of pharmacological effects, which include anticarcinogenic, antiallergic, vasoprotective, hypolipidemic, antioxidant, and anti-inflammatory actions.[23,24] These biological effects of HES are mainly associated with their antioxidant properties. Histopathologically, several investigations have demonstrated that HES has radioprotective effect against normal tissues exposed to RT.[25-28] This study was performed to evaluate the protective effect of HES against γ-irradiation-induced acute and chronic lung injury in male Sprague–Dawley rats.

Materials and Methods

Animals

In this study, chemical materials including HES (CAS registry number: 520-26-3) and phosphate-buffered saline tablet (PBS) were purchased from Sigma Chemical Co. (St. Louis, MO, USA). Healthy adult male Sprague–Dawley rats were purchased from the Center for Comparative and Experimental Medicine, Shiraz University of Medical Sciences (SUMS), Shiraz, Iran. The rats weighed around 220 ± 5 g and were housed in accordance with particular practices described in "The Guide for The Care and Use of Laboratory Animals" arranged by SUMS in the university animal house. The practices involved some specific measures which include as follows: characteristics of animal natural life in captivity situation, using spacious cages, preparing appropriate ventilation and light, handling with care, giving standard pellet diet and water *ad libitum*, etc. All the animals were housed in certain circumstances including temperature (23 ± 2°C), humidity (55% ±5%), and light (12 h of light and dark cycle). Besides, four animals were separately housed together in polypropylene cages containing sterile husk bedding during the experiments, and this study was conducted based on the instructions issued by the SUMS' Ethical Committee.

Animal exposure

Rats were anesthetized before exposing to radiation using ketamine at a dose of 80 mg/kg and xylazine at a dose of 5 mg/kg with an intraperitoneal injection. Accordingly, the rats were immobilized in the supine position by taping the extremities on a well-ventilated plexiglass container. A cobalt-60 γ-radiation source (Theratron Phoenix, Canada) was used to irradiate the animals in the Department of RT, Nemazee Teaching Hospital, Shiraz, Iran. In three groups, simultaneously, the anesthetized rats were irradiated locally on the thorax. The source-to-skin distance was 55 cm with a dose rate of 300 mGy/min at room temperature. The rats were irradiated with a single dose of 18 Gy γ-rays. In fact, this dose was selected according to the results published by Tahamtan *et al*., in which they declared that a single dose of 18 Gy develops considerable radiation lung injury.[29]

HES was dissolved in PBS (pH 7.6) and then administered orally using a ball-tipped needle for seven consecutive days before exposure to γ-irradiation. In addition, the drug was freshly prepared every day. Dose of 100 mg/kg was selected for this study based on the previous reports by Rezaeyan *et al*., Hosseinimehr and Nemati, and Pradeep *et al*. They have shown that 100 mg/kg has protective effect against radiation-induced damage in lung, heart, liver, kidney and bone marrow.[30,31] To prepare this dose, 22 mg of HES was dissolved in 2 ml of PBS.

Experimental design

In this course of action, 50 male rats were randomly separated into three groups. Group 1 (sham): Fourteen rats were earmarked as controls which only received PBS for 7 days. Group 2 (RT): Eighteen rats received PBS for 7 days and exposed to γ-irradiation 1 h after the last dose of PBS. Group 3 (HES + RT): Eighteen rats were treated with HES for 7 days and exposed to γ-irradiation 1 h after the last dose of HES. After the last administration of PBS at the 7th day, like rats in RT and HES + RT groups, the rats of sham group were anesthetized. In each group, eight rats were sacrificed 24 h after RT for acute histopathological evaluation. Moreover, 26 animals remained (sham = 6, RT = 10, and HES + RT = 10) were sacrificed 8 weeks after RT for chronic histopathological evaluation.

Histopathological evaluation

Rats were anesthetized with ketamine and xylazine. After extracting the lungs from the chest, tissue was fixed, infused with 10% neutral-buffered formalin introduced through the airways, and then laid into paraffin. Whole-mount sections of the lungs were cut (5 μm), processed, and stained with H and E, Masson's trichrome (MTC), and acid-fast (AF). All the histological works were performed at the Unit of Pathology, Faghihee Teaching Hospital, Shiraz, Iran. The blinded histopathological evaluation was carried out using the light microscope (Olympus BX41TF, Japan). Semi-quantitative scoring of each variable was performed by a histopathologist using the following scales: (1) No change, (2) mild, (3) moderate, and (4) severe injury. In the acute phase, the descriptive items for radiation-induced lung injuries were as follows: Presence of neutrophils, macrophages, lymphocytes and incidence of inflammation, erythrocytes (red blood cell [RBC]), hyaline arteriosclerosis, vascular thickness, alveolar thickness, and collapse. On the other hand, those of chronic phase included the presence of macrophages, neutrophils, and lymphocytes; incidence of inflammation, alveolar thickness, vascular thickness, pulmonary edema, thrombosis and pulmonary fibrosis; and presence of mast cells. Sections were stained using H and E for general tissue characterization.[32] Moreover, collagen accumulation was assessed by preparing tissue sections with MTC stain.[33,34] The AF stain was used to evaluate mast cells.[35,36] The lung index was calculated as lung index = (lung weight/body weight) ×100.

Statistical analysis

In this study, data were analyzed using a commercially available statistical software package (SPSS® for Windows v. 19, Chicago, IL, USA). Histopathological evaluations were analyzed by the Pearson Chi-square test and a pair-wise comparison with Mann–Whitney. Furthermore, to evaluate the body weight, lung weight, and lung index, a one-way ANOVA test with *post hoc* Tukey honestly significant difference was performed. The survival rate was evaluated with Kaplan–Meier method. The results are presented as mean ± standard deviation. We considered $P < 0.05$ as statistically significant difference.

Results

Physical examination and survival rate

Figure 1 and Table 1 illustrate the results of the survival rate, body weights, lung weights, and lung indexes of control versus experimental rats evaluated 8 weeks after local-thorax irradiation. Before irradiation, rats were preadministered with 100 mg/kg/d of HES for seven consecutive days, and then, monitoring was done to observe their reaction daily and bimonthly. The results showed that the rats received 18 Gy radiation exhibited symptoms of discomfort which was characterized by reduction not only in physical activity but also in uptake of food and water. Besides, the radiation-exposed groups showed symptoms of radiation sickness such as irritability, ruffling of hair, weight loss, emaciation, and epilation. On the contrary, those rats which were preadministered with HES had reduced symptoms of radiation sickness and significantly enhanced physical activity, body weight, and survival rate.

Histopathological examination

Acute phase

At 24 h postirradiation, the sham, RT, and HES + RT groups were evaluated through histopathological observation of the lung sections [Figure 2]. Meanwhile, the descriptive factors examined include the presence of neutrophils, macrophages, and lymphocytes and incidence of inflammation, erythrocytes (RBC), hyaline arteriosclerosis, vascular thickness, alveolar thickness, and collapse. According to the results, between-group analysis demonstrated only a significant difference in the inflammation, lymphocyte, macrophage, and neutrophil ($P = 0.001$, $P = 0.009$, $P = 0.001$, $P = 0.001$, respectively). Between-group analysis was performed by a pair-wise comparison with Mann–Whitney test and $P < 0.05$, which indicates a significant difference [Table 2]. The results indicated significant increases in inflammation, lymphocyte,

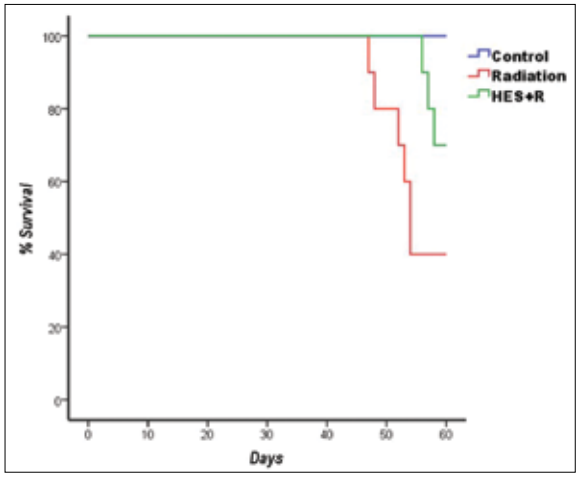

Figure 1: Dose-dependent effect of hesperidin on the survival rate of rats observed for an experimental duration of 60 days. Sham group: Six rats out of six were survived. Radiotherapy group: Four rats out of ten survived. Hesperidin + radiotherapy group: Seven rats out of ten survived.

Table 1: Effect of hesperidin treatment on body weight, lung weight, and lung index of rats exposed to γ-irradiation

	Body weight (g)	Lung weight (g)	Lung index
Sham	312.16±16.3	2.33±0.26	0.74±0.06
RT	227.16±28.2[a]	3.97±0.57[a]	1.78±0.42[a]
HES + RT	302.00±11.2[b]	3.00±0.19[b]	0.99±0.07[b]

Values are expressed as mean±SD. $P<0.05$, statistically significant when compared between groups versus [a]Sham group, or [b]RT group. RT: Radiotherapy, HES + RT: Hesperidin + radiotherapy, SD: Standard deviation

macrophage, and neutrophil frequency in RT group when compared with sham group ($P = 0.001$). In the HES + RT group, treatment with HES contributed a decrease in these factors to near normal values when compared to RT group ($P = 0.003$, $P = 0.017$, $P = 0.001$, $P = 0.001$, respectively).

Chronic phase

With respect to the lung sections in the sham, RT, and HES + RT groups at 8 weeks after radiation, histopathological evaluations were conducted to characterize the chronic changes in lung tissues after RT [Figures 3-5]. The descriptive factors examined were the presence of macrophages, lymphocytes, and neutrophils (inflammatory cells), incidence of inflammation, alveolar thickness, vascular thickness, pulmonary edema, thrombosis, pulmonary fibrosis, and infiltration of mast cells.

The statistical results of the left lung were found to be as follows: A significant difference between groups was observed in the presence of inflammatory cells, incidence of inflammation, alveolar thickness, vascular thickness, and pulmonary fibrosis, and presence of mast cells, but with the exception of pulmonary edema and thrombosis. The pair-wise comparison was performed in the experimental groups [Table 3]. Compared to the sham group, the radiation-induced lung injury factors were significant in the RT group ($P < 0.05$). A majority of factors such as frequency of inflammatory cells and mast cells and the incidence of inflammation, pulmonary fibrosis, alveolar thickness, and vascular thickness increased in irradiated lungs as compared to the sham group. Pulmonary edema and thrombosis signs were not found in the left lung of each group. The administration of HES before radiation reduced the vascular damage ($P = 0.013$) and the incidence of fibrosis ($P = 0.012$), inflammation ($P = 0.006$), frequency of mast cell ($P = 0.033$), macrophage ($P = 0.001$), lymphocyte ($P = 0.026$), and neutrophil ($P = 0.013$) in the HES + RT group when compared to RT group, but no significant difference was observed for vascular thickness ($P > 0.05$). Besides, except lymphocyte, pulmonary edema, and thrombosis, a significant difference was spotted for these factors to compare between the groups of HES + RT and sham.

In the right lung, according to the results, a significant difference between groups was found in all of the mentioned histopathological factors ($P < 0.05$). To pair-wise comparison in the groups of radiation and control, all of these factors showed a significant difference ($P < 0.05$) [Table 3]. To pair-wise comparison in the groups of HES + R and radiation, the HES administration reduced signs of pulmonary fibrosis ($P = 0.005$), alveolar thickness ($P = 0.016$), pulmonary edema ($P = 0.004$), thrombosis ($P = 0.001$), mast cells ($P = 0.003$), inflammation ($P < 0.001$), and inflammatory cells ($P < 0.05$). As similar to the left lung, HES cannot

Table 2: Effect of hesperidin treatment at 24 h postirradiation on histopathological factors in the lung tissue of rats

	Sham	RT	HES + RT
Inflammation	1.13±0.354	3.13±0.835[a]	1.63±0.518[b]
Lymphocyte	1.13±0.354	3.13±0.835[a]	1.88±0.835[b]
Macrophage	1.38±0.744	3.63±0.518[a]	1.75±0.707[b]
Neutrophil	1.25±0.463	3.25±0.707[a]	1.63±0.518[b]

Values are expressed as mean±SD $P<0.05$, statistically significant when compared between groups versus [a]Sham group, or [b]RT group.
RT: Radiotherapy, HES + RT: Hesperidin + radiotherapy, SD: Standard deviation

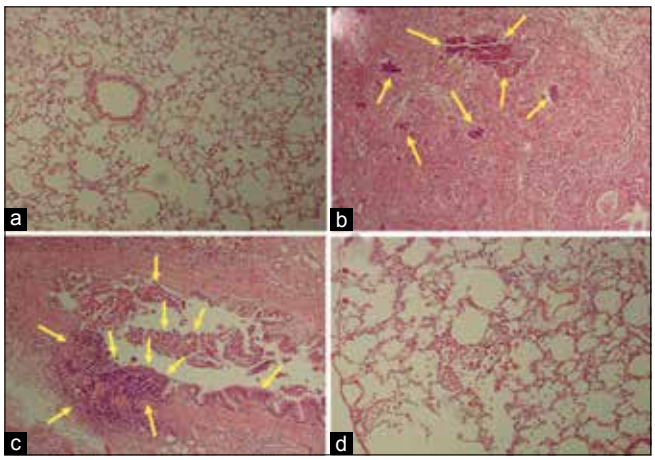

Figure 2: Histopathological investigation of the radioprotective effects of hesperidin and radiation damage in the acute phase (24 h). (a) Sham: Alveolar space, bronchioles, and vascular bed are seen normal. (b) Radiotherapy: Severe interstitial inflammation and pulmonary edema is seen. (c) Radiotherapy: Severe inflammation of bronchial wall is seen with destruction of bronchus. (d) Hesperidin + radiotherapy: Mild inflammation was observed. The arrows indicate an accumulation of lymphocyte, macrophages, and neutrophils in lung tissue (H and E, ×100).

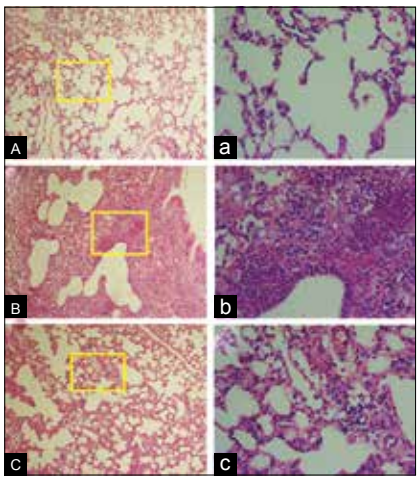

Figure 3: Histopathological investigation of the radioprotective effects of hesperidin and radiation damage in the chronic phase (8 weeks). (A and a) Sham: Alveolar space, bronchioles, and vascular bed are seen normal. (B and b) Radiotherapy: Acute inflammation in the alveolar space, thickening of alveolar and pulmonary edema is seen with polymorphonuclear leukocyte (neutrophils accumulation). (C and c) Hesperidin + radiotherapy: Mild inflammation was observed. The yellow frame shows a magnification of ×400. (H and E, ABC: Magnification ×100, abc: Magnification ×400).

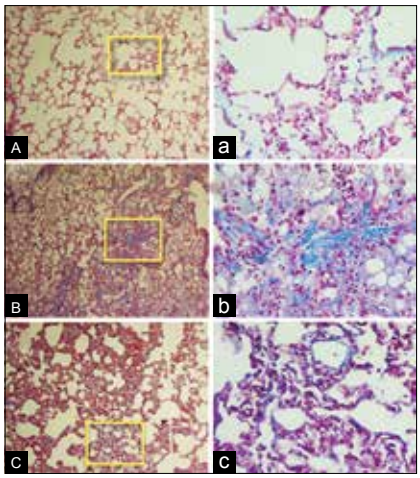

Figure 4: Histopathological investigation of the radioprotective effects of hesperidin and radiation damage in the chronic phase (8 weeks). (A and a) Sham: Alveolar space, bronchioles and vascular bed are seen normal. (B and b) Radiotherapy: Acute collagen deposition is seen. (C and c) Hesperidin + radiotherapy: Deposition of collagen is seen as mild. Collagen deposition is seen light blue. The yellow frame shows a magnification of ×400. (Massonæs trichrome staining, ABC: Magnification ×100, abc: Magnification ×400).

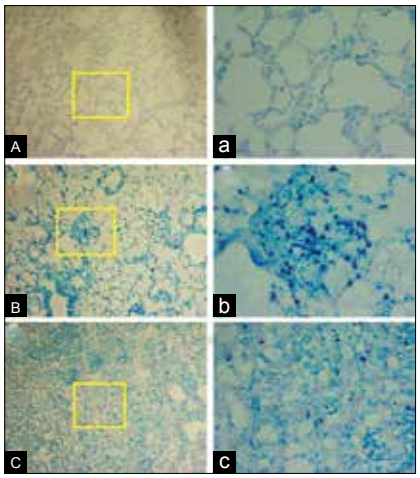

Figure 5: Histopathological investigation of the radioprotective effects of hesperidin and radiation damage in the chronic phase (8 weeks). (A and a) Sham: Alveolar space, bronchioles and vascular bed are seen normal. (B and b) Radiotherapy: Acute mast cells infiltration is seen. (C and c) Hesperidin + radiotherapy: Infiltration of mast cells is seen as mild. Mast cells are seen dark blue points. The yellow frame shows a magnification of ×400. (Acid-fast staining, ABC: Magnification ×100, abc: Magnification ×400).

reduce vascular thickness ($P = 0.698$). In addition, comparing the groups of HES + R and control, a significant difference was observed for these factors except for lymphocyte, inflammation, pulmonary edema, and thrombosis ($P > 0.05$). Overall, in the radiation group, the microscopic results and statistical analysis show histopathological damage in the left lung lesser than the right lung. Further, in the HES + R group, HES treatment reduced lung injury in the left lung more than the right lung, except lymphocyte and inflammation.

Discussion

Radiation-induced tissue damage is mediated generally by either direct attack on the genetic material or by generating ROS by the radiolysis of water (activation of redox systems and inhibition of antioxidant system) that assault the cellular macromolecules. Lung tissue damage includes damage to endothelial cells by increasing the permeability, edema, and fibrin accumulation of ECM. These changes are associated with an inflammatory response, including accumulation and activation of macrophage, inflammatory cells, chemokines, cytokines, and endothelial–leukocyte adhesion molecules that are attached to the damaged area or involved in inflammation.[8] Since ROS play the main role in radiation toxicity, administration of antioxidants may be important for patients who have experienced RT to deter normal tissues from damages.

Animals receiving higher doses of radiation are usually reported to exhibit signs of radiation sickness.[37] In this study, rats that received 18 Gy of γ-irradiation showed signs of discomfort, characterized by a decreased physical activity, and decreased uptake of food and water. In contrast, the rats that were treated with HES showed reduced signs of radiation sickness and appeared normal. Treatment with HES showed for 7 days significantly improved their body weight and lung weight. This result is very important because it is an important side effect in lung radiation adversely impacts nutritional intake which accounts for fatigue and weakness of patients. Therefore, it is established beyond doubt that malnutrition reduces treatment probability, survival, and quality of life.[38-40]

Radiation-induced inflammatory response is related to various cellular and molecular pathways. Molecular pathways including exudation of several cytokines such as tumor necrosis factor-α, interferon-γ, transforming growth factor-β, interleukin-1 (IL-1), IL-6, and IL-8. These cytokines increase expression of MAPKs, NF-κB, NADPH oxidase, inducible nitric oxide synthase (iNOS), and cyclooxygenase-2. NADPH oxidase is generated by neutrophils and iNOS is induced by macrophages.[41] Inflammatory response in the lung tissue is described by vascular thickness change, leukocytes infiltration, and increased number of macrophages, neutrophils, and lymphocytes. On the other hand, pieces of evidence indicated that mast cells have been involved in inflammation and have been associated with early and delayed radiation damages, including tissue remodeling and fibrosis.[42,43] Preclinical reports on the role of mast cells in radiation injury show that these cells were associated with radiation fibrosis and collagen deposition in the lung tissue of rat.[44,45]

In this investigation, radiation increased the counts of macrophages, neutrophils, and lymphocytes and that resulted in the occurrence of inflammation at 24 h postirradiation [Table 2]. Supplementation with HES before irradiation reduces inflammatory cells including macrophages, neutrophils, and

Table 3: Effect of hesperidin treatment at 8 weeks postirradiation on histopathological factors in the lung tissue of rats

	Control	RT	HES + RT
Macrophage			
Left lung	1.33±0.211	3.20±0.200[a]	2.00±0.149[b]
Right lung	1.50±0.224	3.80±0.133[a]	2.20±0.200[b]
Lymphocyte			
Left lung	1.50±0.224	3.10±0.180[a]	2.30±0.260[b]
Right lung	1.33±0.211	3.70±0.153[a]	2.20±0.291[b]
Neutrophil			
Left lung	1.50±0.224	3.10±0.180[a]	2.30±0.213[b]
Right lung	1.50±0.224	3.70±0.153[a]	2.50±0.269[b]
Inflammation			
Left lung	1.33±0.211	3.30±0.213[a]	2.20±0.249[b]
Right lung	1.33±0.211	3.90±0.100[a]	2.00±0.333[b]
Fibrosis			
Left lung	1.17±0.167	3.10±0.233[a]	2.10±0.233[b]
Right lung	1.33±0.211	3.60±0.163[a]	2.40±0.306[b]
Mast cell			
Left lung	1.00±0.00	2.90±0.233[a]	2.10±0.277[b]
Right lung	1.33±0.211	3.60±0.221[a]	2.20±0.291[b]
Alveolar thickness			
Left lung	1.00±0.00	2.90±0.180[a]	1.90±0.277[b]
Right lung	1.33±0.211	3.60±0.163[a]	2.60±0.306[b]
Vascular thickness			
Left lung	1.00±0.00	2.20±0.249[a]	2.20±0.249
Right lung	1.00±0.00	2.70±0.153[a]	2.50±0.307
Pulmonary edema			
Left lung	1.00±0.00	1.00±0.00	1.00±0.00
Right lung	1.00±0.00	2.00±0.00[a]	1.40±0.163[b]
Thrombosis			
Left lung	1.00±0.00	1.00±0.00	1.00±0.00
Right lung	1.17±0.167	2.00±0.00[a]	1.30±0.153[b]

Values are expressed as mean±SD. $P<0.05$, statistically significant when compared between groups versus [a]Sham group, or [b]RT group. RT: Radiotherapy, HES + RT: Hesperidin + radiotherapy, SD: Standard deviation

lymphocytes resulting in reduced inflammation [Figure 2]. This reveals HES can decrease acute inflammatory pathways induced by exposure to γ-radiation. In the RT group, histopathological evaluation of the lung sections at 8 weeks after irradiation showed an increase in inflammation, fibrosis, alveolar thickness, vascular thickness, pulmonary edema, and number of mast cells and inflammatory cells [Table 3]. The pulmonary edema and thrombosis signs were not found in the left lung of radiation group. In the left lung of radiation group, histopathological damage is lesser than the right lung. Supplementation with HES before radiation could reduce inflammation, fibrosis, and number of mast cells, inflammatory cells, alveolar thickness, pulmonary edema, and thrombosis significantly [Figures 3-5]. Furthermore, reduction of vascular thickness was not significant. Overall, in the HES + R group, HES treatment reduced lung injury in the left lung more than the right lung, except lymphocyte and inflammation.

According to previous studies, oral administration of HES can reduce γ-radiation-induced damage in the lung tissue of rats. HES acts by scavenging free radicals and by maintaining intracellular superoxide dismutase (SOD) and glutathione levels, thereby preventing lipid peroxidation and tissue damage.[28] In another similar study, the irradiation of the whole thorax of the rats with 18 Gy, a single dose of X-ray resulted in oxidative stress and histopathological changes in the heart tissue. The early oxidative stress is associated with the increased malondialdehyde level and decreased SOD enzyme activity. Long-term changes such as inflammation, fibrosis, increased mast cells and macrophages, plaque, vascular leakage and myocardial degeneration were observed in both right and left ventricles. Preadministration of HES is used to ameliorate oxidative stress, histopathological changes, and subsequent cell death after radiation treatment, which can cause the increased risk of heart diseases during years after RT.[27] Some studies showed HES supplement reduces oxidative and pathologic damages induced by IR in the liver, heart, and kidney.[25,26,31]

These investigations show that HES ameliorates inflammation signs including reduction of macrophages accumulation specially. Macrophages have a major role in acute and chronic inflammation and oxidative stress in lung tissues. Hence, administration of supplements that alleviate of macrophage activity can be advantageous. HES also has been reported to exert a protective effect on lung tissues that include modulated expression of pro-inflammatory cytokines and chemokines, reduction of polymorphonuclear neutrophils secretion in the airway, and improved pulmonary edema and lung morphology. HES effectively reduces pulmonary vascular permeability and leads to ameliorate pulmonary edema.[46] Hence, HES may protect the integrity of the alveolar membrane, resulting in the prevention of the infiltration of mast cells, and significantly improves lung morphology. Thus, HES has anti-inflammatory and specific protective effects against inflammatory disorders which are done through a mechanism involving the antioxidant activity of free radicals.

Conclusions

It is known that HES has pharmacological effects including antioxidant, anti-inflammatory, and anticarcinogenic actions. The present study indicates that HES significantly diminishes γ-radiation-induced damage in the lung tissues of rats. It seems that HES may be used as a natural radioprotector with anti-inflammatory and antioxidant functions to prevent oxidative stress caused by IR in a short-term after irradiation and acute and chronic inflammation of lung tissue. Based on the results of this study, it is concluded that HES can be a candidate for treating and preventing radiation-induced damage to the tissues, particularly for patients undergoing RT. However, additional investigations are needed to understand the molecular and cellular mechanisms associated with the radioprotective properties of HES in the lungs.

Financial support and sponsorship

Nil.

Conflicts of interest

There are no conflicts of interest.

References

1. Lett JT. Damage to cellular DNA from particulate radiations, the efficacy of its processing and the radiosensitivity of mammalian cells. Emphasis on DNA double strand breaks and chromatin breaks. Radiat Environ Biophys 1992;31:257-77.
2. Dainiak N, Tan BJ. Utility of biological membranes as indicators for radiation exposure: Alterations in membrane structure and function over time. Stem Cells 1995;13 Suppl 1:142-52.
3. Ertekin MV, Koçer I, Karslioglu I, Taysi S, Gepdiremen A, Sezen O, *et al.* Effects of oral *Ginkgo biloba* supplementation on cataract formation and oxidative stress occurring in lenses of rats exposed to total cranium radiotherapy. Jpn J Ophthalmol 2004;48:499-502.
4. Najafi M, Fardid R, Takhshid MA, Mosleh-Shirazi MA, Rezaeyan AH, Salajegheh A. Radiation-induced oxidative stress at out-of-field lung tissues after pelvis irradiation in rats. Cell J 2016;18:340-5.
5. Ringborg U, Bergqvist D, Brorsson B, Cavallin-Ståhl E, Ceberg J, Einhorn N, *et al.* The Swedish Council on Technology Assessment in Health Care (SBU) systematic overview of radiotherapy for cancer including a prospective survey of radiotherapy practice in Sweden 2001 – summary and conclusions. Acta Oncol 2003;42:357-65.
6. Stone HB, Coleman CN, Anscher MS, McBride WH. Effects of radiation on normal tissue: Consequences and mechanisms. Lancet Oncol 2003;4:529-36.
7. Citrin D, Cotrim AP, Hyodo F, Baum BJ, Krishna MC, Mitchell JB. Radioprotectors and mitigators of radiation-induced normal tissue injury. Oncologist 2010;15:360-71.
8. Marks LB, Yu X, Vujaskovic Z, Small W Jr., Folz R, Anscher MS. Radiation-induced lung injury. Semin Radiat Oncol 2003;13:333-45.
9. Yarnold J, Brotons MC. Pathogenetic mechanisms in radiation fibrosis. Radiother Oncol 2010;97:149-61.
10. Kong FM, Ten Haken R, Eisbruch A, Lawrence TS. Non-small cell lung cancer therapy-related pulmonary toxicity: An update on radiation pneumonitis and fibrosis. Semin Oncol 2005;32 2 Suppl 3:S42-54.
11. Gross NJ. Experimental radiation pneumonitis. IV. Leakage of circulatory proteins onto the alveolar surface. J Lab Clin Med 1980;95:19-31.
12. Takishima T, Shimura S. Definition and classification of pulmonary fibrosis. In: Takishima T, editor. Basic and Clinical Aspects of Pulmonary Fibrosis. Boca Raton, FL: CRC Press; 1994. p. 293-303.
13. Weller K, Foitzik K, Paus R, Syska W, Maurer M. Mast cells are required for normal healing of skin wounds in mice. FASEB J 2006;20:2366-8.
14. Galli SJ, Tsai M. Mast cells: Versatile regulators of inflammation, tissue remodeling, host defense and homeostasis. J Dermatol Sci 2008;49:7-19.
15. Maltby S, Khazaie K, McNagny KM. Mast cells in tumor growth: Angiogenesis, tissue remodelling and immune-modulation. Biochim Biophys Acta 2009;1796:19-26.
16. Arpin D, Perol D, Blay JY, Falchero L, Claude L, Vuillermoz-Blas S, *et al.* Early variations of circulating interleukin-6 and interleukin-10 levels during thoracic radiotherapy are predictive for radiation pneumonitis. J Clin Oncol 2005;23:8748-56.
17. Chen Y, Williams J, Ding I, Hernady E, Liu W, Smudzin T, *et al.* Radiation pneumonitis and early circulatory cytokine markers. Semin Radiat Oncol 2002;12 1 Suppl 1:26-33.
18. Greenberger JS. Radioprotection. *In Vivo* 2009;23:323-36.
19. Nair CK, Parida DK, Nomura T. Radioprotectors in radiotherapy. J Radiat Res 2001;42:21-37.
20. Maurya DK, Devasagayam TP, Nair CK. Some novel approaches for radioprotection and the beneficial effect of natural products. Indian J Exp Biol 2006;44:93-114.
21. Tiwari AK. Imbalance in antioxidant defense and human diseases: Multiple approach of natural antioxidants therapy. Curr Sci 2001;81:1179-87.
22. Barthe GA, Jourdan PS, McIntosh CA, Mansell RL. Radioimmunoassay for the quantitative determination of hesperidin and analysis of its distribution in Citrus sinensis. Phytochemistry 1988;27:249-54.
23. Tommasini S, Calabrò ML, Stancanelli R, Donato P, Costa C, Catania S, *et al.* The inclusion complexes of hesperetin and its 7-rhamnoglucoside with (2-hydroxypropyl)-beta-cyclodextrin. J Pharm Biomed Anal 2005;39:572-80.
24. Emim JA, Oliveira AB, Lapa AJ. Pharmacological evaluation of the anti-inflammatory activity of a citrus bioflavonoid, hesperidin, and the isoflavonoids, duartin and claussequinone, in rats and mice. J Pharm Pharmacol 1994;46:118-22.
25. Kalpana KB, Devipriya N, Srinivasan M, Vishwanathan P, Thayalan K, Menon VP. Evaluating the radioprotective effect of hesperidin in the liver of Swiss albino mice. Eur J Pharmacol 2011;658:206-12.
26. Pradeep K, Ko KC, Choi MH, Kang JA, Chung YJ, Park SH. Protective effect of hesperidin, a citrus flavanoglycone, against κ-radiation-induced tissue damage in Sprague-Dawley rats. J Med Food 2012;15:419-27.
27. Rezaeyan A, Haddadi GH, Hosseinzadeh M, Moradi M, Najafi M. Radioprotective effects of hesperidin on oxidative damages and histopathological changes induced by X-irradiation in rats heart tissue. J Med Phys 2016;41:182-91.
28. Rezaeyan A, Farid R, Haddadi GH, Takhshid MA, Hosseinzadeh M, Najafi M, *et al.* Evaluating radioprotective effect of hesperidin on acute radiation damage in the lung tissue of rats. J Biomed Phys Eng 2016;6:165-174.
29. Tahamtan R, Shabestani Monfared A, Tahamtani Y, Tavassoli A, Akmali M, Mosleh-Shirazi MA, *et al.* Radioprotective effect of melatonin on radiation-induced lung injury and lipid peroxidation in rats. Cell J 2015;17:111-20.
30. Hosseinimehr SJ, Nemati A. Radioprotective effects of hesperidin against gamma irradiation in mouse bone marrow cells. Br J Radiol 2006;79:415-8.
31. Pradeep K, Park SH, Ko KC. Hesperidin a flavanoglycone protects against gamma-irradiation induced hepatocellular damage and oxidative stress in Sprague-Dawley rats. Eur J Pharmacol 2008;587:273-80.
32. Gamble M. The hematoxyline and eosin. In: Bancroft JD, Gamble M, editors. Theory and Practice of Histological Techniques. 6th ed. Philadelphia, PA: Churchill Livingstone/Elsevier; 2008. p. 121-34.
33. Jones ML, Bancroft JD, Gamble M. Connective tissues and stains. In: Bancroft JD, Gamble M, editors. Theory and Practice of Histological Techniques. 6th ed. Philadelphia, PA: Churchill Livingstone/Elsevier; 2008. p. 135-60.
34. Sheehan D, Hrapchak B. Theory and Practice of Histotechnology. 2nd ed. Ohio: Battelle Press; 1980.
35. Eagle RC. Eye Pathology: An Atlas and Text. 2nd ed. Philadelphia, PA; London Lippincott Williams & Wilkins; 2010.
36. Loew JM, Macon WR. Lymph nodes. In: Gattuso P, Reddy VB, David O, Spitz DJ, Haber MH, editors. Differential Diagnosis in Surgical Pathology. 2nd ed. Philadelphia, PA: W.B. Saunders; 2010. p. 761.
37. Meister M. The Health Effects of Low-Level Radiation. New York: American Council on Science and Health; 2005. p. 2-4.
38. Platek ME, Reid ME, Wilding GE, Jaggernauth W, Rigual NR, Hicks WL Jr., *et al.* Pretreatment nutritional status and locoregional failure of patients with head and neck cancer undergoing definitive concurrent chemoradiation therapy. Head Neck 2011;33:1561-8.
39. Isenring E, Bauer J, Capra S. The scored patient-generated subjective global assessment (PG-SGA) and its association with quality of life in ambulatory patients receiving radiotherapy. Eur J Clin Nutr 2003;57:305-9.
40. Ross PJ, Ashley S, Norton A, Priest K, Waters JS, Eisen T, *et al.* Do patients with weight loss have a worse outcome when undergoing chemotherapy for lung cancers? Br J Cancer 2004;90:1905-11.
41. Ding NH, Li JJ, Sun LQ. Molecular mechanisms and treatment of radiation-induced lung fibrosis. Curr Drug Targets 2013;14:1347-56.
42. Zheng H, Wang J, Hauer-Jensen M. Role of mast cells in early and delayed radiation injury in rat intestine. Radiat Res 2000;153(5 Pt 1):533-9.
43. Richter KK, Langberg CW, Sung CC, Hauer-Jensen M. Increased transforming growth factor beta (TGF-beta) immunoreactivity is independently associated with chronic injury in both consequential

and primary radiation enteropathy. Int J Radiat Oncol Biol Phys 1997;39:187-95.
44. Watanabe S, Watanabe K, Oishi T, Aiba M, Kageyama K. Mast cells in the rat alveolar septa undergoing fibrosis after ionizing irradiation. Ultrastructural and histochemical studies. Lab Invest 1974;31:555-67.
45. Ward WF, Molteni A, Ts'ao CH, Hinz JM. Captopril reduces collagen and mast cell accumulation in irradiated rat lung. Int J Radiat Oncol Biol Phys 1990;19:1405-9.
46. Yeh CC, Kao SJ, Lin CC, Wang SD, Liu CJ, Kao ST. The immunomodulation of endotoxin-induced acute lung injury by hesperidin *in vivo* and *in vitro*. Life Sci 2007;80:1821-31.

Technical Note

Evaluation of Intensity Modulated Radiation Therapy Delivery System using a Volumetric Phantom on the Basis of the Task Group 119 Report of American Association of Physicists in Medicine

Raphaela Avgousti, Christina Armpilia, Ioannis Floros[1], Christos Antypas

Department of Radiology, Medical Physics Unit, Aretaieion Hospital, University of Athens, Greece, [1]Department of Radiotherapy Physics, Nottingham University Hospital, NHS Trust, Nottingham, United Kingdom

Abstract

The current work describes the implementation of the American Association of Physicists in Medicine (AAPM)'s Task Group 119 report on a volumetric phantom (Delta^4, Scandidos, Uppsala, Sweden) following the stated dose goals, to evaluate the step-and-shoot intensity modulated radiation therapy (IMRT) system. Delta^4 consists of diode detectors, lying on two crossed planes, measuring the delivered dose, and providing two-dimensional dosimetric information. Seven plans of different goals and complexity were performed, with individual structure sets. TG199 structure sets and plans were transferred and implemented on the Delta^4 phantom taking into account its cylindrical geometry. All plans were delivered with a 6 MV linear accelerator equipped with multileaf collimator of 1 cm thickness. Plan results for each test met the recommended dose goals. The evaluation was performed in terms of dose deviation, distance to agreement, and gamma index passing rate. In all test cases, the gamma index passing rate was measured >90%. Delta^4 phantom has proven to be fast, applicable, and reliable for the step-and-shoot IMRT commissioning following TG119's recommended tests. Although AAPM's TG119 report is referring to the implementation of test plans that do not correspond to patient plans, it could be used as an evaluation tool of various IMRT systems, considering the local treatment planning system and the delivery system.

Keywords: Commissioning, intensity modulated radiation therapy, quality assurance, volumetric phantom

Received on: 11-10-2016 **Review completed on: 29-11-2016** **Accepted on: 01-12-2016**

Introduction

There are many articles and reports referring to the commissioning and the verification process of intensity-modulated radiation therapy (IMRT) system consisting of a linear accelerator (linac) equipped with a multileaf collimator (MLC) and a treatment planning system (TPS) with an inverse planning option. The American Association of Physicists in Medicine (AAPM) 2003 Guidance Document[1] refers to the planning and delivery techniques that are used to enhance the prospects for more accurate and trustworthy results in IMRT commissioning. The document states that the verification measurements are initially implemented on a phantom plan, where the beam segments and the position of the MLCs have to be checked. In clinical routine and for patient-specific quality assurance (QA), a patient plan is transferred on a phantom computed tomography study, recalculating the specific dose distribution on the phantom geometry to be delivered in the phantom. The resulting dose distribution is measured using either ionization chambers, films, or other detectors. The resulting measurement is then compared to the predicted dose to the phantom[1] and the objective is to coincide the planned dose distributions with the measured one.

In 2009, AAPM Task Group (TG) 119[2,3] focused on the problem of quantifying the overall performance of an IMRT system. The

Access this article online	
Quick Response Code:	Website: www.jmp.org.in
	DOI: ***

Address for correspondence: Mrs. Raphaela Avgousti, Department of Radiology, Medical Physics Unit, Aretaieion Hospital, University of Athens, Greece. E-mail: raphaela.avgousti@gmail.com

How to cite this article:

report recommends a set of test cases, to assess the accuracy of planning and delivery process of IMRT treatments. It basically refers that those tests should be performed at a primary level in every institution to be able to proceed on IMRT treatments. TG119 recommends verification measurements with ionization chamber for one-dimensional (1D) point measurements and film for two-dimensional (2D) measurements, all performed on a solid water phantom. It is essential to study many different cases and run multiple measurements during the commissioning process to be as accurate as possible and make comparisons between IMRT delivery systems. Performing treatment plans of different type and complexity may arise unidentified inaccuracies of the local treatment and delivery system procedure and hence lead institutions to improve the IMRT process.

Although AAPM TG119 suggests 1D and 2D measurements, it has not been applied so far in literature with a volumetric phantom. The aim of this study is the implementation of AAPM's TG119 Report on a volumetric dosimetric phantom to evaluate step-and-shoot IMRT procedure at our department.

Materials and Methods

All measurements were carried out at Aretaieion University Hospital in a 6 MV photon beam linac Siemens Oncor Impression. It is equipped with an MLC of 82 leaves in the X-axis and a nominal width of 1 cm at the isocenter. The Y-axis jaws could move independently creating the desirable field length. The treatment planning was done on the local TPS Oncentra V4.3 (Nucletron, Elekta). The dose distribution for all the test cases was calculated using a collapsed cone convolution algorithm both for optimization process and for final dose calculation. The calculation grid used during the planning process was 0.15 cm.

Gamma index: A quantitative tool for dose distribution comparison

The idea of dose deviation (DD) was introduced by Van Dyk *et al*.[4] It referred to the comparison between two dose distributions at low dose gradient areas. Mistreatments that may occur during setup and alignment of a detector system showed a great influence on the results of the comparison. To confront those drawbacks, Van Dyk introduced another quantitative tool, described by the distance to agreement (DTA) for low dose at low gradient areas. It was applied then by Harms *et al*.,[5] as a software tool, introducing the idea of the closest distance between two dose distributions, which lie at the same dose level. To achieve more precise and accurate results, Low[6] combined the two parameters, DD and DTA, into one factor, the gamma index. This factor is satisfied when both variables DD and DTA pass specific criteria. Many groups have attempted to develop methods for the improvement of the calculation of gamma index, with Stock *et al*.[7] in 2005, to introduce 2D gamma analysis and gamma histograms for complex dose distributions.

Hence, within the gamma index, DTA, and DD were summarized to one evaluation tool for the verification of a treatment plan. Gamma criteria of 3 mm DTA and 3% DD were used for the evaluation of IMRT treatment plans. The criteria's threshold, as Low stated, could be modified depending on the clinical needs that are examined.[6] Moreover, it is possible to set an acceptable benchmark passing rate, below which, the gamma index is unacceptable and above that, passes the criteria. In this work, a passing rate of 90% and above for the gamma index (3% DD/3 mm DTA) was considered as acceptable.[8]

Delta^4 phantom

All test cases, investigated in this work, were planned and delivered on Delta^4 Phantom (Scandidos, Uppsala, Sweden). Delta^4 is a cylindrical, polymethylmethacrylate phantom, consisting of two orthogonal detector planes in a crossed array. It consists of 1069 p-type silicon diodes that can measure point doses and can be used for QA of patient-specific treatment delivery. The detector planes spatial resolution is 5 mm at the central area of 6 cm × 6 cm and 10 mm at the outer area in each plane. The cylindrical phantom has diameter and length of 22 cm and 40 cm, respectively.[9]

For the verification of a patient treatment plan, it was applied on a Delta^4 phantom and the dose distribution inside the phantom was recalculated in the TPS. The comparison between the calculated and the measured radiotherapy (RT) dose was translated to DTA, DD, and gamma index. The evaluated gamma passing rate is only given for the measured points in the two detector planes, therefore the analysis is limited to the measurement points.[9] Diodes that received a dose less than a certain percentage of the maximum absorbed dose was ignored in the analysis. These ignored readings typically were located in the low gradient regions where the diode response is less reliable.[10] In this work, dose values below 10% of the dose maximum were excluded from the final result. It has to be emphasized that there is not a direct calculation of the delivered dose for every point within the phantom. However, according to the manufacturer, a 3D calculation of the delivered dose is available, even if the planned control points are missing. This interpolation method theoretically uses depth dose distributions for different field sizes, calculated with the TPS for the Delta^4 phantom and processed by its software. The 3D dose determination for a single beam in the cylindrical Delta^4 phantom requires the planned dose to be known in the complete cylindrical volume, while the measured dose to be known in the two orthogonal detector planes.

The planned dose for each beam is renormalized using the ratio between the planned and the measured dose at the intersection point of the beam with the detector plane. Finally, the dose is calculated for all the radiation fields.[11] The above process has been carried out during the calibration of the phantom, which is recommended by the manufacturer to be performed once a year including the wing uniformity response, directional dependence, and absolute dose calibration.

Reference treatment planning data, such as DICOM RT objects, beam arrangement, and structures from the original plan were transferred to the Delta[4] system. The software has a variety of tools for displaying the differences between the measured and the calculated dose. The gamma analysis was performed based on the formulae by Low *et al*.[12] The histograms of DD, DTA, gamma index,[6] and the passing rates were calculated by the Delta[4]'s software (Scandidos, Uppsala, Sweden). For the statistical calculation, all detectors from both the detector boards were used.

Before the evaluation of an IMRT plan, two more measurements were done by delivering 100 cGy with a 10 cm × 10 cm field at gantry angles of 0° and 90°, in order to check the phantom for positional corrections and linac output constancy.[13] These setup corrections were then applied to the rest of the measurements performed with the same phantom position.

American Association of Physicists in Medicine Task Group-119 report

TG119 report suggests seven test cases for the evaluation of the IMRT procedure. Each case included a target and peripheral normal structure shapes in a DICOM format, which were imported in the TPS. Thereafter, the DICOM RT structures were fused and registered on the dosimetric phantom. Each test also included specific dose goals [Tables 1-5] and beam arrangement to be applied. The seven tests were of varying type and complexity, and hence different optimization criteria had to be used. Each case required certain specific measurements to be performed for testing the accuracy of both delivery and planning systems, through comparison of the results with the published values in the report.

Preliminary/forward planning test cases

Test P1: Anterior-posterior: Posterior-anterior and Test P2: Bands

Test P1 is a simple, parallel-opposed setup of the phantom using anterior-posterior: Posterior-anterior (AP: PA), 10 cm × 10 cm fields to a dose of 200 cGy to the isocenter.

Test P2 (Bands test) is also a simple, parallel-opposed setup using a series of adjacent AP: PA fields, to create a set of five bands, 3 cm wide and a total field length of 15 cm. This was achieved by opening the jaws at Y-axis up to 15 cm at field length, while the MLC's, which lie in X-axis, were moving asymmetrically producing gradually a field width of 15 cm of 3 cm per time). The proposed dose escalation to be achieved was 40–200cGy, in five 40cGy steps.

Inverse planning test cases

Test I1: Multitarget

Multitarget consists of three cylindrical targets, which are stacked along the axis of rotation of the gantry. Each has a diameter of 4 cm and length of 4 cm. The objective of the test is to deliver different doses to each target, with the central target receiving the largest dose per fraction, and the superior and targets receiving 50% and 25% of the prescribed dose respectively. Dose goals are specified as D99, referring to the dose of 99% of the volume and D10, referring to the dose of 10% of the volume respectively, for each and every target [Table 1].

Test I2: Mock prostate

At the mock prostate test case, the planning target volume (PTV) is expanded 0.6 cm around the clinical target volume of the

Table 1: Treatment planning statistics for multitarget

Planning parameter	Plan goal (cGy)	Plan results (cGy)	TG119 institutions
Central target D99	>5000	4845	4955
Central target D10	<5300	5266	5455
Superior target D99	>2500	2571	2516
Superior target D10	<3500	3554	3412
Inferior target D99	>1250	1258	1407
Inferior target D10	<2500	2717	2418

Table 2: Treatment planning statistics for mock prostate

Planning parameter	Plan goal (cGy)	Plan results (cGy)	TG119 institutions
Prostate D95	>7560	7913	7566
Prostate D5	<8300	8237	8143
Rectum D30	<7000	6529	6536
Rectum D10	<7500	7410	7303
Bladder D30	<7000	4766	4304
Bladder D10	<7500	6888	6269

Table 3: Treatment planning statistics for mock head/neck

Planning parameter	Plan goal (cGy)	Plan results (cGy)	TG119 institutions
PTV D90	5000	4992	5028
PTV D99	>4650	4586	4704
PTV D20	<5500	5381	5299
Cord maximum	<4000	3826	3741
Right parotid D50	<2000	1722	1798
Left parotid D50	<2000	1838	

Table 4: Treatment planning statistics for mock C-shape (easier)

Planning parameter	Plan goal (cGy)	Plan results (cGy)	TG119 institutions
PTV D95	5000	5068	5010
PTV D10	<5500	5463	5440
Core D10	<2500	2461	2200

Table 5: Treatment planning statistics for C-shape (harder)

Planning parameter	Plan goal (cGy)	Plan results (cGy)	TG119 institutions
PTV D95	5000	4008	5011
PTV D10	<5500	5647	5702
Core D10	<1000	968	1630

prostate with a posterior concavity. The bladder and the rectum are also included in the structure set and need to be protected. Dose goals for prostate PTV, are specified as D95 and D5, referring to the dose of 95% and 5%, respectively. In addition, rectum and bladder have to be protected, and dose has to be kept under specific limits. D30 and D10, which are referring to the dose of 30% and to the dose of 10% of the volume, respectively, have to be characterized [Table 2].

Test I3: Mock head/neck

The PTV head/neck test case includes all anterior volume from the base of the skull to the upper neck, including the posterior neck nodes. The parotid glands and the spinal cord are also outlined and have to be protected. For the PTV, dose goals are specified as D99, D90, and D20 describing the respective dose percentages of the target. For the parotids, D50 was used, referring to the dose received by 50% of the volume, whereas the maximum dose for the cord has to be kept under 4000 cGy [Table 3].

Test I4 and I5: C-shape

The last two IMRT plans refer to a C-shaped target that surrounds a central avoidance structure. The center core is a cylinder 1 cm in radius and is located in the inner arc of the PTV. Two versions of this test case, with different numerical goals but with the same beam arrangements, were examined. In the first and easier one, the central core must be kept under 50% of the target dose, while in the second and harder test case the central core has to be kept below 20% of the target dose. For both cases, PTV dose goals are specified as D95, aka the dose to 95% of the volume and D10, aka the dose to 10% of the volume. For the core, D10 needs to meet individual criteria, which are stricter for the harder case [Tables 4 and 5].

Results

The proposed dose goals from TG119 and plan results from the local TPS are shown in Tables 1-5, individually for all the tests performed at our department. Mean values achieved by the institutions referred to the TG119 report are also shown in Tables 1-5, respectively. Results refer to the doses in cGy of the different PTV's and to the organs at risk that have to be protected according to TG119.

Planning parameters, including number of fields, segments and monitor units (MU's), and the gamma analysis results of each test case, including DD, DTA, and gamma index passing rates, are also presented in Table 6.

Test P1: Anterior-posterior: Posterior-anterior and P2: Bands

The percentage of gamma passing rate of the test P1 is 99.3%, and for the test, P2 is 99.7%. For the simple irradiation of parallel-opposed fields, AP: PA and bands test, the results of gamma index were high. Those tests could also be performed as a primary accuracy check of a delivery system for everyday practice.

Tests I1: Multitarget

The gamma passing rate for the multitarget was calculated at 98.1%. Test case I1 represents a concomitant target IMRT, asking from the planner to achieve gradually different doses to the three targets. The DD pass percentage was 81.7% and the DTA pass percentage was 95.1%.

Test I2: Mock prostate

The gamma passing rate for test I2 was 99.6%, while the pass percentages of DD and DTA were 80.1% and 98.6% respectively. Dose distribution at axial projection and on the Delta^4 planes and the gamma index results are also provided [Figure 1].

Test I3: Mock head/neck

The gamma passing rate for the I3 test case was 98.6%, while the pass percentages of DD and DTA were 83.1% and 94.2% respectively. The mock structures of the spinal cord and the parotid glands showed a decline in dose, while target receives at least 95% of the prescribed dose [Figure 2].

Tests I4 and I5: C-shape

For each case of the C-shape test, different objectives and constraints had to be achieved. For the easier case, the pass percentage of gamma index was 95.2%, while that for DD and DTA were 48.8%, and 87.8% respectively and are presented below [Figure 3]. For the harder case, the gamma index pass percentage was 90.3%. For the DD and DTA, the pass percentages were 48.2% and 86.7% respectively.

Discussion

For each TG119 test case, there were specific dose goals that had to be fulfilled by the IMRT system, including the TPS,

Table 6: Results of dose deviation, distance to agreement, and gamma index for all the test cases

Test case	Fields number	Segments number	MU	Dose deviation (%)	Distance to agreement (%)	Gamma index (%)
P1 - Anterior-posterior: posterior-anterior	2	2	274	85.4	96.5	99.3
P2 - Bands	10	10	227	91.5	98.8	99.7
I1 - Multitarget	7	61	492	81.7	95.1	98.1
I2 - Prostate	7	46	507	80.1	98.6	99.6
I3 - Head/neck	9	80	1213	83.1	94.2	98.6
I4 - C-shape (easier)	9	70	1204	48.8	87.8	95.2
I5 - C-shape (harder)	9	60	1368	48.2	86.7	90.3

MU: Monitor unit

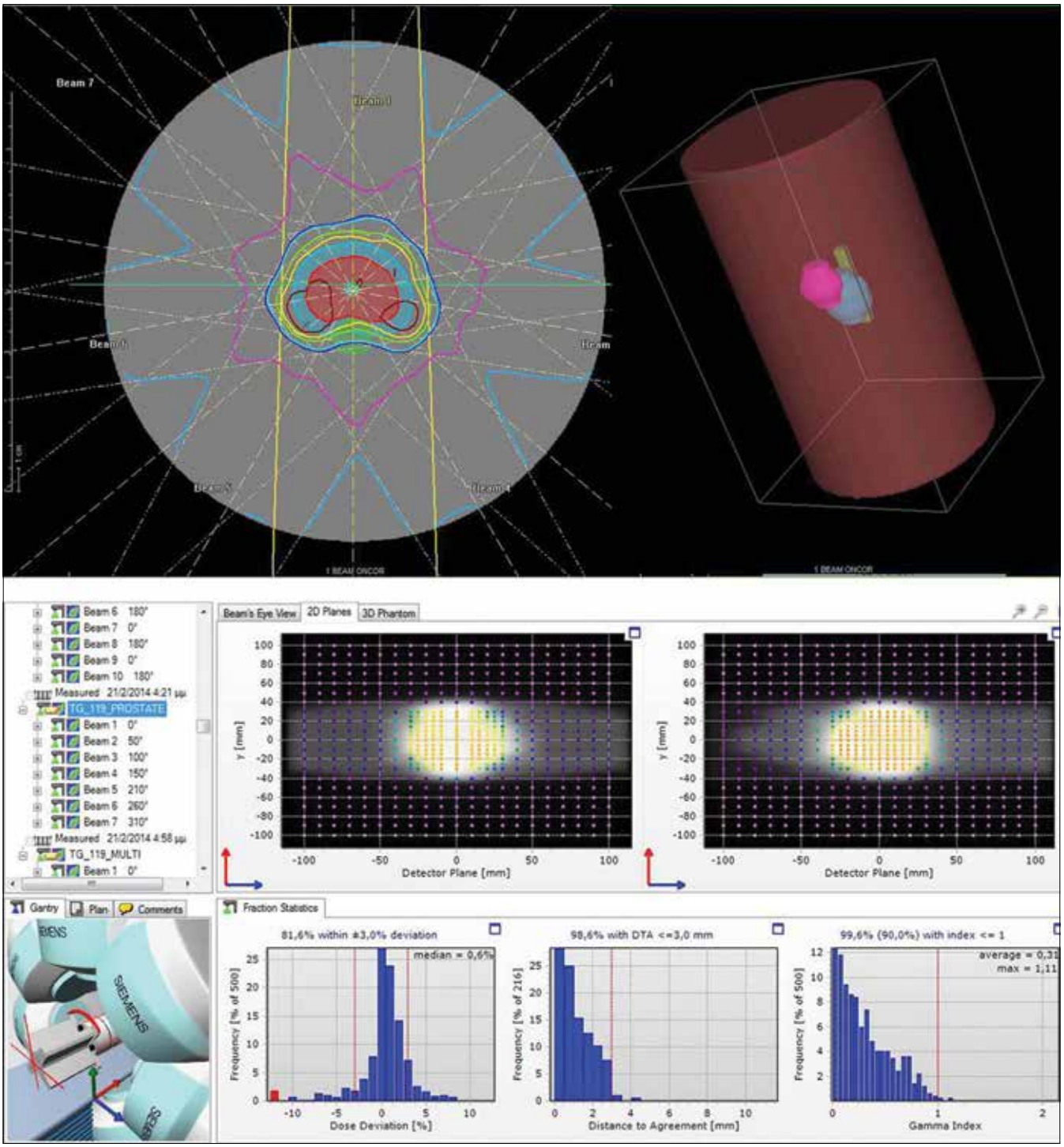

Figure 1: Dose distribution, dose deviation, distance to agreement, and gamma index of test case I2: Prostate.

the optimization algorithm, and the linac's MLC system. In Tables 1-5, the plan results of our IMRT system are presented. As it can be seen most of our plan results met the TG119 recommended dose goals.

The multitarget test case was satisfied for most of the planning goals, except the D99 for the central target with a difference of 3.1% lower dose coverage than the required constraint and the D10 for the superior target with a difference of 1.5% higher value than the TG119's constraint. These differences are low and could be considered as acceptable, while the rest parameters satisfied the TG119 needs. Considering the results of the institutions with the dose goals of TG119, there was a difficulty in achieveing the goals of D99 and D10 of the central target by 0.9% lower and 2.9% higher than the asked values, respectively.

Regarding mock prostate test case, all the specified goals were met. Like the other institutions, the doses to critical organs

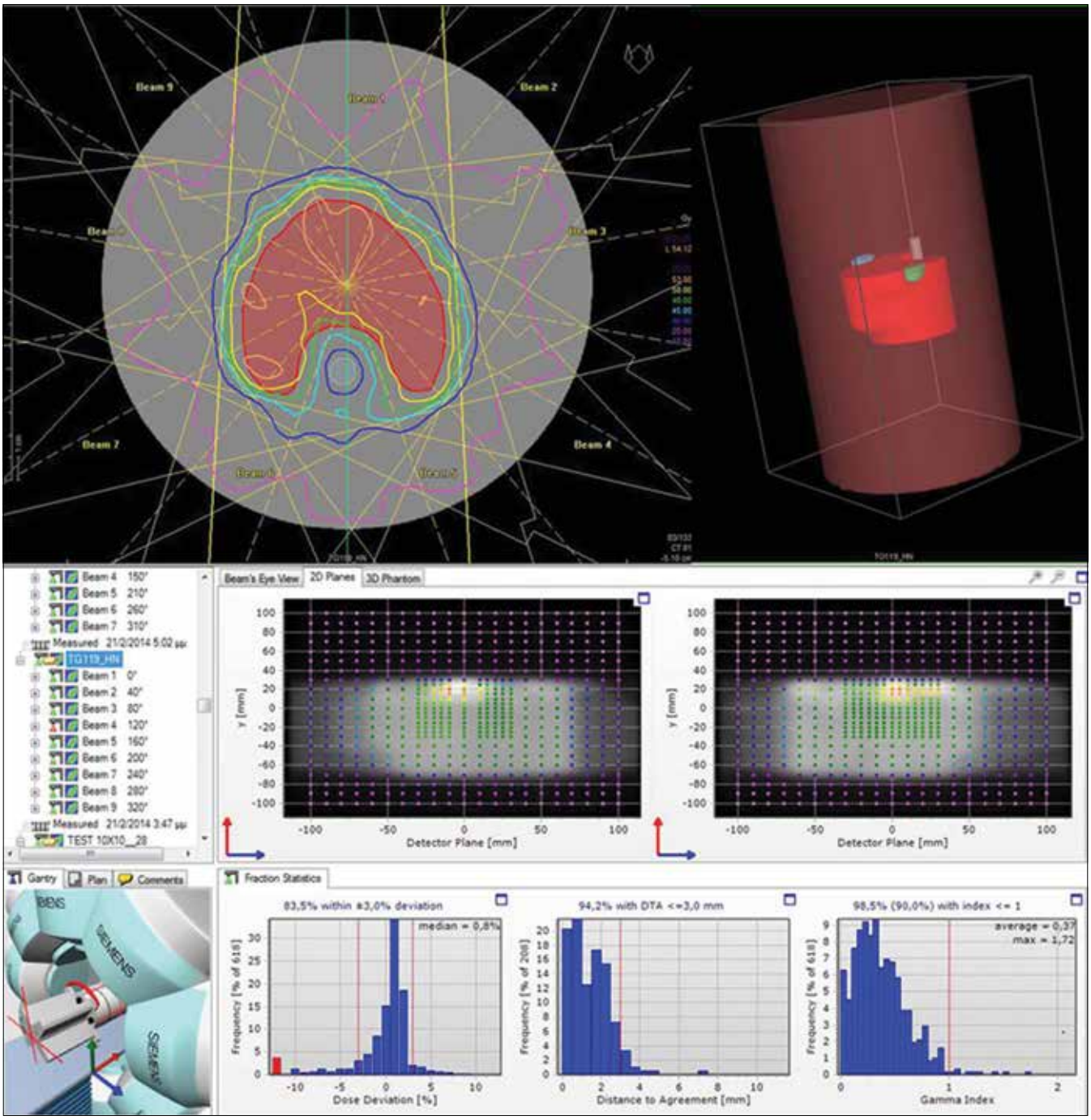

Figure 2: Dose distribution, dose deviation, distance to agreement, and gamma index of test case I3: Head/neck.

were kept much lower than the proposed doses. Furthermore, the dose coverage at the PTV both for the D95 and the D5 did satisfy the stated goals.

For the head/neck test case there was a 1.4% deficiency in reaching the goal for D99 of the PTV and also a deficiency of 0.2% in achieving the goal of PTV D90, while PTV D20 stayed below 2.2% the required dose. On the other hand, the published results in the report satisfied all the goals both for the PTV and for organ-at-risks (OARs). However, due to the fact that the deviations of the dose that we measured are lower than 3% of the proposed dose, they could be considered as acceptable.

In the easy case of C-shape, the objectives referring to PTV were satisfied with the core to be kept under the proposed dose. TG119 results for the easy case of C-shape were also acceptable for the D95 and D10 of the PTV, and also the core kept under the asked limits. However, in the harder case of C-Shape, there was a disability to keep PTV D10 lower than the goal, and there was a deficiency in meeting the benchmark value of D95 for PTV. Nevertheless, the cord dose was kept lower

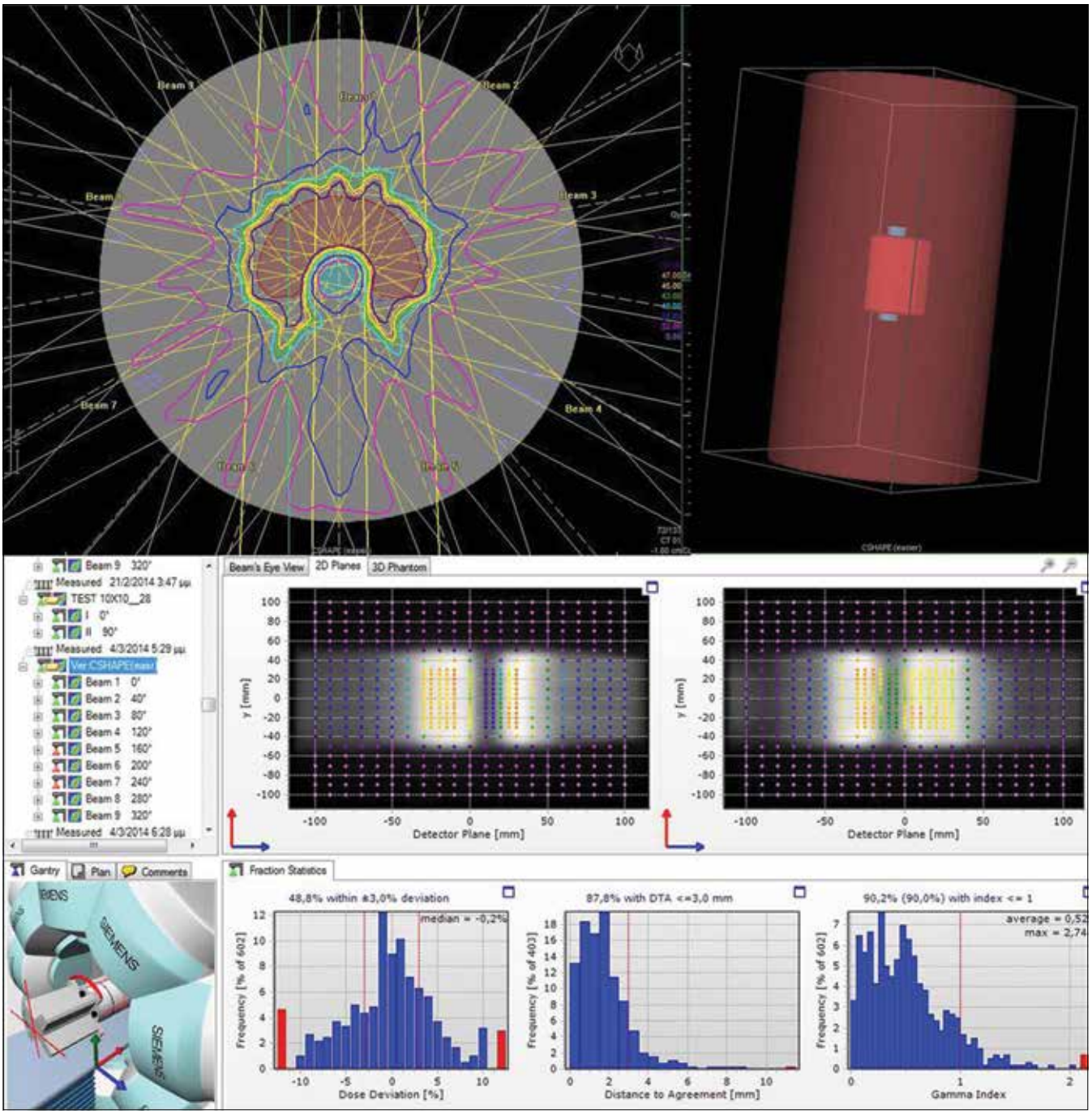

Figure 3: Dose distribution, dose deviation, distance to agreement, and gamma index of test case I2: C-shape (easier).

than 1000 cGy. Unlike other institutions, we chose to preserve the core and underdose the PTV in order to stay below the core constraint. The report's results, on the contrary, satisfied the dose coverage of PTV95 by remaining 0.2% above the proposed goal, but at the same time, PTV D10 exceeded the proposed value by 3.7% and also D10 for the core exceeded by 63% of the required constraint.

Another basic purpose of the implementation of the tests was to check if the measured dose from the diodes of the phantom agreed with the planned dose from the TPS. The comparison included measuring the percentages of DD, DTA, and from those two the percentage of gamma index. It is essential, these three parameters to be combined for more accurate results. Acceptance criteria of 3% DD, 3 mm DTA, and 90% threshold of the passing rate for the gamma index were used. As presented in Table 4, in all test cases, the gamma index passing rate was measured >90%. Furthermore, in each test case DTA was measured closer to the gamma index value than the DD value, respectively. However, in the C-shape test cases, even though the gamma index has been satisfied, DD or/

and DTA have been measured relatively low. The above has been stated by Low *et al*.,[14] to prove that it is not obligatory for the acceptance of gamma index percentage to conclude to also acceptable percentages of DD and DTA. In particular, it is mentioned that DTA tool is more intense and variable at steep dose gradient regions, where as the spatial discrepancy of dose distributions is rather low. In clinical practice, a treatment plan, in order to be accepted, must be verified by comparing the measured dose with the planned dose. Different practice has to be followed for different cases, referring to the criteria that a plan needs to satisfy depending on tumor/critical organs and taking into account the uncertainties of spatial resolution. Nevertheless, Low *et al*.[14] studied and have proved that these two vectors tend to conclude to similar results. As an illustration, all above measurements have shown this tendency of DTA to the gamma index pass percentage. The DD pass percentage on the other hand, shows a general decline to most of the test cases, despite gamma index's acceptable percentage. The DD pass percentage was the lowest for the harder case of C-shape test at 50%. The complexity of the planning goals for the individual plans was varied according to the objectives and the constraints given in TG119. The measured DD, DTA, and gamma index histograms of the forward plans resulted in high pass percentages. The two forward plans can be used as an initial cross-check of the planning and the delivery system, before the IMRT procedure. The IMRT plans resulted in acceptable pass percentages of the gamma index and did meet the criteria asked from the report. In addition, from IMRT results it was revealed an increase in the planned MU's with the complexity of the plans and respectively a decrease in the gamma passing rate.

Summing up, Delta^4 provides a thorough data analysis and a relatively faster way to take measurements without necessitating further QA systems. Measurements take place on the two planes of the phantom, where a 3D dose distribution of the dose could be computed by the software of the phantom through an interpolation method. A major advantage using a volumetric phantom for the implementation of TG119 is that one measurement is enough to calculate absolute doses at different points corresponding to points in PTVs and OARs. The measurement procedure with the volumetric phantom gives much more information than point dose measurement with an ionization chamber. The Delta^4 phantom can be set-up easily, and positional errors could be diminished to the minimum. It is important that the initial calibration and the commissioning process of Delta^4 has to be accomplished with rigorous and careful measurements to ensure patient specific QA tests are accurate.[8] Last but not least, it should be noted that TG119 report refers to commissioning process of an IMRT system at a primary level. Consequently, it cannot be used directly on the clinical practice, because it refers to methods that should be followed in order to test the IMRT planning and delivery system before perform IMRT plans on actual patients. In addition, the report's test cases refer to specific mock structures but in real patient cases there might be multiple OARs, and also the size of PTVs/OARs may differ. The requirements to fulfill according to TG119 report were of high intricacy both for the planning and for the delivery system. Comparing our results with those of other institutions, it was concluded that even if they are similar in most of the test cases, (except the test case of harder C-shape), they cannot be compared directly. This is basically because institutions referred in this report used different delivery and planning systems. Results reported in TG119 report refer to mean values of doses that were achieved by all institutions collectively and not individually.

Conclusion

Delta^4 phantom has proven to be fast and reliable for the step-and-shoot IMRT commissioning following TG119's recommended tests. AAPM TG119 test cases have been applied successfully on the Delta^4 volumetric phantom, providing accurate results at a primary level and before any clinical use. It has to be noted that the test cases refer to theoretical objectives and constraints but not to practical guidelines on performing IMRT plans on actual patients. Nevertheless, the TG119 report could be used as an evaluation tool of different IMRT systems between institutions, in order to compare results for different combinations of planning and delivery techniques.

Financial support and sponsorship

Nil.

Conflicts of interest

There are no conflicts of interest.

References

1. Galvin JM, Low D, Palta JR, Rosen I, Sharpe MB, Xia P, *et al*. AAPM REPORT: Guidance Document on Delivery, Treatment Planning, and Clinical Implementation of IMRT: Report of the IMRT Subcommitte of the AAPM Radiation Therapy Committee; 2003.
2. Ezzell GA, Burmeister JW, Dogan N, LoSasso TJ, Mechalakos JG, Mihailidis D, *et al*. IMRT commissioning: Multiple institution planning and dosimetry comparisons, a report from AAPM Task Group 119. Med Phys 2009;36:5359-73.
3. TG-119 IMRT Commissioning Tests Instruction for Planning, Measurement, and Analysis Version 10/21/2009, Digital File Support (www,aapm.org/pubs/tg119/default.asp)
4. Van Dyk J, Barnett RB, Cygler JE, Shragge PC. Commissioning and quality assurance of treatment planning computers. Int J Radiat Oncol Biol Phys 1993;26:261-73.
5. Harms WB Sr., Low DA, Wong JW, Purdy JA. A software tool for the quantitative evaluation of 3D dose calculation algorithms. Med Phys 1998;25:1830-6.
6. Low DA. Gamma dose distribution evaluation tool. J Phys Conf Ser 2010;250:12071.
7. Stock M, Kroupa B, Georg D. Interpretation and evaluation of the gamma index and the gamma index angle for the verification of IMRT hybrid plans. Phys Med Biol 2005;50:399-411.
8. Low DA, Moran JM, Dempsey JF, Dong L, Oldham M. Dosimetry tools and techniques for IMRT. Med Phys 2011;38:1313-38.
9. Scandidos, Delta4PT user manual. Uppsala, Sweden: Scandidos.
10. Nilsson J, Karlsosn Hauer A, Bäck A. IMRT patient-specific QA Using the Delta4 Dosimetry System and Evaluation Based on ICRU 83 Recommendations". Paper Presented at: 7th International Confernsce on 3D RAdiation Dosimetry; 2013.
11. Calvo O, Gutiérrez A, Stathakis S, Mavridis P, Moral S, Esquivel C,

Shi C, Papanikolaou N. Validation of the Delta4 dosimetry phantom against ionometic measurements. Med Phys 2009;36:2610.
12. Low DA, Harms WB, Mutic S, Purdy JA. A technique for the quantitative evaluation of dose distributions. Med Phys 1998;25:656-61.
13. Antypas C, Floros I, Rouchota M, Armpilia C, Lyra M. MLC positional accuracy evaluation through the picket fence test on EBT2 films and a 3D volumetric phantom. J Appl Clin Med Phys 2015;16:5185.
14. Low DA, Morele D, Chow P, Dou TH, Ju T. Does the dose distribution comparison technique default to the distance to agreement test in clinical dose distributions? Med Phys 2013;40:071722.

Technical Note

Response of Nanodot Optically Stimulated Luminescence Dosimeters to Therapeutic Electron Beams

Y. Retna Ponmalar[1,2], Ravikumar Manickam[1], S. Sathiyan[1], K. M. Ganesh[1], R. Arun[1], Henry Finlay Godson[1,2]

[1]Department of Radiation Physics, Kidwai Memorial Institute of Oncology, Bengaluru, Karnataka, [2]Department of Radiotherapy, Christian Medical College, Vellore, Tamil Nadu, India

Abstract

Response of Al_2O_3:C-based nanoDot optically stimulated luminescence (OSL) dosimeter was studied for the dosimetry of 6, 9, 12, 16, and 20 MeV therapeutic electron beams. With reference to ionization chamber, no change in the response was observed with the change in the energy of electron beams for the field size from 6 cm × 6 cm to 25 cm × 25 cm, dose rates from 100 MU/min to 600 MU/min, and the linearity in the response up to 300 cGy. The fading of the transient signal was higher for 20 MeV electron beam than that of 6 MeV electron beam by about 5% as compared to value at 20 min after irradiation. The depletion of OSL signal per readout in 200 successive readouts was also found to change with dose and energy of electron beam from 6 MeV (9% and 12% per readout at 2 and 10 Gy, respectively) to 20 MeV (9% and 16% at 2 and 10 Gy, respectively). The OSL sensitivity changed in the range from 2% to 6% with accumulated doses from 2 to 8 Gy and with electron energy from 6 to 20 MeV, but the sensitivity could be reset using an optical annealing treatment. Although negligible fading for postirradiation storage from 20 min to several months, acceptable precision and linearity in the desired range, and high reproducibility makes nanoDot dosimeters very attractive for the dosimetry of therapeutic electron beams, a note should be made for changes in sensitivity at doses beyond 2 Gy and electron beams energy dependence in reuse, short-term fading, and signal depletion on repeated readout.

Keywords: Dosimetric characteristics, electron beam, nanoDot dosimeter, radiotherapy

Received on: 23-04-2016 **Review completed on: 03-09-2016** **Accepted on: 13-11-2016**

Introduction

Megavoltage electron beam therapy is an important treatment modality in radiotherapy, providing unique choice to treat superficial tumors.[1,2] Electron beams have been produced initially by betatrons, and by microtrons followed by linear accelerators.[3] An appropriate dosimeter must be used to determine the dose accurately at a point with minimum perturbation of electron fluence.[4] The drawbacks of the dosimeters such as destructive technique, annealing process[5,6] and ineffectualness in reestimating the dose with thermoluminescent dosimeters, reduced lifetime with metal oxide semiconductor field effect transistors (MOSFETs) [7,8] necessity for corrective actions required with diode,[9,10] cumbersome measurements with cables (MOSFET, diodes),[11] and non-suitability in patient dosimetry with plane-parallel ionization chamber (gold standard in electron beam dosimetry)[12] persist the necessity to explore new dosimetric method for dosimetric verification.[13] The dosimeters that are based on the luminescence properties of solids are highly suitable for *in vivo* and in-phantom measurements as they are available in small sizes providing high spatial resolution and wider dose range coverage with high precision.[14-16] Optically stimulated luminescence dosimeter (OSLD) has been introduced into radiation dosimetry, yet it is well known as a suitable dosimeter in space dosimetry and personal dosimetry over a decade.[17-22] Despite the ability to measure small and large doses with high accuracy and precision, the drawback is that it has to be enclosed in a light-proof case owing to the nature of optically stimulated luminescence (OSL) phenomenon in the phosphor material (Al_2O_3:C).[23] However, this drawback is easily overcome by encapsulating the

Access this article online	
Quick Response Code:	Website: www.jmp.org.in
	DOI: ***

Address for correspondence: Dr. M. Ravikumar, Department of Radiation Physics, Kidwai Memorial Institute of Oncology, Hosur Road, Bengaluru - 560 029, Karnataka, India. E-mail: drmravi59@yahoo.com

How to cite this article:

sensitive element in a water equivalent light-tight plastic casing. A form factor difference of 50% with standard dot dosimeters enables to place this dosimeter in more restricted spaces, for instance, eyelid. The reported results of electron beam energy dependency with dot OSLD,[24,25] optical fiber,[19,26] and nanoDot[27] was <1%. However, higher response of 1.9% was observed in the uncorrected data of electron beams with 6 MV photon beam.[28] Schembri observed a discrepancy of 3.7% between electron (6–22 MeV) and 6 MV photon beams with OSL film.[29] This significant difference points out the need for detailed investigations with careful attention to the experimental conditions. In addition, the other dosimetric responses with therapeutic electron beams such as field size, reproducibility, long-term fading effect, reader stability, and signal depletion per readout of nanoDot OSLD were studied, and the results were discussed.

Materials and Methods

The OSLDs used were commercially available nanoDot dosimeters (Landauer, Inc., Glenwood, USA), and they are 5 mm diameter and 0.2 mm thick discs of Al_2O_3:C. These discs are encased in a 10 mm × 10 mm × 2 mm light-tight plastic case to prevent depletion of optical signals due to light. The bar code information in the nanoDot OSLD enables identification of each dosimeter and recording of the reading with ease. InLight microStar reader (Landauer Inc., Glenwood, USA) was used to read the optical signals of the OSLDs, with the reader warm up time of 10 min. The reader system includes an external PC, installed with a special software system to acquire the data, export to Microsoft Excel spreadsheet for analysis, and an optical annealing unit with recommended bleaching time of 6 h. During readout, OSLD is stimulated with a light of wavelength 540 nm, and the luminescence emitted is of wavelength 420 nm. The optically bleached OSLDs were read before irradiation, and the postirradiation readout was done after the transient signal decay. The resultant OSL counts reported were the difference between the pre- and post-irradiation optical signals of OSLD. The stability of the reader was checked before each readout session to ensure that the variations are within limits recommended by the manufacturer. With the intrinsic system check, reader stability was assessed by measuring the background counts (DRK) from photomultiplier tube (PMT), the counts from ^{14}C (CAL), a small exempt source to indicate the consistency of the PMT and counts from PMT to check the stability of the beam intensity of the light-emitting diode. The values within the tolerance limit indicate the acceptable stability of the reader. In every measurement, four OSLDs were used and average of 4 readings of OSL counts represents each data point of the measurement. Unless stated otherwise, the precision in the measurements was <2% (1 σ).

The ionometric measurements were performed with a calibrated NACP-02 parallel plate ionization chamber developed by Nordic Association of Clinical Physicists. The chamber has a sensitive volume of 0.16 cm^3, incorporated with a front window of thickness 0.5 mm made of graphite covered with a mylar foil of 0.1 mm thickness as water proof. The dose 1 electrometer (Scanditronix Wellhofer AB, Sweden) of high precision is used along with the chamber and maintained at a polarizing voltage of 200 V. The ion chamber and electrometer were calibrated in absorbed dose to water according to TRS 398 reference dosimetry protocol in a Cobalt-60 beam. The data obtained with OSLDs was compared with ion chamber measurement wherever applicable.

Measurements with electron beams were performed in a Clinac DHX linear accelerator (Varian Medical Systems, Palo Alto, CA, USA). During irradiation, the dosimeters were placed at the reference depths [Table 1] corresponding to their electron energies (6, 9, 12, 16, and 20 MeV) with various electron applicators at 100 cm source to surface distance (SSD). The irradiations were done with a nominal dose rate of 400 MU/min and a known dose of 200 cGy was delivered for all dosimetric measurements unless otherwise mentioned. Measurements were carried out in plastic water phantoms made of white polystyrene material of size 30 cm × 30 cm with various thicknesses having a density of 1.04 g/cm^3. The slabs of 10 cm thickness were used for backscatter in all irradiation set ups. A specially designed perspex slab with a groove arrangement was used to place OSLDs with minimized air gap during measurements.

Results and Discussion

To ensure batch heterogeneity, element correction factor (ECF) for each OSLD (ratio of the average signal of the batch to the individual OSL signal) was calculated. For uniform irradiation, ^{60}Co beam was chosen to simultaneously irradiate the OSLDs to a known dose of 2 Gy at 5 cm depth with a field size of 20 cm × 20 cm. The histogram [Figure 1] shows the distribution of ECF values from 0.90 and 1.07 better than the reported distribution[30] and a coefficient of variation <1.5%. This could be attributed to the improved production process of the supplier. Ninety percent of the dosimeters fall within 5% of the mean. The ECF obtained was applied to the raw readings of OSL in the successive uses in all measurements.

Figure 2 shows the dose response of OSLDs from 50 cGy to 1000 cGy with electron beams. The response was linear (with R^2 values ranging from 0.997 to 0.998) in the range from 50 cGy to 300 cGy above which supralinearity was observed up to 10 Gy, the maximum dose delivered. Similar behavior

Table 1: Reference depths for each energy level

Cone size (cm^2)	Reference depth (cm) for electron energies				
	6 MeV	9 MeV	12 MeV	16 MeV	20 MeV
6×6	1.27	1.97	2.80	3.67	4.51
10×10	1.27	1.97	2.80	3.70	4.68
15×15	1.28	1.97	2.78	3.70	4.69
20×20	1.26	1.98	2.78	3.69	4.69
25×25	1.28	1.97	2.80	3.70	4.69

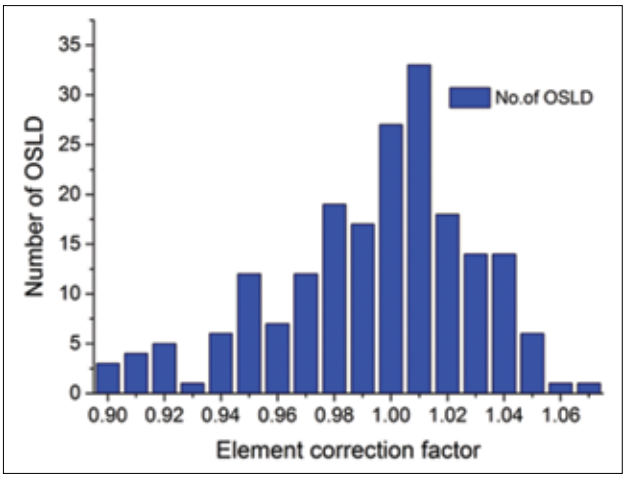

Figure 1: Histogram of the distribution of element correction factors of 200 optically stimulated luminescence dosimeters.

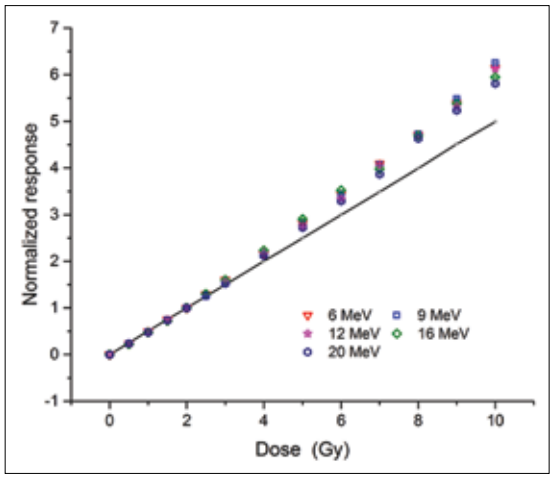

Figure 2: Dose response of nanoDot optically stimulated luminescence dosimeters with electron beams of different energies

was observed for all five electron (6, 9, 12, 16, and 20 MeV) energies. As expected and evident, the supralinearity of OSLDs to therapeutic electron beam is similar to that of therapeutic photons beams at doses >2 Gy.[7,24,25,29,31-33]

To establish the field size dependency, nanoDots were irradiated with electron applicators of 6 cm × 6 cm, 10 cm × 10 cm, 15 cm × 15 cm, 20 cm × 20 cm and 25 cm × 25 cm. A dose of 200 cGy was delivered by positioning the dosimeters at the reference depth of each energy level with 100 cm SSD. The measurement uncertainty was calculated, and it was found to be <1.5%. This indicates the independency of nanoDot response with field size. The results obtained suggest that OSLD can be used instead of ion chamber in the relative output factor measurement as there is no change in trend in the effect of OSL response compared to ion chamber.[7] However, it may be noted that for 6 MV photon beams, Schembri and Heijmen[29] reported a maximum discrepancy of 2.5% with the use of OSL, but there is no such study for electron beams. In addition, no dose rate dependence was observed for dose rates from 100 MU/min to 600 MU/min for a dose of 200 cGy delivered at the reference depths of electron energies with 15 cm × 15 cm electron cone applicator (SSD = 100 cm). Within the measurement uncertainty, this study confirms the dose rate independence of nanoDot OSLDs for the dose per pulse. Yukihara *et al*.[28] have also shown the dose rate variation of 1% in the response of OSL package of polyester film up to 1000 MU/min, with 9 MeV electron beam.

The variation in the energy response of OSL dosimeter was tested with five different electron energies of 6, 9, 12, 16, and 20 MeV and compared with 6 MV photon beams by delivering 200 cGy [Table 2]. A maximum variation of 2.1% was observed for 9 MeV electron when compared with 6 MV photon beam.

To investigate the reproducibility of OSLDs with repeated irradiations, the dosimeters were exposed to identical doses three times in three different ways. First, OSLDs were irradiated to a dose of 8 Gy with an increment of 2 Gy

Table 2: Variation in energy response of optically stimulated luminescence dosimeter

Energy (MeV)	Percentage variation in the response of nanoDot OSLD		Percentage of SD
	In comparison with 6 MV (%)	In comparison with 12 MeV (%)	
6	+2.0	+0.8	0.46
9	+2.1	+0.9	0.53
12	+1.2	-	0.43
16	+1.0	−1.0	0.37
20	+0.9	−1.0	0.48
Published results in comparison with 6 MV photon beams			
Dunn *et al.*	A variation of 1.6±1.6% with nanoDot (20 MeV)		
Yukihara *et al.*	A variation of 1.9% with OSL films (6, 9,12, 16 and 20 MeV)		
Schembri and Heijmen	A variation of 3.7% with OSL films (6-22 MeV)		

OSLD: Optically stimulated luminescence dosimeter, SD: Standard deviation, OSL: Optically stimulated luminescence

and read after every exposure of 2 Gy with a minimum wait period of 10 min. The exposed OSLDs were optically bleached after each irradiation (bleach) and made ready for the next exposure. Second, the absorbed dose in the OSLDs was accumulated to a dose of 8 Gy in steps of 2 Gy without bleaching (accum) the dosimeters, and the OSLDs were readout. Third, OSLDs were irradiated to a dose of 8 Gy in a single session (SS), and the readout was done after the wait period. The OSLD irradiations were carried out with 6, 12, and 20 MeV electron beams at their corresponding reference depths in phantom with 15 cm × 15 cm applicator. Figures 3a-c show the response of dosimeters when they are bleached in between irradiations (bleach), accumulated the OSL signals without bleaching (accum), and irradiation of OSLD in a SS for 6, 12, and 20 MeV, respectively. The error bar represents the standard deviation of OSLD readings during readout. The accumulated response of OSLD was

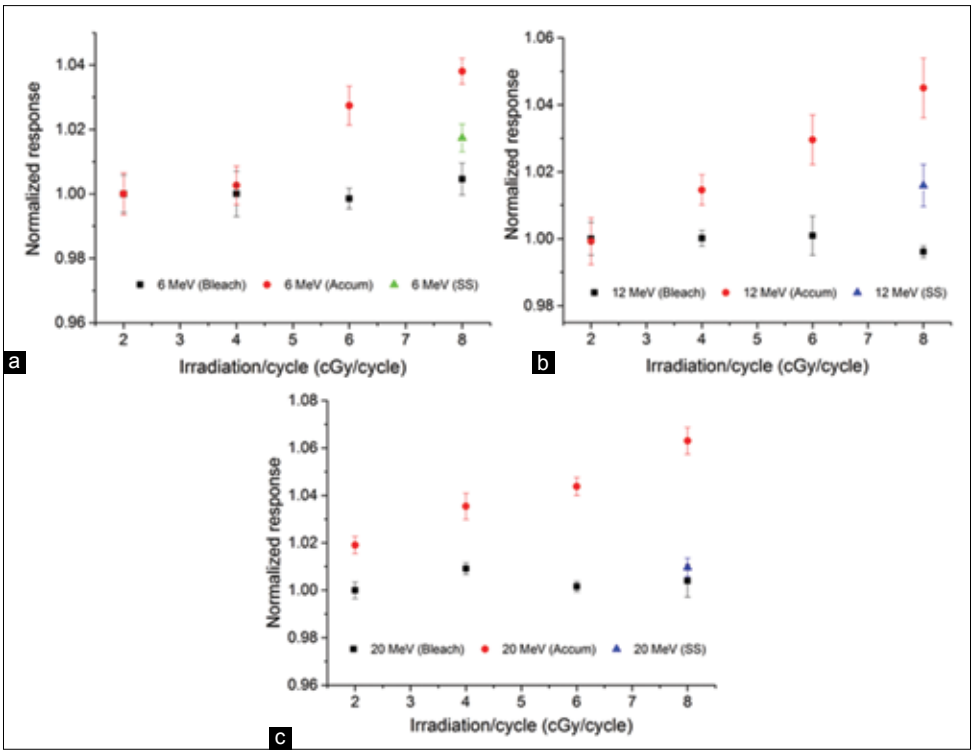

Figure 3: Reproducibility of optically stimulated luminescence dosimeters when irradiated to a total dose of 8 Gy with an increment of 2 Gy with bleach (bleach), without bleach (accum), and single session for (a) 6 MeV (b) 12 MeV (c) 20 MeV.

found to increase with dose and energy. The percentage difference observed between bleached and accumulated response was 3.9% in 6 MeV, 4.4% in 12 MeV, and 5.9% in 20 MeV electron beams at 8 Gy. The response variation of OSLDs due to accumulation of dose in an SS was found to be <2% with optically bleached OSLDs. A maximum difference of 7% with 6 MV photon beam was reported by Miller and Murphy.[34] In our study, it has been noticed that the response of nanoDot OSLDs without accumulation of dose had shown no change in sensitivity. As the optical bleach extends the useful life of OSLD, it can be conveniently used multiple times eliminating the supralinear effect. A supralinear corrective action is required if the OSLDs are irradiated with high doses (HDs) more than 3 Gy or if the doses are accumulated without bleaching. However, the ability to optically reset and reuse the nanoDot OSLD is the extreme beneficial feature of this dosimeter in large scale dosimetry program where more than hundred OSLDs would be used.[30]

The decay in OSL signal as a function of time was assessed by exposing nanoDot OSLDs to a low dose of 2 Gy and a HD of 10 Gy with 6, 9, 16, and 20 MeV electron beams at the reference depths with 100 cm SSD and an applicator size of 15 cm × 15 cm. The dosimeters were stored at room temperature and checked for the periods of (a) short-term (s/min/h), (b) mid-term (few days), and (c) long-term (months). OSLDs were read immediately after irradiation as early as 40 s, every day for the first 5 days, and then once a week for 5 weeks. The long-term fading was evaluated by taking OSLD reading

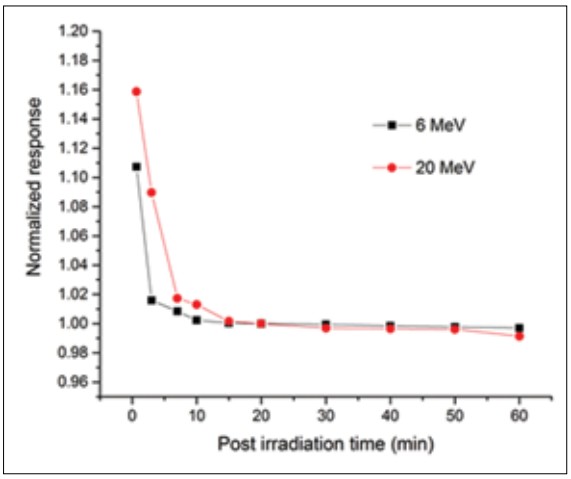

Figure 4: Post-irradiation fading of optically stimulated luminescence response from 40 s to 60 min following irradiation to 2 Gy of 6 MeV and 20 MeV electrons.

monthly once for about 8 months. Figure 4 shows the transient signal decay in OSL signal as a function of time with 6 and 20 MeV electron beams for 2 Gy. The rapid drop in the optical signal response due to the transient signal from the unstable electron traps depend on the energy of electrons. The drop in signal from 40 s to 20 min was found to be 10.7% for 6 MeV beam, whereas 15.9% for 20 MeV electron beams. It was evident from the graph that a minimum wait period of at least 10–15 min after the irradiation is required to achieve stable readout; accordingly, this was followed during all other measurements. The fading beyond 20 min post-irradiation was

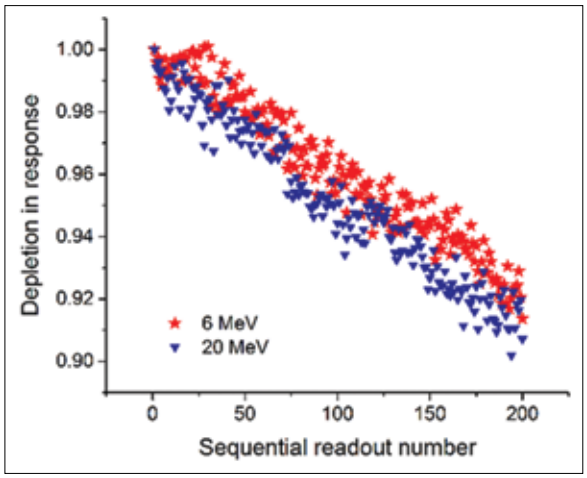

Figure 5: Depletion in response of optically stimulated luminescence dosimeters (irradiated to 2 Gy) during sequential readout (200 times) with 6 and 20 MeV electrons.

found to be similar (0.2%) for 6 and 20 MeV beams. The decay rate of fading stayed constant in every 1 month period (<1%), and the same effect was observed over a period of 8 months.

The signal loss during successive readout of OSL dosimeter was analyzed by exposing OSLDs to 2 Gy and 10 Gy of 6, 12, and 20 MeV electron beams (100 cm SSD) with 15 cm × 15 cm applicator at the reference depths. The OSLDs were read two hundred times successively, and the signal depletion per readout is shown in Figure 5. The percentage reduction in signal with electron beams of 6 MeV and 20 MeV for a dose of 200 cGy was 8.6%, and 9.3%, respectively. With a dose of 1000 cGy, the variation was 12.3% for 6 MeV and 15.8% for 20 MeV electron beams. These results indicate that the depletion rate depends on dose and energy involved during irradiation.

Conclusion

The electron beam energy dependence of nanoDot OSLDs was studied for the linearity of dose response, dose rate, field size, reproducibility, reader stability, fading characteristics, and depletion of signal per readout. Although negligible fading for post-irradiation storage from 20 min to several months, acceptable precision and linearity in the desired range, and high reproducibility make nanoDot dosimeters very attractive for the dosimetry of therapeutic electron beams, a note should be made for changes in sensitivity at doses beyond 3 Gy and electron beams energy dependence in reuse, short-term fading, and signal depletion on repeated readout.

Acknowledgment

This study was supported by a grant (AERB/CSRP/58/06/2014) from the Atomic Energy Regulatory Board, India.

Financial support and sponsorship

Nil.

Conflicts of interest

There are no conflicts of interest.

References

1. Hogstrom KR, Almond PR. Review of electron beam therapy physics. Phys Med Biol 2006;51:R455-89.
2. Amin MN, Heaton R, Norrlinger B, Islam MK. Small field electron beam dosimetry using MOSFET detector. J Appl Clin Med Phys 2010;12:3267.
3. Strydom WY, Parker WI, Olivares MA. Electron beams: Physical and clinical aspects. In: Podgorsak EB, editor. Radiation Oncology Physics: A Handbook for Teachers and Students. Vienna: International Atomic Energy Agency (IAEA); 2005. p. 273-99.
4. Eveling JN, Morgan AM, Pitchford WG. Commissioning a p-type silicon diode for use in clinical electron beams. Med Phys 1999;26:100-7.
5. Attix FH. Introduction to Radiological Physics and Radiation Dosimetry. Hoboken, NJ: John Wiley and Sons; 2008.
6. Essers M, Mijnheer BJ. *In vivo* dosimetry during external photon beam radiotherapy. Int J Radiat Oncol Biol Phys 1999;43:245-59.
7. Viamonte A, da Rosa LA, Buckley LA, Cherpak A, Cygler JE. Radiotherapy dosimetry using a commercial OSL system. Med Phys 2008;35:1261-6.
8. Chung JB, Lee JW, Suh TS, Lee DH, Choe BY, Kim YS, *et al.* Dosimetric characteristics of standard and micro MOSFET dosimeters as *in-vivo* dosimeter for clinical electron beam. J Korean Phys Soc 2009;55:2566-70.
9. VanDam J, Marinello G. Methods for *in vivo* dosimetry in external radiotherapy. ESTRO Booklet on Physics for clinical Radiotherapy No.1, Leuven- Apelddoorn, Belgium: Garant Publishers; 1994.
10. Yorke E, Alecu R, Ding L, Fontenla D, Kalend A, Kaurin D, *et al*. Diode *in vivo* dosimetry for patients receiving external beam radiation therapy. Report of the American Association of Physicists in Medicine (AAPM) Task Group 62.AAPM Report No.87 (Madison, WI: Medical Physics Publishing 2005).
11. Scalchi P, Francescon P. Calibration of a MOSFET detection system for 6-MV *in vivo* dosimetry. Int J Radiat Oncol Biol Phys 1998;40:987-93.
12. Electron beams with mean energies at the phantom surface below 15 MeV. Supplement to the recommendations by the Nordic Association of Clinical Physics (NACP) 1980. Acta Radiol Oncol 1981;20:401-15.
13. Kinhikar RA, Sharma PK, Tambe CM, Mahantshetty UM, Sarin R, Deshpande DD, *et al.* Clinical application of a OneDose MOSFET for skin dose measurements during internal mammary chain irradiation with high dose rate brachytherapy in carcinoma of the breast. Phys Med Biol 2006;51:N263-8.
14. Pradhan AS, Lee JI, Kim JL. Recent developments of optically stimulated luminescence materials and techniques for radiation dosimetry and clinical applications. J Med Phys 2008;33:85-99.
15. Pradhan AS. A concern on in-phantom photon energy response of luminescence dosimeters for clinical applications. J Med Phys 2010;35:187-8.
16. Paliwal B, Tewatia D. Advances in radiation therapy dosimetry. J Med Phys 2009;34:108-16.
17. Yukihara EG, Yoshimura EM, Lindstrom TD, Ahmad S, Taylor KK, Mardirossian G. High-precision dosimetry for radiotherapy using the optically stimulated luminescence technique and thin Al_2O_3:C dosimeters. Phys Med Biol 2005;50:5619-28.
18. Aznar MC, Andersen CE, Bøtter-Jensen L, Bäck SA, Mattsson S, Kjaer-Kristoffersen F, *et al.* Real-time optical-fibre luminescence dosimetry for radiotherapy: Physical characteristics and applications in photon beams. Phys Med Biol 2004;49:1655-69.
19. Andersen CE, Marckmann CJ, Aznar MC, Bøtter-Jensen L, Kjaer-Kristoffersen F, Medin J. An algorithm for real-time dosimetry in intensity-modulated radiation therapy using the radioluminescence signal from Al_2O_3:C. Radiat Prot Dosimetry 2006;120:7-13.
20. Yukihara EG, McKeever SW. Optically stimulated luminescence (OSL) dosimetry in medicine. Phys Med Biol 2008;53:R351-79.
21. Yukihara EG, McKeever SW. Optically Stimulated Luminescence: Fundamentals and Applications. West Sussex, UK: John Wiley and Sons; 2011.
22. Mrčela I, Bokulić T, Izewska J, Budanec M, Fröbe A, Kusić Z. Optically stimulated luminescence *in vivo* dosimetry for radiotherapy: Physical characterization and clinical measurements in ^{60}Co beams. Phys Med Biol 2011;56:6065-82.

23. Kerns JR, Kry SF, Sahoo N. Characteristics of optically stimulated luminescence dosimeters in the spread-out Bragg peak region of clinical proton beams. Med Phys 2012;39:1854-63.
24. Jursinic PA. Characterization of optically stimulated luminescent dosimeters, OSLDs, for clinical dosimetric measurements. Med Phys 2007;34:4594-604.
25. Reft CS. The energy dependence and dose response of a commercial optically stimulated luminescent detector for kilovoltage photon, megavoltage photon, and electron, proton, and carbon beams. Med Phys 2009;36:1690-9.
26. Andersen CE, Aznar MC, Bøtter-Jensen L, Bäck SÅ, Mattsson S, Medin J. Development of optical fibre luminescence techniques for real time *in vivo* dosimetry in radiotherapy. Vol. 2. Vienna: IAEA; 2003. p. 353-60.
27. Kim DW, Chung WK, Shin DO, Yoon M, Hwang UJ, Rah JE, *et al.* Dose response of commercially available optically stimulated luminescent detector, Al_2O_3:C for megavoltage photons and electrons. Radiat Prot Dosimetry 2012;149:101-8.
28. Yukihara EG, Mardirossian G, Mirzasadeghi M, Guduru S, Ahmad S. Evaluation of Al_2O_3:C optically stimulated luminescence (OSL) dosimeters for passive dosimetry of high-energy photon and electron beams in radiotherapy. Med Phys 2008;35:260-9.
29. Schembri V, Heijmen BJ. Optically stimulated luminescence (OSL) of carbon-doped aluminum oxide (Al_2O_3:C) for film dosimetry in radiotherapy. Med Phys 2007;34:2113-8.
30. Dunn L, Lye J, Kenny J, Lehmann J, Williams I, Kron T. Commissioning of optically stimulated luminescence dosimeters for use in radiotherapy. Radiat Meas 2013;51:31-9.
31. Yukihara EG, Whitley VH, Polf JC, Klein DM, McKeever SW, Akselrod AE, *et al.* The effects of deep trap population on the thermoluminescence of Al_2O_3: C. Radiat Meas 2003;37:627-38.
32. Yukihara EG, Whitley VH, McKeever SW, Akselrod AE, Akselrod MS. Effect of high-dose irradiation on the optically stimulated luminescence of Al_2O_3:C. Radiat Meas 2004;38:317-30.
33. Edmund JM, Andersen CE, Marckmann CJ, Aznar MC, Akselrod MS, Bøtter-Jensen L. CW-OSL measurement protocols using optical fibre Al_2O_3:C dosemeters. Radiat Prot Dosimetry 2006;119:368-74.
34. Miller SD, Murphy MK. Technical performance of the Luxel Al_2O_3:C optically stimulated luminescence dosemeter element at radiation oncology and nuclear accident dose levels. Radiat Prot Dosimetry 2007;123:435-42.

Form IV

Statement of ownership and other particulars about the publication, (Journal of Medical Physics) as per Rule 8

1. Place of publication	M/s Wolters Kluwer India Private Limited A-202, 2nd Floor, The Qube, C.T.S. No.1498A/2 Village Marol, Andheri (East), Mumbai - 400 059, India.
2. Periodicity of its publication	Quarterly (January, April, July and October)
3. Printer's name	Mr. Hemant Rameshchandra Manjrekar
Nationality	Indian
(a) Whether a citizen of India?	Yes
(b) If a foreigner, the country of origin	NA
Address	B9, Kanara Business Center, Off Link Road, Ghatkopar (East), Mumbai – 400075, India
4. Publisher's name	Mr. Hemant Rameshchandra Manjrekar
Nationality	Indian
(a) Whether a citizen of India?	Yes
(b) If a foreigner, the country of origin	NA
Address	B9, Kanara Business Center, Off Link Road, Ghatkopar (East), Mumbai – 400075, India
5. Editor's name	Dr. A. S. Pradhan
Nationality	Indian
(a) Whether a citizen of India?	Yes
(b) If a foreigner, the country of origin	NA
Address	Journal of Medical Physics, C/o Radiological Physics & Advisory Division, Bhabha Atomic Research Centre, CTCRS, Anushaktinagar, Mumbai - 400094, India. E-mail: editor@jmp.org.in
6. Names and addresses of individuals who own the newspaper and partners or shareholders holding more than one per cent of the total capital	Association of Medical Physicists of India (AMPI), C/o Radiological Physics and Advisory Division, Bhabha Atomic Research Centre, Anushaktinagar, Mumbai-400094.

I, Mr. Hemant Rameshchandra Manjrekar, hereby declare that the particulars given above are true to the best of my knowledge and belief.

Dated: ***will update later — Hemant Manjrekar

Technical Note

Assessment of Regional Pediatric Computed Tomography Dose Indices in Tamil Nadu

A. Saravanakumar, K. Vaideki[1], K. N. Govindarajan[2], S. Jayakumar[3], B. Devanand

Departments of Radiology and [2]Medical Physics, PSG Hospitals, [1]Department of Applied Science, PSG College of Technology, [3]Department of Physics, PSG Institute of Technology and Applied Research, Coimbatore, Tamil Nadu, India

Abstract

The aim of this article is to assess Tamil Nadu pediatric computed tomography (CT) diagnostic reference levels (DRLs) by collecting radiation dose data for the most commonly performed CT examinations. This work was performed for thirty CT scanners installed in various parts of the Tamil Nadu region. The patient cohort was divided into two age groups: <1 year, and 1–5 years. CT dose indices were measured using a 10 cm^3 pencil ion chamber with pediatric head and body polymethyl methacrylate phantoms. Dose data such as volumetric CT dose index ($CTDI_v$) and dose length product (DLP) on a minimum of twenty average-sized pediatric patients in each category were recorded to calculate a mean site $CTDI_v$ and DLP value. The rounded 75th percentile was used to calculate a pediatric DRL for each hospital, and then region by compiling all results. Data were collected for 3600 pediatric patients. Pediatric CT DRL for two age groups: <1 year ($CTDI_v$ and DLP of head [20 mGy, 352 mGy.cm], chest [7 mGy, 120 mGy.cm] and abdomen [12 mGy, 252 mGy.cm]), and 1–5 years ($CTDI_v$ and DLP of head [38 mGy, 505 mGy.cm], chest [8 mGy, 132 mGy.cm] and abdomen [14 mGy, 270 mGy.cm]) for select procedures have been calculated. Proposed pediatric DRLs of $CTDI_v$ and DLP for head procedure were lower, and for chest and abdomen procedures were higher than European pediatric DRLs for both age groups.

Key words: Diagnostic reference level, pediatric computed tomography, pediatric computed tomography diagnostic reference level, volumetric computed tomography dose index

Received on: 06-07-2016 **Review completed on: 30-10-2016** **Accepted on: 07-11-2016**

Introduction

Children are being referred for computed tomography (CT) scan due to the latter's speed, accuracy, flexibility, and accessibility. This has been mainly due to the introduction of fast spiral scanning, which obviates the need for sedation to keep children motionless, thereby permitting scans of younger or less cooperative children.[1] In the US, about 33% of all pediatric CT procedures are in children aged 10 or younger, with 17% of children aged five or younger.[2] At these ages, the organs and tissues are inherently more radiation sensitive to the oncogenic effects due to the larger quantity of cells that are separating and reproducing.[3-5] The International Commission on Radiological Protection (ICRP) states that children are 2–3 times more radiosensitive as compared to adult patients, due to the effect of cell division in developing organs and the longer anticipated lifetime for developing cancer cells.[6,7] The radiation-induced effects are also elevated in pediatric patients due to wider and enlarged cellular circulation of red bone marrow, and their higher postexposure life expectancy.[8,9] With this sharp radio-sensitivity now well documented, and to better inform radiographers about the significance of limiting the unwanted radiation dose to pediatric patients[10] the European Commission (EC) has, in its recommendations published in the year 2000, stressed the need for optimization of pediatric CT radiation dose.[11] The Food and Drug Administration (FDA) has also published related recommendations in 2002[12] about pediatric radiation dose optimization. While the use of CT scan for pediatric cases has increased unlike adult examination protocols, most of the times the exposure parameters used in

Access this article online	
Quick Response Code:	Website: www.jmp.org.in
	DOI: ***

Address for correspondence: Dr. K. N. Govindarajan, Department of Medical Physics, PSG Hospitals, Coimbatore - 641 004, Tamil Nadu, India. E-Mail: kngrajan@gmail.com

How to cite this article:

the older CT scanner are not always optimized to suit children. The result is that pediatric patients are being given considerably larger radiation doses than required for an optimum image quality.[13,14]

As children are intrinsically more sensitive to the effects of X-rays than adults, there is an urgent need to optimize CT exposure protocols for pediatric patients. The objective of optimization in CT exposures is to obtain acceptable image quality with minimum dose to the patients; reduction of dose in itself is not the objective of medical exposures. From this point of view, in recent times, much work has been done on optimization of scanning parameters in routine clinical conditions.[15-18] The foundation of optimization is the establishment of diagnostic reference levels (DRLs), first proposed by the ICRP in 1996[19] and later introduced into European[20] and Irish legislation.[21]

ICRP defines DRLs as "a form of investigation level applied to an easily measured quantity, usually the absorbed dose in air or tissue-equivalent material at the surface of (or inside) a simple standard phantom or a representative patient." This definition strongly emphasizes that DRLs are not the dose limits and do not help distinguish between good and poor medical practice. Although dose limits for occupational exposures must not be exceeded, patient DRLs may be exceeded if clinically necessary. DRLs also differ from dose limits for occupational exposure because they are not used to constrain individual patient exposures; this is because a dose higher than the standard dose may be required depending on the patient's body size and weight. DRLs are a tool for identifying facilities with unusually high doses and for promoting the optimization process.

Separate DRLs have been established for each country and/or region because equipment and procedure protocols can vary between different facilities in countries or regions, mainly due to different patient sizes and their weights. It is usually defined for a large collection of data at the 75th percentile. It can be defined at local level for a minimum number of 10–20 patients and preferably for a much larger number. By averaging such data from a large number of hospitals, the national DRLs can be estimated.[22,23] Hence, establishing national DRL would definitely ensure a safer pediatric CT diagnosis from patient's perspective. The purpose of DRLs is optimization of the imaging technique rather than radiation dose reduction to patients. If a justified examination does not provide the necessary clinical information because of too low dose resulting in an inadequate image quality, then the patient has been exposed needlessly to radiation. In clinical practice, it is assumed that the necessary dosage, within stipulated margins, will be used. In this line, it is essential to initially establish zonal DRL, namely, South, North, East, West and central and finally consolidate them to arrive at the pediatric DRL for the country. Thus, the objective of our study was to measure radiation dose for most commonly performed pediatric head, chest, and abdomen procedures in the radiology department in Tamil Nadu hospitals and suggest/derive pediatric DRLs, compare them with the internationally recommended DRLs and to suggest dose reduction methods without disturbing image quality.

Materials and Methods

Selection of computed tomography scanners

When attempting to establish regional CT DRLs which are applicable to all hospitals in Tamil Nadu, it is essential to sample as many hospitals as possible. The hospitals incorporated were equally spread over in the state of Tamil Nadu. This work was performed in thirty CT scanners which include both conventional and multidetector CT (MDCT) types installed at various major cities (Chennai, Coimbatore, Madurai, Salem, Erode, Tirupur, Namakkal, Trichy, Vellore, Dindigul, Dharmapuri, Hosur, Thiruvarur). The selection of the scanners was based on the number of pediatric patients investigated. The average number of pediatric patients scanned each day in the Tamil Nadu region was 3000: From this 1100 for head, 900 for chest and 1000 for abdomen CT procedures were performed. The total number of patients examined each day in the region was approximately 9000. Table 1 summarizes the make and model of the CT scanners involved in this study.

Radiation dose calibration

Before collecting the patient dose data, CT dose index (CTDI) measurements were carried out on all CT scanners by using calibrated 100 mm pencil ionization chamber (DCT10 RS, S/N 1636) and solidose electrometer 400 (S/N 4253) of RTI Electronics, Sweden. For this purpose, polymethyl methacrylate head (10 cm diameter) and body (16 cm diameter) phantoms were used.[24] The dosimetry methods recommended in the European guidelines[20] were followed. The individual approximate patient dose data were estimated from the phantom $CTDI_v$ and DLP measurements. It should be noted that phantom measurements are only a measure of the actual patient dose. Furthermore, it requires correction for different pediatric patient diameter.

Computed tomography dose measurements

Before initiating measurements in hospitals, a questionnaire was prepared to collect data regarding the pediatric CT protocols and clinical practices adopted by the hospitals in Tamil Nadu. These data helped to record the pediatric CTDI values for different scanning protocols adopted by the various departments. Participants were asked to extract from the scanner library, data for twenty patients belonging to each examination type and each age group in thirty CT departments (a total of 120 [20 (patients) × 3 (sites) × 2 (age group)] × 30 = 3600 procedures). In each category of machine, the lowest, highest, and mean physical parameters and operating parameters of both age group of pediatric patients are presented in Tables 2 and 3. Each row in this table refers to the parameters of the scanners mentioned in Table 1 in the same order.

This data abstraction has been done as per "Nationwide Evaluation of X-ray Trends" protocol.[25] The questionnaire contains a number of parameters including (i) make and model of the CT scanner, (ii) patient physical parameters

Table 1: Make and model of the computed tomography scanners involved in this study

Number of slice	Make	Models	Tamil Nadu (number of units)
Single	Hitachi	Pratico	1
	Philips	Secura	1
	Siemens	Emotion	1
Dual/4 slice	Hitachi	CXR4	1
	Philips	Brilliance Big Bore	1
	Siemens	Emotion Duo	2
	Toshiba	Asteion	2
	GE	High speed dual	3
	Siemens	Somatom	2
	Toshiba	Asteion	1
	GE	Lightspeed QX-I Quad CT	2
16	Philips	Brilliance	1
	Siemens	Somatom Emotion	1
	Toshiba	Aquilion	2
	GE	Brivo and LightSpeed	2
64	Siemens	Somatom Sensation	2
	Toshiba	Aquilion	1
	GE	High-speed VCT	1
128	Siemens	Somatom Definition AS and Edge	2
	GE	Optima 660	1
	Total		30

GE: General electric

such as height, weight, lateral diameter and anteroposterior diameter, (iii) indication, (iv) interested organ, (v) phase such as pre- and post-contrast, arterial phase, venous phase, full bladder, and delay phase, (vi) routine scan parameters such as tube potential, tube current, scan time, rotation time, slice thickness, slice beam collimation, pitch, total slices, field of view, start couch level and end couch level, (vii) dose-related data such as displayed volumetric CTDI and DLP.

The majority of the hospitals have followed almost similar exposure parameters for chest and abdomen procedures. However, the newer scanner systems like 64 slice, 128 slice CT machines use AEC/care kV technique for pediatric patients. Some of the CT centers have used larger scan length for routine brain and abdomen procedures. Further, it was noted that individual CT radiographers selected different scan parameters for the same type of pediatric patients.

CT dose experiments were carried out by placing the standard head and body phantom at the isocenter of the CT scanner and applying one axial slice of a clinical head protocol in sequential scan mode. The dose received by the phantom at the five positions for a set of scan parameters was measured by placing the ion chamber in one hole at a time while plugging the rest of holes with acrylic rods.

The CTDI is defined as:[26]

$$\text{CTDI} = (1/nT) \int D_z \, dz \text{ (integration limits from } -50 \text{ mm to } +50 \text{ mm)} \quad (1)$$

where, n is the number of data channels in the multiscan CT scanner, T is the slice thickness corresponding to one channel and the integration is done over the length of the pencil chamber (100 mm). The CTDI was measured as per the above definition by the pencil chamber-electrometer system and displayed on the dosimeter unit. CTDI is defined for a single complete rotation of the CT scanner. Using these dose values, the other CT dose indices, namely, weighed CTDI ($CTDI_w$), $CTDI_v$, and DLP were calculated using the following relations:

$$\text{Weighted } CTDI_w = 1/3\ (CTDI_{100,c}) + 2/3\ (CTDI_{100,p}) \quad (2)$$

$$\text{Volumetric } CTDI_v = CTDI_w/\text{pitch} \quad (3)$$

$$DLP = CTDI_v \times \text{scan length} \quad (4)$$

Results and Discussion

Before carrying out the regional dose estimation, complete QA (electrical, mechanical, and radiation checks) was performed for all the machines involved in this work. One among these tests was the measurement of $CTDI_w$ for standard protocol involving tube potential of 80 kV, 100 kV, and 120 kV, tube current-time product of 100 mAs and 5 mm slice thickness. These values were compared with the $CTDI_w$ displayed on the console to ensure that the measured and displayed values agreed as per Atomic Energy Regulatory Board standards (maximum ± 18%).[27]

The CT dose indices were measured based on the five point method proposed by European guidelines using standard CTDI phantoms and suitable detector. The pediatric CTDI phantom was placed on the couch and aligning the central axis of the phantom with isocentre point of the gantry. As per FDA's recommendation the dose is measured at the four peripheral holes as well as the central hole. The measured $CTDI_v$ and DLP of pediatric head, chest and abdomen procedures for

Table 2: Lowest, highest and mean of the operating parameters

Type of machine	Head				Chest				Abdomen			
	Tube potential (kV)	Tube current time product (mAs)	Scan length (cm)	Pitch	Tube potential (kV)	Tube current time product (mAs)	Scan length (cm)	Pitch	Tube potential (kV)	Tube current time product (mAs)	Scan length (cm)	Pitch
Single slice	100, 120	100, 180	10, 18	Axial	100, 120	100, 160	15, 25	1.0	100, 120	100, 180	15, 25	1.0
	110	160	16		105	120	20		105	125	22	
Dual slice	100, 120	110, 200	10, 20	Axial	100, 110	100, 180	18, 25	0.9, 1.2	100, 110	100, 180	15, 30	0.9, 1.1
	110	175	15		105	130	22	1.0	105	124	25	1.0
4 slice	100, 120	100, 250	10, 20	0.8, 1.1	100, 110	90, 150	16, 26	0.8, 1.3	100, 110	100, 180	15, 30	0.9, 1.4
	115	150	15	0.9	105	100	24	1.0	100	120	26	1.2
16 slice	100, 110	80, 200	10, 23	0.9, 1.0	100, 120	80, 140	15, 25	1.0, 1.1	100, 120	80, 160	15, 30	1.0, 1.6
	105	110	20	1.0	110	109	23	1.5	110	140	25	1.2
64 slice	100, 110	100, 200	10, 25	0.6, 1.1	80, 110	90, 160	15, 28	1.0, 1.4	80, 110	90, 180	15, 30	1.0, 1.2
	108	128	19	1.0	96	110	22	1.1	98	135	26	1.1
128 slice	80, 100	80, 160	10, 25	0.5, 1.0	80, 100	90, 140	15, 22	1.0, 1.6	80, 100	60, 180	15, 30	1.0, 1.4
	90	135	18	0.9	90	100	20	1.1	90	115	25	1.2

Table 3: Pediatric patient physical parameters in Tamil Nadu region

Pediatric patient physical parameters	Age group (years)	
	0-1	1-5
Weight (kg)	2.5-4.5	4-15
Height (cm)	40-80	80-130
Antero-posterior diameter (cm)		
Head	5-10	8-14
Chest	5-10	5-13
Abdomen	5-13	5-15
Lateral diameter (cm)		
Head	4-11	5-14
Chest	5-13	8-15
Abdomen	5-15	6-18
Abdominal circumference (cm)		
Head	4-12	5-14
Chest	4-13	5-15
Abdomen	5-14	5-18

both age groups at different CT departments are presented in Figures 1 and 2.

Figures 1 and 2 show that the large variations in CT radiation doses for pediatric head, chest, and abdomen procedures were noted for both age groups. This may be attributed to scans conducted without optimization of tube voltage and tube current-time product (mAs) with respect to the patient anatomy and organ of interest. Out of thirty CT departments, twenty CT departments have followed larger scan length for routine procedures; this will also give rise to an increase in the patient dose. Further, in this work, it was observed that based on the experience and knowledge of the radiographers, the selection of exposure parameters was altered from the default values. Those who have experience, have selected appropriate scan parameters when compared with newer radiographers; this also contributes to minimize radiation dose. Further, in this study, latest advancements and concepts in CT technology and selection of techniques such as detector arrangements, detector size, number of detectors, scan speed, tube rotation time, and type of detector (e.g., stellar detector in Siemens CT) available in recent MDCT scanners have been employed with reduction of radiation dose when compared with older CT scanners for pediatric patients.

Further, using overall calculated $CTDI_v$ and DLP value for both age groups of pediatric patients, the 75th percentile of $CTDI_v$ and DLP for head, chest and abdomen procedures thus calculated was taken as their respective third quartile values for each group of pediatric patients. The pediatric CT DRL proposed for Tamil Nadu region in south India has been compared with DRL recently proposed by EC[28] in Tables 4 and 5 [extracted from Figures 1 and 2].

From Tables 4 and 5, it was observed that the 75th percentile of $CTDI_v$ of pediatric head is lower than European DRL for both age groups. For chest and abdomen procedures, the 75th percentile of $CTDI_v$ is higher than European DRL

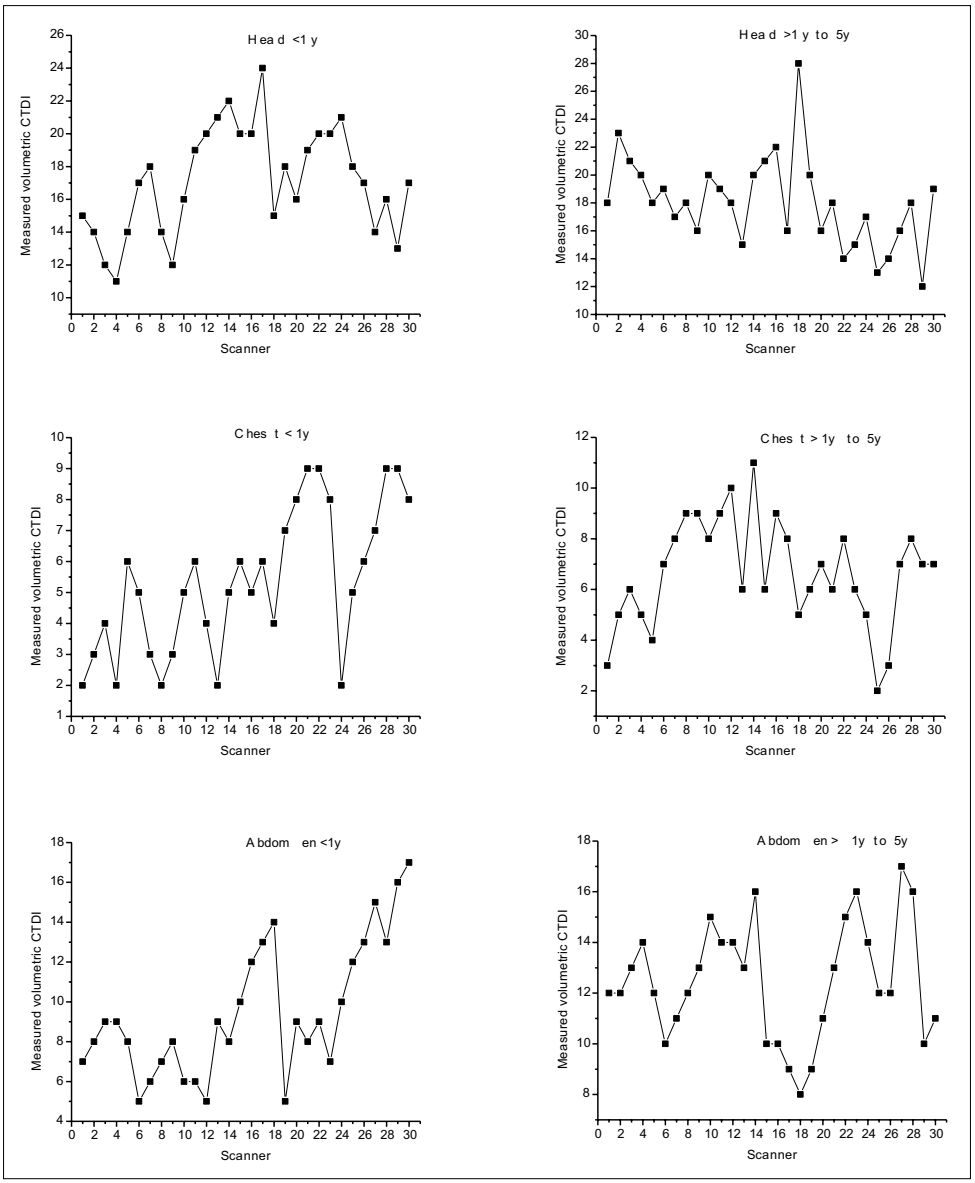

Figure 1: Calculated volumetric computed tomography dose index for <1 year and 1–5 years age group of pediatric patients for select procedures.

Table 4: Mean, range and third quartile values for volumetric computed tomography dose index for select procedures

Study region	Age group in year	Volumetric CTDI (mGy)			
		Mean	Range	Third quartile value of Tamil Nadu 2015	Pediatric European DRL 2015
Head	<1	17	11-24	20	25
	1-5	18	12-28	20	38
Chest	<1	5	2-9	7	3.3
	1-5	7	2-11	8	5.6
Abdomen	<1	9	5-17	12	5.7
	1-5	12	8-17	14	5.7

CTDI: Computed tomography dose index, DRL: Diagnostic reference level

for both age groups. This may be attributed to selection of greater exposure parameters for pediatric chest and abdomen procedures as compared to European practice. Following the European regulations, it becomes necessary to take into account the body size and habitus for selection of optimum machine parameters (e.g., tube voltage and mAs) for the

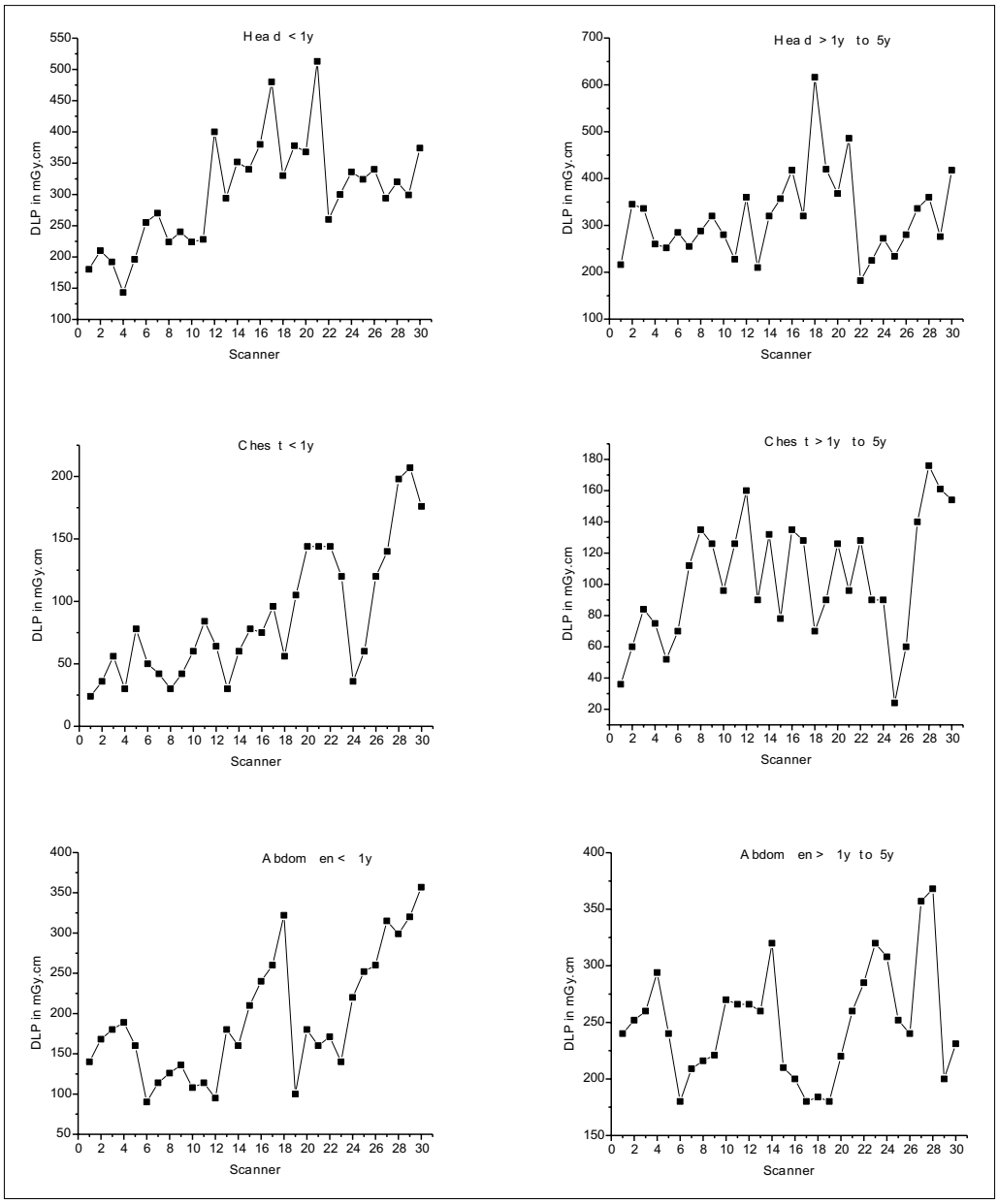

Figure 2: Calculated dose length product for <1 year and 1–5 years age group of pediatric patients for select procedures.

Table 5: Mean, range and third quartile values for dose length product for select procedures

Study region	Age group in year	DLP (mGy.cm)			
		Mean	Range	Third quartile value of Tamil Nadu 2015	Pediatric European DRL 2015
Head	<1	300	143-513	352	300
	1-5	304	182-616	360	505
Chest	<1	69	24-207	120	80
	1-5	96	24-176	132	115
Abdomen	<1	175	90-357	252	160
	1-5	246	180-368	270	170

DLP: Dose length product

required diagnostic information with minimum dose to the patient. In addition, it was observed that the 75th percentile of DLP of pediatric head for 0–1 year old patients is higher and for 1–5 years old patients is lower than European PiDRL, and for chest and abdomen procedures was higher than European pediatric DRL for both age groups. This is mainly

because of choosing higher scan length for both procedures and both age groups.

From this study, it is suggested that it is very important to justify CT examinations in advance and once the decision for CT scan is taken, it is mandatory to adopt the ALARA principle strictly. In this line, radiologists should play essential advisory role with referring clinicians. When equal or greater diagnostic yields are expected, CT should be replaced by alternative imaging modalities such as sonography, magnetic resonance imaging, or radionuclide voiding cystography. On the other hand, radiologists should make every effort to reduce the pediatric radiation dose of CT examinations while maintaining diagnostic quality when CT is indicated. Furthermore, minimizing the scan range of CT examinations as required is a straightforward way to achieve this goal. CT radiographer should follow the strategies for pediatric CT dose optimization methods, namely, body size adopted CT protocols, tube current modulation, optimal tube voltage, scan modes, appropriate pitch, appropriate scan length, and field of view to reduce the pediatric CT radiation dose for selected procedures.

Conclusion

This study reports the regional pediatric CT DRLs for head, chest and abdomen procedures for the first time in Tamil Nadu region. More than 3600 individual patients' data were recorded and studied. The experimentally measured $CTDI_v$ and DLP values for all procedures were compared with displayed control console values (maximum ± 18%). Tamil Nadu pediatric CT DRL values have been proposed for $CTDI_v$ and DLP of head, chest, and abdomen procedures for <1 year and 1–5 years age group of patients. These proposed DRL values were compared with the pediatric European DRL values and strategies for pediatric CT dose reduction have been suggested. In this line, all clinicians who request pediatric CT should frequently assess its suitability on a case-by-case basis. When used carefully, CT is a valuable imaging modality for both age groups of children.

Financial support and sponsorship

Atomic Energy Regulatory Board, Mumbai and PSG College of Technology, Coimbatore, Tamil Nadu, India.

Conflicts of interest

There are no conflicts of interest.

References

1. Donnelly LF, Emery KH, Brody AS, Laor T, Gylys-Morin VM, Anton CG, *et al.* Minimizing radiation dose for pediatric body applications of single-detector helical CT: Strategies at a large Children's Hospital. AJR Am J Roentgenol 2001;176:303-6.
2. Lam W, Wendy WM Lam. Pediatric CT radiation risks: What you should know. Med Bull 2006;11:5-7.
3. Brenner David J. One size does not fit all: Reducing risks from pediatric CT. ACR Bull 2001;57:20-3.
4. Frush DP, Donnelly LF, Rosen NS. Computed tomography and radiation risks: What pediatric health care providers should know. Pediatrics 2003;112:951-7.
5. Wakeford R. The cancer epidemiology of radiation. Oncogene 2004;23:6404-28.
6. 1990 recommendations of the international commission on radiological protection. Ann ICRP 1991;21:1-201.
7. UNSCEAR. Sources and Effects of Ionizing Radiation. New York: UNSCEAR; 2000.
8. Pierce DA, Shimizu Y, Preston DL, Vaeth M, Mabuchi K. Studies of the mortality of atomic bomb survivors. Report 12, Part I. Cancer: 1950-1990. Radiat Res 1996;146:1-27.
9. Preston DL, Ron E, Tokuoka S, Funamoto S, Nishi N, Soda M, *et al.* Solid cancer incidence in atomic bomb survivors: 1958-1998. Radiat Res 2007;168:1-64.
10. Chodick G, Kim KP, Shwarz M, Horev G, Shalev V, Ron E. Radiation risks from pediatric computed tomography scanning. Pediatr Endocrinol Rev 2009;7:29-36.
11. Bongartz G, Golding S, Jurik A, Leonardi M. European Commission. European Guidelines on Quality Criteria for Computed Tomography (Report EUR 16262). Luxemburg: European Commission; 1999.
12. Feigal DW Jr. FDA public health notification: Reducing radiation risk from computed tomography for pediatric and small adult patients. Int J Trauma Nurs 2002;8:1-2.
13. Brenner D, Elliston C, Hall E, Berdon W. Estimated risks of radiation-induced fatal cancer from pediatric CT. AJR Am J Roentgenol 2001;176:289-96.
14. Sternberg S. CT Scans in Children Linked to Cancer Later. USA Today, 01 April, 2001.
15. Hamberg LM, Rhea JT, Hunter GJ, Thrall JH. Multidetector row CT: Radiation dose characteristics. Radiology 2003;226:762-72.
16. Jangland L, Sanner E, Persliden J. Dose reduction in computed tomography by individualized scan protocols. Acta Radiol 2004;45:301-7.
17. Boone JM, Geraghty EM, Seibert JA, Wootton-Gorges SL. Dose reduction in pediatric CT: A rational approach. Radiology 2003;228:352-60.
18. Radiological protection and safety in medicine. A report of the International Commission on Radiological Protection. Ann ICRP 1996;26:1-47.
19. European Community. On health protection of individuals against the dangers of ionizing radiation in relation to medical exposure. Council directive 97/43 (Euratom). J Radiol Prot 1998;18:133-7.
20. European Guidelines on Quality Criteria for Computed Tomography. Report EUR 16262. Brussels, Belgium: European Commission; 2000.
21. Staniszewska MA. Evaluation of patient exposure in computerised tomogram in Poland. Radiat Prot Dosimetry 2002;98:437-40.
22. McCollough CH, Rochester MN. Diagnostic Reference Levels, American College of Radiology; 2010. Available from: http://WWW.IMAGEWISELY.ORG. [Last accessed on 2016 Nov 10].
23. CT Dose Profiler, Probe for Evaluation of CT Systems Manual-Version 5.2A, RTI, Sweden. Available from: http://www.rti.se/. [Last accessed on 2013 May 20].
24. Saravanakumar A, Vaideki K, Govindarajan KN, Jayakumar S, Devanand B. Cost-effective pediatric head and body phantoms for computed tomography dosimetry and its evaluation using pencil ion chamber and CT dose profiler. J Med Phys 2015;40:170-5.
25. Nationwide Evaluation of X-ray Trends (N.E.X.T). Tabulation and Graphical Summary of 2000 Survey of Computed Tomography; 2007. Available from: http://www.crcpd.org/PDF/NEXT2000CTProl.pdf. [Last accessed on 2016 Nov 14].
26. Saravanakumar A, Vaideki K, Govindarajan KN, Jayakumar S Establishment of diagnostic reference levels in computed tomography for select procedures in Pudhuchery, India. J Med Phys 2014;39:50-5.
27. AERB/RSD/MDX-CT/QAR/2010, Acceptance/Performance Test for Computed Tomography (CT) Scanner; 2010. Available from: http://www.aerb.gov.in/cgi-bin/X-Ray/XRAYuserform.asp. [Last accessed on 2016 Nov 14].
28. European Guidelines on DRLs for Pediatric Imaging, Final Complete Draft for PiDRL Workshop; 30 September, 2015. p. 38. Available from: http://www.eurosafeimaging.org. [Last accessed on 2015 Nov 05].

Bystander Effect and Second Primary Cancers following Radiotherapy: What are its Significances?

Sir,

Over last two decades, there has been an increasing interest in bystander effect in radiotherapy. Now, millions of people around the world undergo radiotherapy. On the other hand, in parallel with recent progresses in cancer therapy, there is an increasing life expectancy for cancer patients. However, these may cause growing concerns related to long-term consequences of radiotherapy including secondary malignancies. These concerns are more important for pediatric cancer patients. The risk of secondary cancer among pediatric patients who have undergone radiotherapy is considered to be up to ten folds than in adult patients.[1]

Possibly, bystander effect is one of the most interesting biological responses to ionizing radiation that may be involved in second primary cancer occurring years after radiotherapy. According to the *in vitro* and *in vivo* studies conducted so far, there is a direct link between bystander effect and cancer hallmark in non-irradiated cells. The direct role of the bystander effect in the induction of medulloblastoma in the non-targeted brain of mice has been investigated by Mancuso *et al*.[2]

In clinical studies, the best example of the role of the bystander effect in second primary cancer induction, is a high incidence of secondary lung cancer among patients who have had radiotherapy for prostate, ovarian, and rectal cancer. Induction of secondary cancers is more obvious for long-term survivors.[3] The prevalence of secondary lung cancer among these patients has been one of the most common malignancies within years after treatment, while received radiation dose with lung has been reported as lower than 0.5 Gy.[4] Hence, in addition to the need to understand the importance of this phenomenon in different situations, it is crucial to consider bystander effect as an important factor in selecting the treatment modalities.

According to different studies that have been conducted so far, different biological and physical factors are involved in damages induced by bystander effect. Two important biological factors are sex specificity and tissue specificity. Similar to direct irradiation, bystander signals are more obvious in males as compared to females.[5] Among physical factors, the role of dose, dose rate, linear energy transfer (LET), and fractionation have been investigated in several *in vitro* and *in vivo* studies.[6] Although it is predictable that an increase in cell damage, along with the increased LET, results in more obvious damages in bystander cells, the effect of fractionation against direct irradiation has less sparing effect on bystander cells.[7] Moreover, the effect of dose and dose rate are controversial.[8]

To the best of our knowledge, the basic mechanisms of bystander effect include inflammatory responses, antioxidant system suppression, epigenetic modulators, and so on.[5,9,10] Although, it seems that complete mechanisms of this phenomenon remain to be elucidated. Based on the importance of bystander effect in radiation treatment of cancer, it seems that the risk of secondary malignancies caused by this phenomenon should be considered in the near future. For this aim, it is crucial we consider life expectancy and sex of patients, numbers of fractionation, LET, and other factors.

Financial support and sponsorship

Nil.

Conflicts of interest

There are no conflicts of interest.

Masoud Najafi, Ashkan Salajegheh[1], Abolhasan Rezaeyan[2]

Department of Medical Physics and Biomedical Engineering, Faculty of Medicine, Tehran University of Medical Sciences, [2]Department of Medical Physics, Faculty of Medicine, Iran University of Medical Sciences, Tehran, [1]Department of Radiology, School of Paramedical, Shiraz University of Medical Sciences, Shiraz, Iran

Address for correspondence: Dr. Masoud Najafi, Department of Medical Physics and Biomedical Engineering, Faculty of Medicine, Tehran University of Medical Sciences, Tehran, Iran.
E-mail: masoudnajafi67@yahoo.com

References

1. Kumar S. Second malignant neoplasms following radiotherapy. Int J Environ Res Public Health 2012;9:4744-59.
2. Mancuso M, Pasquali E, Leonardi S, Tanori M, Rebessi S, Di Majo V, *et al.* Oncogenic bystander radiation effects in patched heterozygous mouse cerebellum. Proc Natl Acad Sci U S A 2008;105:12445-50.
3. Goldberg Z, Lehnert BE. Radiation-induced effects in unirradiated cells: A review and implications in cancer. Int J Oncol 2002;21:337-49.
4. Kleinerman RA, Boice JD Jr., Storm HH, Sparen P, Andersen A, Pukkala E, *et al.* Second primary cancer after treatment for cervical cancer. An international cancer registries study. Cancer 1995;76:442-52.
5. Chai Y, Calaf GM, Zhou H, Ghandhi SA, Elliston CD, Wen G, *et al.* Radiation induced COX-2 expression and mutagenesis at non-targeted lung tissues of gpt delta transgenic mice. Br J Cancer 2013;108:91-8.
6. Baskar R. Emerging role of radiation induced bystander effects: Cell communications and carcinogenesis. Genome Integr 2010;1:13.
7. Mothersill C, Seymour CB. Bystander and delayed effects after fractionated radiation exposure. Radiat Res 2002;158:626-33.
8. Gow MD, Seymour CB, Byun SH, Mothersill CE. Effect of dose rate on the radiation-induced bystander response. Phys Med Biol 2008;53:119-32.

9. Najafi M, Fardid R, Takhshid MA, Mosleh-Shirazi MA, Rezaeyan AH, Salajegheh A. Radiation-induced oxidative stress at out-of-field lung tissues after pelvis irradiation in rats. Cell J 2016;18:340-5.
10. Najafi M, Fardid R, Hadadi G, Fardid M. The mechanisms of radiation-induced bystander effect. J Biomed Phys Eng 2014;4:163-72.

Access this article online

Quick Response Code:

Website: www.jmp.org.in

DOI: 10.4103/jmp.JMP_124_16

How to cite this article: Najafi M, Salajegheh A, Rezaeyan A. Bystander effect and second primary cancers following radiotherapy: What are its significances? J Med Phys 2017;42:XX.

JMP_89_16R8

Issue of "In Water Calibration Certificate" for Cobalt-beam Quality at 10 cm Reference Depth - Is it Admissible Under TRS 398 Protocol?

Sir,

Cobalt-60 teletherapy beams are used in treating cancer, in most of the developing countries and countries with large population. For dosimeters used for output calibrations in high-energy photon and electron beams in linear accelerators, cobalt-60 beam qualities are still in use for specification of calibration factors in the calibration protocols such as TRS 277,[1] TRS 381,[2] TRS 398,[3] and TG 51.[4] In TRS 398,[3] the reference condition for calibration factor $N_{d,w}$ is indicated as 5 g/cm^2 (5 cm depth) in water. However, TRS 398 gives the reference conditions for the determination of absorbed dose to water as either 5 or 10 g/cm^2 (5 or 10 cm) depths. Absorbed dose at depth of dose maximum (d_{max}) is to be arrived at using percentage depth dose (PDD) (if source to surface distance [SSD] is 80 or 100 cm) or using tissue maximum ratios (TMR) for isocenter coinciding with specified depths (source axis distance 80 or 100 cm) referred from "standard tables."[5] When these measured outputs are applied for treatment planning calculations, the output at d_{max} in cGy/min is used along with PDD at desired depths. The relevant physical factors and their significance were clearly outlined earlier.[6,7] Whether we use 5 cm or 10 cm as the reference depth for calibration, once the respective PDDs[5] are taken for respective field sizes, it is expected to give the same results. Most of the IAEA-accredited secondary standard laboratories follow TRS 398 protocol for giving $N_{d,w}$ at cobalt energy at reference depth d = 5 g/cm^2 (PTW,[8] Iba[9]). In the recent past in India,[10] a reference depth of d = 10 cm in water is followed.

To validate the above point, a question was raised, whether the same traceability of dose would be valid for all field sizes, had the calibration factor $N_{d,w}$ been provided from 5 to 10 cm. A need for this aspect is brought out because, in the clinics, a 10 × 10 reference output is used along with PDDs or TMRs for treatment planning. A 0.6 cc Farmer ionization chamber (TM 30013, PTW) along with Unidos Electrometer (T 10008, PTW) at polarizing voltage of + 300 V measured ionization charge in nC in a Co-60 teletherapy unit (Theratron 780E, M/s Theratronix, Canada) using a 30 cm × 30 cm × 30 cm water phantom. The water phantom (PTW) has 5 cm and 10 cm water level line marks above the chamber center. The factors for field output variation (ratios of dosimeter corrected readings only) at 10 cm depth, normalized to 10 cm × 10 cm, showed variation from 0.862 to 1.218 from 5 cm × 5 cm field to 35 cm × 35 cm fields (σ = 0.8%). Similar factors for 5 cm depth showed factors variable from 0.903 to 1.145 for respective fields. When the chamber is kept at the surface of water phantom with chamber center aligned with the same level, the field factors varied from 0.948 to 1.097. For chamber with build-up cap, with no water surrounding the chamber, at the same 80 cm source to chamber center, the variation was found to be 0.961–1.073. It was therefore apparent that scatter conditions at various geometries give rise to different normalization factors with reference field of 10 cm × 10 cm.

It could be observed that for larger field sizes there are about 6.1% higher factors for 10 cm depth calibration against the same values with 5 cm depths. To understand this effect, a simple calculation with the interaction volume for 5 cm circular field at SSD = 80 cm with base at 5 cm depth (using truncated cone method) revealed an excess volume of interaction of primary flux by 470 ml at depth of 10 cm; a 30 cm diameter field at 80 cm SSD produces an additional scatter volume of 23,780 ml. When we took the measured head scatter factors multiplied by PDD ratios, and peak scatter factor ratios (obtained from BJR Supplement 25[5]), better agreement with measured field factors was seen at 5 cm depth compared to 10 cm depth. In literature, in general, it has been documented that the variation in estimated calibration factors in water ($N_{d,w}$) at various depths is within experimental uncertainty. It was also well documented that variation in the water to air stopping power with respect to depth is not larger than 0.5%, and perturbation effects are assumed constant beyond the depth of dose maximum. It is highlighted that for linear accelerator photons, 10 cm recommended depth is indicated in all the protocols because of the reason of definition

of beam flatness at 10 cm depths by manufacturers. Our measurements in telecobalt beam in 6 occasions have shown variation of calibrated absorbed doses at d_{max} (arrived from 5 to 10 cm) within ±0.5%, which may be within the uncertainty in ion-chamber dose estimates. This may therefore imply that TRS 398 protocol could be interpreted that it allows the use of 10 cm depth for issue of $N_{d,w}$ certification as practiced in one of the Secondary Standard Dosimetry Laboratories.[10]

Acknowledgment

The author thanks Director, Cachar Cancer Hospital and Research Center (CCHRC), for kind permission to publish the present work.

Financial support and sponsorship

Nil.

Conflicts of interest

There are no conflicts of interest.

Ramamoorthy Ravichandran

Cachar Cancer Hospital and Research Center, Silchar, Assam, India

Address for correspondence: Dr. Ramamoorthy Ravichandran, Cachar Cancer Hospital and Research Center, Silchar - 788 015, Assam, India.
E-mail: ravichandranrama@rediffmail.com

References

1. IAEA. Absorbed Dose Determination in Photons and Electron Beams: International Code of Practice. Tech. Report Series No. 277. Vienna: IAEA; 1997a.
2. IAEA. The Use of Plane Parallel Ion Chambers in High Energy Electron and Photon Beams: International Code of Practice for Dosimetry. Tech. Report Series 381. Vienna: IAEA; 1997b.
3. IAEA. Absorbed Dose Determination in External Beam Radiotherapy: International Code of Practice for Dosimetry. Tech. Report Series No. 398. Vienna: IAEA; 2000.
4. Almond PR, Biggs PJ, Coursey BM, Hanson WF, Huq MS, Nath R, *et al.* AAPM's TG-51 protocol for clinical reference dosimetry of high-energy photon and electron beams. Med Phys 1999;26:1847-70.
5. BIR. Central Axis Depth Dose Data for Use in Radiotherapy: 1996. Supplement No. 25. London, England: British Institute of Radiology; 1996.
6. Meredith WJ, Massey JB. Fundamental Physics of Radiology. 3rd ed. London: John Wright and Sons Ltd.; 1977. p. 469-73.
7. Sathiyan S, Ravikumar M, Ravichandran R. Measurements of radiation absorbed doses in high energy radiotherapy beams: A comparison of different calibration protocols. J Med Phys 2003;28:18-22.
8. Calibration Certificate from PTW, Freiburg, Germany (Certificate No. 1101857, 2011).
9. Calibration Certificate from Iba, Neurenberg, Germany (Certificate Nos. 17063,67,1603032,2016).
10. Calibration Certificates from RSDL, RSS, BARC, India (Certificate Nos. 1429 (2009),1910 (2013).

Access this article online

Quick Response Code:

Website: www.jmp.org.in

DOI: 10.4103/jmp.JMP_89_16

How to cite this article: Ravichandran R. Issue of "In water calibration certificate" for cobalt-beam quality at 10 cm reference depth - Is it admissible under TRS 398 protocol? J Med Phys 2017;42:XX-XX.

Erratum

Erratum: Clinical implications of Eclipse analytical anisotropic algorithm and Acuros XB algorithm for the treatment of lung cancer

In the article titled, "Clinical implications of Eclipse analytical anisotropic algorithm and Acuros XB algorithm for the treatment of lung cancer" published in pages 219-223, issue 4, vol. 41 of Journal of Medical Physics,[1] the fifth and sixth sentences under the section "Introduction" are written incorrectly as 'Type "A" was proposed by Knöös *et al*.[3] which were based on measurements and accounts for correction for patient contours and heterogeneities. Type "B" was proposed by Ojala *et al*.[4] which were based on superposition and convolution techniques.' instead of 'Type "A" and "B" were proposed by Knöös *et al*.[3] Type "A" was based on measurements and accounts for correction for patient contours and heterogeneities. Type "B" was based on superposition and convolution techniques. Ojala *et al*.[4] proposed type "C ".'

Reference

1. Krishna GS, Srinivas V, Reddy PY. Clinical implications of Eclipse analytical anisotropic algorithm and Acuros XB algorithm for the treatment of lung cancer. J Med Phys 2016;41:219-23.

Reviewers List, 2016

We gratefully acknowledge the services of following experts who have given their valuable time and cooperation in reviewing the manuscripts

A Jirasek, *Canada*
A Shukla K, *India*
Al Mutaz M. Abdalla, *United Arab Emirates*
Alok K Singh Kushwaha, *India*
Ambika Sahai Pradhan, *India*
Ananthanarayanan Sankaran, *India*
Andrzej Niemierko, *USA*
Anuj Soni, *India*
Archana Gautam, *USA*
Ashok Bakshi, *India*
B Satish Rao, *India*
Bhudatt Paliwal R, *USA*
Bhuwan Chandra Bhatt, *India*
Biju Keshavkumar, *India*
BS Rao, *India*
Challapalli Srinivas, *India*
Chandra Joshi Prakash, *Canada*
Chithra Nair, *USA*
Choryi Ng, *China*
D Deshpande D, *India*
David Eaton, *United_Kingdom*
Devesh Mishra R, *India*
G Panayiotakis, *Greece*
G.C. Jagetia, *India*
Ganesan Ramanathan, *Australia*
Ganesh Narayanasamy, *USA*
Gopalkrishna Kurup, *India*
habib zaidi, *Switzerland*
Harold DSouza, *United_Kingdom*
Hema Vaithianathan, *Australia*
Huijun Xu, *USA*
Indra Das J, *USA*
J Velmurugan, *India*
Jamema Swamidas, *India*
James CL Chow, *Canada*
John Schreiner, *Canada*
K J MariaDas, *India*
K.M. Ganesh, *India*
K.N. Govindrajan, *India*
Kanta Chhokra, *India*
Kevin Jordan, *Canada*
kirisits christian, *Austria*
Komanduri Ayyangar, *USA*
KV Subbaiah, *India*
L Nithya, *India*
Lalit M Aggarwal, *India*
Lisa Karam, *USA*
M Kehwar, *USA*
M Ravi Kumar, *India*
Ma Jiasen, *USA*
Manoj Semwal, *India*
N Chegeni, *Iran*
N Gopishankar, *India*
N Nagaiah, *India*
Nagesh N Bhat, *India*
Nan Qin, *USA*
P Jursinic, *USA*
P K Dash Sharma, *India*
P Venkatachalam, *India*
Palani Selvam, *India*
Patrick Langechuan Liu, *USA*
Paul Ravindran B, *India*
Prabhakar Ramachandran, *India*
Pramilla Sawant, *India*
Pratik Kumar, *India*
Prince Gyekye Kwabena, *Ghana*
Raghavendra Holla, *India*
Raghuram K Nair, *India*
Rajesh Kinikar, *India*
Rajesh Kumar, *India*
Ramamoorthy Ravichandran, *India*
Ramkrushn S Vishwakarma, *India*
Ravi Teja Seethamraju, *USA*
Roshan Livingstone Samuel, *India*
S Mahalakshmi, *India*
S Panneerselvam, *India*
S Sharma D, *India*
Shanta Appukutan, *India*
Siva Sarasanandarajah, *Australia*
Slav Yartsev, *Canada*
Subhash Kheruka, *India*
Sudesh Deshpande, *India*
Sujoy Chatterjee, *India*
Surendra Rustgi, *USA*
Tharmar Ganesh, *India*
Tim Olding, *Canada*
Tomas Kron, *Australia*
V Sathiyanarayanan, *India*
Varatharaj Chnadraraj, *India*
Vasu Vasu, *United_Kingdom*
Wilbroad Muhogora, *Tanzania*
Xiao Jin, *USA*
YB Cihan, Turkey

The fastest and easiest way to keep track of your QA data

Track-it

The New QA Data Management Solution by PTW

Tracking. Trending. Reporting.
On one single platform.

Anytime. Anywhere. Your way.

PTW DOSIMETRY INDIA PVT.LTD
ACE Towers, 2nd Floor, 73/75, Dr. Radhakrishnan Road, Mylapore, Chennai - 600 004.
Ph : 044 - 4207 9999 Telefax : 044 - 4207 2299 E-mail : info@ptw-india.in Web : www.ptw-india.in

PTW
Knowing what responsibility means

Film is a ~~hassle~~. *snap*

GafChromic introduces FilmQA-PRO Verification Software for IMRT QA.

You know that film gives you a more complete picture than electronic arrays. What's more, emerging techniques like SRS and RapidArc™ are better suited to film because film lets you shoot from any angle. But film may feel hard to work with and time-consuming. All that changes. Now FilmQAPro™ 3.0 is taking full advantage of what we've built into GafChromic™ film. One-scan analysis lets you do calibration and plan verification simultaneously. So you eliminate variables, and post-exposure growth no longer gets between you and your results. You get answers in minutes. And multi-channel dosimetry ensures the integrity of your measurement. Finally, software that makes film easy. With help from FilmQAPro 3.0, the future is film.

GAFCHROMIC® Films for Radiotherapy:

(1) Gafchromic® EBT3 and EBT3-1417 (2) Gafchromic® RTQA2-1010 (3) Gafchromic® RTQA2-111

Let's take care.

Exclusively distributed in India by:

LATESTECH INTERNATIONAL

GafChromic

17-G/319, Vasundhara, Ghaziabad-201012, INDIA
Telephone: 0120-2881252 Fax: 91-120-2881179
Mob: 09873278842 Email: latestech@rediffmail.com

RADIATION ONCOLOGY

MEDITRONIX

PRODUCTS & SERVICES

Having representing the best technologies for over 35 years, we have understood the treatment needs which changes with the newer challenges everyday. Today, we represent world's premium brands for different modalities of cancer diagnosis and treatment.

Fluke 35040 Dosimeter

A2J Moving & Fixed Lasers

Precisis Cobalt MLC

Klarity AIO Base Plate

Klarity SBRT System

Klarity Thermoplastics

Ludlum 9DP Pressurised Ion Chamber Survey Meter

Rexon TLD Reader

Par Scientific Block Cutter

CIRS Dynamic Thorax Phantom

Quartz QA Kit

AERB Recognized Calibration Facility For Radiation Measuring Instruments

Radimage HEALTHCARE INDIA Pvt. Ltd.

Radimage Healthcare India Pvt. Ltd.

G-236, Sec-63, Noida - 201 303, India

Tel.: +91 120 2406096, 4263270 Fax: +91 120 2406097

• radimagehealthcare@gmail.com • www.radimageindia.com

(A MEDITRONIX CORPORATION GROUP COMPANY)

Radimage HEALTHCARE INDIA Pvt. Ltd.

AERB Recognised Calibration Laboratory

- **AERB recognised calibration laboratory vide letter no. AERB/RSD/ Recog-Cal04/2014/7963 dt. 12.8.2014**
- **Facility to calibrate any brand or type of Radiation Survey Meter, Area (Zone) Monitor and Pocket Dosimeters. Either analogue or digital**
- **Pick-up and drop through courier can be arranged, if the need arise**
- **Routine turn-around calibration time is 5-6 days**
- **Instrument should always be in working condition, to avoid delays**
- **Calibration validity TWO years**

परमाणु ऊर्जा नियामक बोर्ड
Atomic Energy Regulatory Board
GOVERNMENT OF INDIA

CERTIFICATE OF RECOGNITION OF LABORATORY FOR CALIBRATION OF RADIATION MONITORING INSTRUMENTS (RMIs)

Certificate No. : AERB/RSD/Recog Cal04/2014/7963 | Issuance Date : August 12, 2014 | Expiry Date : August 11, 2016

In accordance with the Rule-29 of Atomic Energy (Radiation Protection) Rules, 2004 and on the basis of review of the Application along with documents submitted, the Atomic Energy Regulatory Board (AERB) hereby grants Recognition to **M/s Radimage Healthcare India Pvt. Ltd., Noida, Uttar Pradesh,** for the purpose of calibration of Radiation Monitoring Instruments (RMIs) up to the range of **900 mGy/hr (90 R/hr).**

This Recognition is subject to the adherence to the requirements specified in the AERB document, entitled "Recognition & Consenting requirements for Calibration Laboratories for Radiation Survey Instruments and Pocket Dosimeters" and compliance with the terms and conditions as applicable and stated overleaf of this Certificate of Recognition.

Competent Authority

Shri Arun Mathur
Executive Director
M/s Radimage Healthcare India Pvt Ltd.,
G-236, Sector -63,
Noida-201303, Uttar Pradesh

Radimage HEALTHCARE INDIA Pvt. Ltd.

Radimage Healthcare India Pvt. Ltd.
G-236, Sec-63, Noida - 201 303, India
Tel.: +91 120 2406096, 4263270 Fax: +91 120 2406097
• radimagehealthcare@gmail.com • www.radimageindia.com
(A MEDITRONIX CORPORATION GROUP COMPANY)

RAVEN
LINAC QA BY LAP

ROSALINA INSTRUMENTS

THE INDEPENDENT ALL-IN-ONE QA DEVICE FOR YOUR DAILY, MONTHLY, AND ANNUAL LINAC QA

One device measures, verifies and records your LINACs optical, mechanical, and radiation parameters.

MECHANICAL AND RADIATION MEASUREMENTS FOR LINEAR ACCELERATORS

DAILY QA*

DOSIMETRY
- x-ray output constancy
- electron output constancy

MECHANICAL
- laser localization
- optical distance indicator (ODI) @ iso
- collimator size indicator

MLC
- qualitative test (i. e. matched segments, aka picket fence)

WEDGES
- morning check-out run for one angle

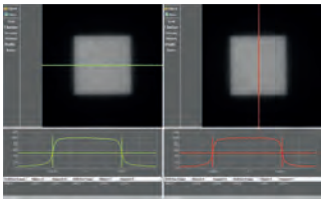

Radiation QA

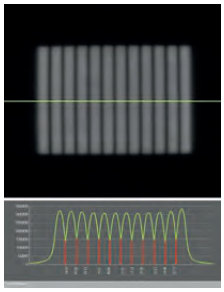

MLC Picket Fence

MONTHLY QA*

DOSIMETRY
- x-ray output constancy
- electron output constancy
- photon beam profile constancy
- photon beam energy constancy
- electron beam profile constancy
- electron beam energy constancy
- dose rate output constancy

MECHANICAL
- light / radiation field coincidence
- distance check device for lasers compared with front pointer
- gantry / collimator angle indicators
- accessory trays
- jaw position indicators (symmetric)
- cross-hair centering (walkout)
- treatment couch position indicators
- wedge placement accuracy
- compensator placement accuracy
- localizing lasers

MLC
- setting vs radiation field for two patterns
- travel speed
- leaf position accuracy

WEDGES
- wedge factor for all energies

ODI & Light Field

ANNUAL QA*

DOSIMETRY
- x-ray flatness change from baseline
- x-ray symmetry change from baseline
- electron flatness change from baseline
- electron symmetry change from baseline
- x-ray / electron output calibration
- spot check of field-size dependent output factors for x-ray
- output factors for electron applicators
- x-ray beam quality
- electron beam quality
- physical wedge transmission factor constancy
- x-ray monitor unit linearity (output constancy)
- electron monitor unit linearity (output constancy)
- x-ray output constancy vs dose-rate
- x-ray output constancy vs gantry angle
- electron output constancy vs gantry angle
- electron and x-ray off-axis factor constancy vs gantry angle

MECHANICAL
- collimator rotation isocenter
- gantry rotation isocenter
- couch rotation isocenter
- coincidence of radiation and mechanical isocenter
- table top sag
- table angle
- table travel maximum range movement in all directions

MLC
- MLC transmission
- leaf position repeatability
- MLC spoke shot
- coincidence of light field and radiation field
- segmental IMRT (step and shoot) test
- moving window IMRT

WEDGES
- check of wedge angle for 60°, full field and spot check for intermediate angle, field size

Rosalina Instruments

127, Bussa Udyog Bhavan,
Tokershi Jivraj Road, Sewri (W),
Mumbai - 400 015.
Tel: 91 22 24166630
Email: support@rosalina.in
Website: www.rosalina.in

Radcal

Radcal Diagnostic
Medical Imaging Quality Assurance

ACCU-GOLD

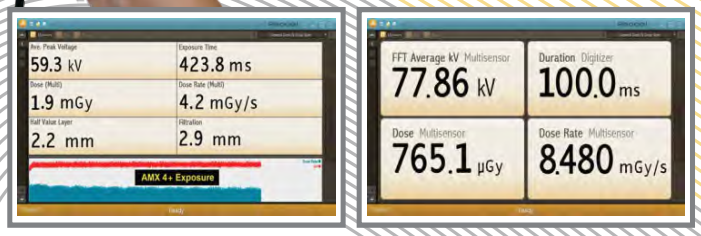

RAPIDOSE

ACCU-PRO

ROSALINA
INSTRUMENTS
127, Bussa Udyog Bhavan, Tokershi Jivraj
Road, Sewri (W), Mumbai - 400 015
Tel : +91 22 24166630
E-mail : support@rosalina.in
Website : www.rosalina.in

Efficiency, accuracy and clinical relevance at the same time

Cornerstones of ScandiDos

INSTANTLY ANALYZE AND APPROVE PLANS	The analysis starts with the Dose - Picture.
QUICKLY AND EASILY FIND THE CAUSE OF DEVIATIONS	If a deviation is noted, the user can easily zoom in on the details.
VERIFY THE DOSE DELIVERY WITHOUT COMPROMISES IN 3D	Reliable QA must be highly accurate and comprehensive. Delta 4®PT measures the dose with high density in the high gradient region with the resolution of 50nGy.
ANALYZE THE CLINICAL RELEVANCE OF A DEVIATION	The level of importance in discrepancy between delivered and planned dose is determined using patient anatomy (e.g. target and risk structures) to gauge the clinical relevance.

THE DIFFERENCE CLEAR

ROSALINA INSTRUMENTS

Registered with Registrar of Newspapers in India
Vide RNI No. MAHENG/2012/44833, Rs 20 for AMPI Members

Editor Dr. A. S. Pradhan. Printed and published by Wolters Kluwer India Private Limited on behalf of Association of Medical Physicists of India, Mumbai and printed at Dhote Offset Technokrafts Pvt. Ltd., Jogeshwari (E), Mumbai - 400 060, India, and published at A-202, 2nd Floor, The Qube, C.T.S. No.1498A/2 Village Marol, Andheri, Mumbai, India